Simulation of mechanoregulation and tissue differentiation in calcium phosphate scaffolds for tissue engineering

Clara Inés Sandino

Doctoral Thesis

Biomedical Engineering Doctoral Program

Supervised by Dr. Damien Lacroix

Departament de Ciència del Materials i Enginyeria Metal·lúrgica

Universitat Politècnica de Catalunya

July 2010

For my family and friends

"La inspiración existe, pero tiene que encontrarte trabajando"

Pablo Picasso

Acknowledgments

I am happy to express my sincere gratitude to those who have contributed to the research performed during the PhD and to the writing of this thesis. During these years many people had helped me not only discussing about models, formulations, cells, etc, but also sharing those things that let me enjoy working.

I would like to thank Dr. Damien Lacroix, director of this thesis, for always taking the time to talk and to help, for his guidance and for his patience. It is a fortune to have him as a supervisor.

I am grateful to Professor Dr. Josep Anton Planell, director of the IBEC, and Dra. Mari Pau Ginebra, director of the biomaterials, biomechanics and tissue engineering group at the UPC, without them this thesis would have not been possible. I would also like to acknowledge the funding by the Government of Catalonia through a FI grant and from the European Commission through the SmartCap project (NMP3-CT2005-013912).

Furthermore I would like to thank Professor Dr. Patrick Prendergast, from the Trinity College Dublin, and Professor Dr. Keita Ito, from the Eindhoven University of Technology, for reviewing this work. Additionally, Professor Prendergast welcomed me to the Trinity College for a three months stay.

I am also grateful to the administrative staff of the CMEM and ESAII at the UPC as well as the staff of the IBEC, for their assistance. In particular Pedro, Guillem and Anton are acknowledged for their informatics support.

I also want to thank former and current group members of the biomaterials, biomechanics, and tissue engineering group at the UPC, as well as the biomaterials, implants and tissue engineering group at the IBEC. I thanks Melba for the very special persons she is and for the incredible amount of things she does for me, specially for taking me out for running. I thanks Milena, Alex, Teresa and Txell for their support and friendship and for the nice times we have share. I also thanks Elisabeth, Montse CH, Carolina, Marta P, Montse E, Emiliano, Miguel, Oscar, Ana, Edgar, Sergio, Johan, Lucia, Aitor, Román, Marta G, Pablo, Marta M, Gemma, Tiziano, Aleix, Lluis, and Noelia. I am also indebted to Ainara and Maria Elena from the biomedical engineering doctoral program for pleasant conversations at the mathematics building.

I would like to express my deep appreciation to my colleagues at the Trinity College in Dublin; Sara, who made my stay at Trinity and in Dublin an incredible fructiferous experience; Hanifeh, for our nice discussions and for all the chocolates we shared; Colin, Feng and Katey for their kindly welcoming; and Damien, who also came for a stay to Barcelona. From the staff, Sheena is specially thanked for her gently care.

It is a pleasure to thank my colleagues and friends of the biomechanics and mechanobiology group. I thank all of them for their friendship and for making fun every day at the office. Jérôme, for his optimism and his comradeship; Sebas, for teaching me that things non necessarily have to be square, symmetric and ordered to be perfect; Ramiro for his life philosophy thoughts; Andy for being always there; Andrea for his smart sense of humor; Jean-Louis for his smile; Sara for her enthusiasm and her friendship; Cecile for her charm and cordiality; Aura for her authenticity; and Martin, who is for me the best definition of what a friend is, thanks also Martin for reading this manuscript as well as reports, presentations and e-mails. I would also like to thank Agnès, Igor, Sol and Juan.

I am indebted to Xavi, Cristina, Sergi and "Los Marines" from the UPC gym for helping me to keep the stress out, and especially Gemma and Pilar, for giving me a smile every morning.

I am also happy to thank my old friends Diana, Verónica and Olga for their long distance support; my flat mates in Barcelona Guille and Meritxell, for taking care of me; and my family, my mother for being an example of discipline and perseverance; my father, María and Tomás for welcoming me with open arms to Colombia; Alejandro and Hayat for funny weekends in Barcelona; Leonardo for Sunday afternoon hot chocolates in Colombia; and of course Luis, Daniela, Alejandra and Sara for being the love of my life.

Publications and Presentations Resulting from this Study

Journal Publications

C. Sandino and D. Lacroix. A dynamical study of the mechanical stimuli and tissue differentiation within a CaP scaffold based on μCT finite element models. Biomechanics and Modeling in Mechanobiology 2010; in press.

C. Sandino, S. Checa, P.J. Prendergast and D. Lacroix. Simulation of angiogenesis and cell differentiation in a CaP scaffold subjected to unconfined compressive strain using a lattice modeling approach. Biomaterials 2010; 31:2446-2452.

C. Sandino, J.A. Planell and D. Lacroix. A finite element study of mechanical stimuli in scaffolds for bone tissue engineering. Journal of Biomechanics 2008; 41:1005-1014.

Other Publications

S. Checa, C. Sandino, D.P Byrne, D.J. Kelly, D. Lacroix and P.J. Prendergast. Computational techniques for selection of biomaterial scaffolds for tissue engineering. Keynote lectures book chapter invited by the International Conference on Tissue Engineering. Leiria, Portugal, 9-12 July 2009.

Congress Oral Presentations

D. Lacroix, M. Koch, C. Sandino, JL. Milan and E. Engel. Biomechanical Study of the Mechanical Stimuli at the Cellular Level in a Bone Tissue Engineering Scaffold. 6th World Congress of Biomechanics, Singapore. 1rd-6th August 2010.

P. Prendergast, A. Lennon, H. Khayyeri, K. Roddy, P. Murphy, C. Sandino and D. Lacroix. Mechanoregulation of Tissue Differentiation, Experiments and Computation. 6th World Congress of Biomechanics, Singapore. 1rd-6th August 2010.

C. Sandino and D. Lacroix. A dynamical FE study of mechanical stimuli in scaffolds for bone tissue engineering. 17th Congress of the European Society of Biomechanics, Edinburgh, Scotland. 5th-8th July 2010.

C. Sandino, S. Checa, P.J. Prendergast and D. Lacroix. An in silico study of the mechanoregulation of angiogenesis and tissue differentiation within a Calcium Phosphate scaffold for bone tissue engineering TERMIS EU Conference 2010. Galway, Ireland. 13th - 17th June 2010. Rapid fire presentation and Poster.

C. Sandino and D. Lacroix. An in Silico Study of the Mechanoregulation of Tissue Differentiation in a Calcium Phosphate Scaffold for Tissue Engineering. 3rd IBEC Symposium on Bioengineering and Nanomedicine. Barcelona, Spain. 1st - 2nd June 2010. Flash presentation and Poster.

C. Sandino, S. Checa, P.J. Prendergast and D. Lacroix. Simulation of Angiogenesis and Cell Differentiation in CaP Scaffolds for Bone tissue engineering. 2nd China-Europe Symposium on Biomaterials in Regenerative Medicine. Barcelona, Spain. 16-20th November 2009.

C. Sandino, J.A. Planell and D. Lacroix. Simulation of tissue differentiation in scaffolds for bone tissue engineering. IV International Conference on Computational Bioengineering. Bertinoro, Italy. 16-18th September 2009.

D. Lacroix, J.L. Milan, C. Sandino, S. Midderhoff, L. Marques and J.A. Planell. Mode of failure of a biomaterial composite scaffold for bone tissue engineering using synchrotron micro-tomography and finite element analysis. 12th International Conference on Fracture. Ottawa, Canada. 12-17th July 2009.

C. Sandino, J.A. Planell and D. Lacroix (2008) μCT based FE models of perfusion fluid flow into scaffolds for bone tissue engineering. 16th congress of the European Society of Biomechanics. Lucerne, Switzerland, 6 - 9 July 2008.

C. Sandino, D Lacroix and J.A. Planell (2007) μCT based FE models of mechanical stimuli in scaffolds for bone tissue engineering. ESB 2007 Workshop. Dublin, Ireland, 26-28 August 2007.

C. Sandino, M.P. Ginebra, J.A. Planell and D. Lacroix D (2006). Estudio por elementos finitos de estímulos mecánicos para la ingeniería de tejidos. XXIX Congreso de la sociedad Ibérica de Biomecánica y Biomateriales. Reus, España, 2- 4 de Noviembre 2006.

D. Lacroix, C. Sandino, M.P. Ginebra and J.A. Planell (2006) L'ingénierie tissulaire pour l'orthopédie pédiatrique. 6th European Research Conference in Pediatric Orthopaedics. Toulouse, France, 5-6 October 2006.

D. Lacroix, C. Sandino, M. Charles-Harris and J.A. Planell (2006) On the use of Mimics FEA to characterize finite element meshes of bone scaffolds. 5th World Congress of Biomechanics. Munich, Germany, 29 July – 4 August 2006. Journal of Biomechanics, 39 (S1) S424

D. Lacroix, C. Sandino, M. Villagomez, M.P. Ginebra and J.A. Planell (2006) A micro-Finite Element analysis of fluidic and solid mechanical stimuli in bone tissue engineering scaffolds. 5th World Congress of Biomechanics. Munich, Germany, 29 July – 4 August 2006. Journal of Biomechanics, 39 (S1) S415

C. Sandino, M.P. Ginebra, J. A. Planell and D. Lacroix (2006) Development of micro-finite element models of tissue engineering based ceramic scaffolds from micro-computed tomography. 7th International Symposium on Computer Methods in Biomechanics and Biomedical Engineering. Antibes, France. 22-25 March 2006. CMBBE2006 Proceedings pp 73-78.

Contents

List of Figures

List of Tables

Abbreviations

2D	Two Dimensions
3D	Three Dimensions
BMP	Bone Morphogenetic Protein
CaP	Calcium Phosphate
CMEM	Ciència del Materials i Enginyeria Metal·lúrgica Material Science and Metallurgical Engineering Department - UPC
CT	Computed Tomography
DMEM	Dulbecco´s Modified Eagle Medium
EC	Endothelial Cell
ESAII	Enginyeria de Sistemes, Automàtica i Informàtica Industrial Automatic Control Department - UPC
FE	Finite Element
IBEC	Institut de Bioenginyeria de Catalunya Institute for Bioengineering of Catalonia
MSC	Mesenchymal Stem Cell
SMC	Smooth Muscle Cells
UPC	Universitat Politècnica de Catalunya Technical University of Catalonia
VEGF	Vascular Endothelial Growth Factor
µCT	Micro Computed Tomography

Abstract

Mechanical stimuli are one of the factors that affect cell differentiation in the process of bone tissue regeneration; therefore, in the development of scaffolds for tissue engineering, mechanical loads can be applied in order to induce cell activity. The specific mechanical stimuli transmitted to cells at a microscopic level when mechanical loads are applied can be studied using numerical techniques. The objective of this thesis was to study the mechanoregulation of tissue differentiation within calcium phosphate scaffolds using micro computed tomographed based finite element models.

Two samples of porous calcium phosphate based materials were used. Congruent finite element meshes, with the solid phase and the interconnected pores discretized, were developed in order to account for the scaffold irregular morphology.

First, a study of the distribution of mechanical stimuli was performed. The solid phase and the fluid flow within the pores were modeled as linear elastic solid material and Newtonian fluid respectively. Compressive strains of 0.5% of total deformation applied to the solid and interstitial fluid flows with inlet velocities of 1, 10 and 100 μm/s applied to the pores were simulated. Similar strain distributions for both materials were found, with compressive and tensile strain maximal values of 1.6% and 0.6% respectively. For the fluid flow models, the fluid velocity in some of the scaffold pores increased to 100 and 1000 times the inlet velocity. This study showed how mechanical loads and fluid flow applied to the scaffolds caused different levels of mechanical stimuli within the samples according to the morphology of the materials.

Next, a study of the mechanoregulation of tissue differentiation over time in a scaffold subjected to *in vitro* loads was performed. The solid phase and the fluid flow were modeled as in the study described above. Compressive strain of 0.5% and fluid flow with constant inlet velocity of 10 μm/s or constant inlet pressure of 3 Pa were applied. Octahedral shear strain and fluid shear stress were used as mechano-regulatory stimuli based on the theory of Prendergast et al. (1997). When a constant velocity was simulated, fluctuations between stimuli equivalent to tissue formation and cell death were predicted due to the increase in the fluid shear stress when tissue started to fill the pores. However, when constant pressure was applied, stimuli equivalent to bone formation were predicted in about half of the pore volume. These results suggest that in order to allow tissue differentiation within a scaffold, the fluid velocity should be decreased when tissue starts mineralizing.

Finally, a study of the angiogenesis and the mechanoregulation of tissue differentiation over time in a scaffold subjected to *in vivo* conditions was performed. Octahedral shear strain and relative fluid velocity were used as mechano-regulatory stimuli. The solid and pore phases were treated as poroelastic materials. Individual cell activity was simulated within the pore domain. Compressive strains of 0.5 and 1% of total deformation were simulated. Most vessels grew in the pores at the periphery of the scaffolds and were blocked by the scaffold walls. Similar capillary networks were formed independently of the magnitude of the mechanical strain applied. When 0.5% of strain was applied, 70% of the pore volume was affected by mechano-regulatory stimuli corresponding to bone formation; however, because of the lack of oxygen, only 40% of the volume was filled with osteoblasts. This study showed the effect of the lack of vascularization in the center of the scaffold on the tissue differentiation.

Such kind of studies, combined with *in vitro* studies, should contribute to the understanding of the process of tissue differentiation within the constructs and therefore to the improvement of scaffold design methods.

Resumen

Los estímulos mecánicos son uno de los factores que afectan a la diferenciación celular en el proceso de regeneración del tejido óseo, por lo tanto, en el desarrollo de andamios para ingeniería de tejidos, se pueden aplicar las cargas mecánicas con el fin de inducir la actividad de las células. Cuando se aplican cargas mecánicas, los estímulos mecánicos específicos transmitidos a las células a nivel microscópico pueden estudiarse mediante técnicas numéricas. El objetivo de esta tesis fue estudiar la mecanoregulación de la diferenciación de tejido en andamios de fosfato de calcio utilizando modelos de elementos finitos basados en micro tomografía axial computarizada.

Dos muestras de materiales porosos basados en fosfato de calcio fueron utilizadas. Se desarrollaron mallas de elementos finitos congruentes, discretizando la fase sólida y los macro poros interconectados, con el fin de tener en cuenta la morfología irregular de los andamios.

En primer lugar, se estudió la distribución de los estímulos mecánicos. La fase sólida y el fluido intersticial se simularon como material elástico lineal y como fluido Newtoniano, respectivamente. Se simuló una compresión del 0.5% en el sólido y un fluido con velocidades de entrada de 1, 10 y 100 μm/s en los poros. Se encontraron distribuciones de deformación similares en las paredes ambos materiales, con valores máximos de 1.6% en compresión y de 0.6% en tracción. En algunos poros, la velocidad del fluido aumentó a 100 y 1000 veces la velocidad de entrada. Este estudio

mostró como estímulos mecánicos macroscópicos pueden causar distintos niveles de estímulos mecánicos microscópicos dentro los andamios, debido a la morfología.

A continuación se realizó un estudio en el tiempo de la diferenciación de tejido en un andamio sometido a condiciones *in vitro*. La compresión y la perfusión se modelaron como en el estudio anterior. Se simularon una compresión del 0.5% y una velocidad de entrada de fluido constante de 10 μm/s o una presión de entrada de fluido constante de 3 Pa. La deformación cortante octaédrica y el esfuerzo cortante del fluido se utilizaron como estímulos mecano-regulatorios basándose en la teoría de Prendergast et al. (1997). Al aplicar velocidad constante, se predijeron fluctuaciones entre los estímulos equivalentes a la formación de tejido y a la muerte celular, debido al aumento en el esfuerzo cortante del fluido cuando el tejido comienza a llenar los poros. Sin embargo, al aplicar presión constante, se predijo estímulo equivalente a la diferenciación de tejido óseo en la mitad del volumen de los poros. Estos resultados sugieren que para permitir la diferenciación de tejido, la velocidad del fluido debe disminuirse cuando el tejido empieza a mineralizarse.

Finalmente, se llevó acabo un estudio en el tiempo de la angiogénesis y de la diferenciación de tejido en un andamio bajo condiciones *in vivo*. La deformación cortante octaédrica y la velocidad relativa del fluido se utilizaron como estímulos mecano-regulatorios. Las fases sólida y porosa fueron tratadas como materiales poroelásticos. Se simuló la actividad individual de las células. Compresiones de 0.5 y 1% fueron simuladas. La mayoría de los vasos crecieron en los poros de la periferia del andamio y se bloquearon por las paredes. Se formaron redes capilares similares independientemente de la magnitud de deformación utilizada. Al aplicar 0.5% de compresión, estímulos correspondientes a la formación de hueso se predijeron en el 70% del volumen de los poros, sin embargo, sólo el 40% del volumen se llenó de osteoblastos debido a la falta de oxigeno. Este estudio mostró el efecto de la falta de vascularización en el centro del andamio en la diferenciación de tejido.

Ese tipo de estudios, combinados con estudios *in vitro*, deberían contribuir a la comprensión del proceso de diferenciación de los tejidos dentro de los andamios y por lo tanto a la mejora de los métodos de diseño de andamios.

CHAPTER 1
Introduction

1.1. TISSUE ENGINEERING

Tissue Engineering is a multidisciplinary field that applies the principles of biology and engineering in order to develop tissue substitutes to restore, maintain, or improve the function of diseased or damaged human tissues when the body is not able to do it by itself (Ratner et al. 2004). The main approach of tissue engineering is to develop a scaffold that mimics the structure of the tissue. This scaffold would be implanted serving as support for cells to migrate, proliferate, differentiate and synthesize extracellular matrix proteins. At the same time, the scaffold should degrade leaving the new healthy tissue.

Many aspects should be considered in the development of scaffolds such as biomaterial composition, scaffold and pore morphology, porosity, pore interconnectivity and material mechanical properties (Navarro and Michiardi 2008). All these aspects affect the mechanical stimuli transmitted to the cells and therefore influence the process of tissue differentiation.

1.2. THE ROLE OF MECHANICAL STIMULI IN BONE TISSUE ENGINEERING

In the 19th century, bone form was related to its function in terms of mechanical loading. For instance, Julius Wolff, in 1892, stated that "The shape and structure of growing bones and adult bones depend on the stresses and strains to which they are subjected. By altering the lines of stress the shape of a bone could be changed" (Wolff 1892). In addition to Wolff´s law, in 1881, Wilhelm Roux proposed that bone formation and functional adaptation are regulated by cells, which are governed by mechanical stimuli, in a self-organizational process (Huiskes 2000).

Since bone tissue differentiation is regulated by mechanical stimuli, it can be used to improve cell proliferation and differentiation and consequently tissue formation within scaffolds. *In vivo,* mechanical loads are induced by body forces, while *in vitro*, mechanical stimuli can be generated by mechanical loading (Meyer et al. 2006), by perfusion fluid flow (Fassina et al. 2005) or by a combination of them (Yang and El Haj 2005).

In vitro the mechanical load applied to the scaffold can be correlated to cell activity, However, it is difficult to determine the specific mechanical stimuli transmitted to each cell since they depend on the location of the cell within the scaffold, the mechanical properties of the material, the morphology of the construct, and the mechanical load applied to the scaffold. This information can be obtained using numerical studies.

1.3. THE ROLE OF NUMERICAL STUDIES IN BONE TISSUE ENGINEERING

The micro mechanical stimuli distribution on the scaffold can be studied by means of numerical techniques, e.g. the FE method. The greatest advantage of this method is its ability to handle arbitrary geometry including non homogeneous and anisotropic materials. The analyzed domain is divided into a finite number of discrete elements, providing the possibility of examining the stress and strain in each discrete point, i.e. node, of the material surface when the scaffold is subjected to mechanical loads.

As well as physical and biological processes in bone can be studied at different scales, from organ level to molecular level, FE models can be developed at different levels or scales (Fig 1.1). Macroscopic models treats tissues, or scaffolds, as a continuum using bulk mechanical properties, while micro models account for the different phases of

tissues, or scaffolds. At the cell level, the internal mechanism of the cell under mechanical loading is studied.

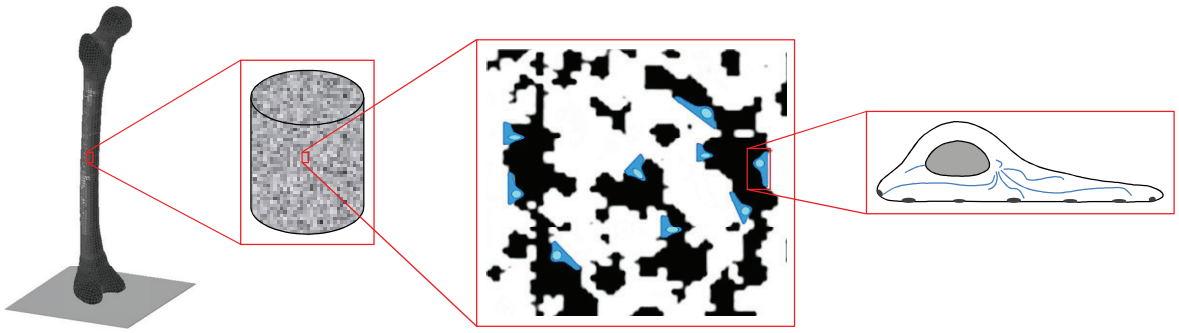

Fig 1.1. Schematic representation of biological tissue multiscale modeling

In order to develop micro FE models, the real architecture of a scaffold can be modeled using μCT images. Using this technique, images of cross sections of the scaffolds can be acquired in a non destructive and non invasive manner. From these images the 3D geometry of scaffolds, discretizing the solid and pore phases, can be reconstructed and virtual models can be obtained.

Two different approaches of FE studies have been used to investigate scaffolds for tissue engineering. On one hand, some studies are focused on investigating the distribution of mechanical stress and strain at each specific location of the scaffold under specific mechanical loads (i.e. compressive loads or perfusion fluid flows) without considering tissue differentiation (Porter et al. 2005, Cioffi et al. 2006, Lacroix et al. 2006, Maes et al. 2009, Milan et al. 2009, Stops et al. 2010a). On the other hand, some tissue differentiation studies apply remodeling theories to simulate the time course of tissue differentiation (Kelly and Prendergast 2006, Byrne et al. 2007, Checa and Prendergast 2010, Milan et al. 2010, Stops et al. 2010b).

1.4. CALCIUM PHOSPHATE AS BIOMATERIAL FOR BONE TISSUE ENGINEERING

The use of CaP cements and glass ceramics for bone tissue engineering is motivated by its structural similarity to the bone mineral phase. They exhibit biocompatible and bioactive behavior and have been used as filler material for bone defect repair and as artificial bone matrix (Ginebra 2009).

This thesis was developed within the frame of the SmartCaP project. The main goal of that project was to implement a novel biomaterial for bone regeneration. This biomaterial would be injectable, porous, and biodegradable and promote osteogenesis and angiogenesis. Novel injectable and porous CaP cements were developed for the project. They consisted of a powder phase and a liquid phase which, after mixing, formed a plastic paste that could be injected in host tissue (ensuring a minimally invasive surgery), and once implanted formed a porous solid body. This process ensured perfect fit at the implant site and good bone-material contact, even in geometrical complex defects. Instead of be injected in the host tissue, the scaffolds could also be molded as cylinders to be used *in vitro* or *in vivo* experiments.

1.5. OBJECTIVES

The main objective of this thesis is to investigate the distribution of the mechanical stimuli and the mechanoregulation of bone tissue differentiation in CaP based porous scaffolds using μCT based FE models.

Specific goals:

1) To reconstruct the real architecture of scaffolds using μCT images in order to analyze the scaffold morphology in terms of porosity and interconnectivity and obtain congruent FE meshes for the solid and the fluid phases.

2) To calculate the distribution of mechanical stimuli within CaP scaffolds when subjected to *in vitro* conditions.

a) The stress and strain within the solid phase due to a compressive mechanical loading and

b) The fluid velocity, fluid pressure and fluid shear stress due to a perfusion fluid flow.

3) To simulate the mechanoregulation of tissue differentiation within the pores of the scaffold when subjected to *in vitro* conditions: compressive loading and perfusion fluid flow; using octahedral shear strain and fluid shear stress as mechanical stimuli.

4) To simulate the mechanoregulation of angiogenesis and tissue differentiation within the pores of the scaffold when subjected to *in vivo* conditions: compressive loading; using octahedral shear strain and relative fluid velocity as mechanical stimuli.

CHAPTER 2
Mechanobiology in Bone Tissue Engineering- State of the Art

2.1. INTRODUCCION

This thesis is mainly concerned about the mechanoregulation of bone tissue differentiation in CaP based porous scaffolds when subjected to *in vitro* mechanical loads. This chapter presents a general description of the tissues that, according to the mechanoregulation concepts, can be differentiated and the cells involved in the process of tissue formation. Then the principal concepts that predict tissue differentiation and angiogenesis in the process of bone regeneration are described as well as their application in scaffolds for tissue engineering.

2.2. SKELETAL TISSUE HISTOMORPHOLOGY

The skeleton provides the structure to bear the weight of the body, protect internal organs from external forces and facilitate movement. It serves as the major store of calcium salts playing an important role in the general metabolism of the body. The adult human skeleton consist of over 200 bones, which can be grouped as long, short, flat, irregular, or sesamoid. These bones are associated with muscles and other non osseous tissues including cartilage, tendons and ligaments. Cartilage provides

articulations between bones, tendons attach muscles to bone and ligaments attach bones to other bones (Martini 1998).

2.2.1. Bone

According to the macroscopic structure of the bone tissue, it can be classified as cortical or trabecular. Cortical (dense or compact) bone is dense in texture and is the shell of many bones, surrounding the trabecular bone in the center. The basic functional unit of cortical bone is the osteon. All osteons are aligned in the same way, making bones very strong when stressed in the direction of osteon alignment. Trabecular (cancellous or spongy) bone consists of thin bars and sheets of bone, called trabeculae, which branch and intersect to form a sponge-like network. This spongy bone is located where bones are not heavily stressed or where the stresses arrive from many directions. The trabeculae are oriented along the stresses lines. Two connective tissues cover bone, the endosteum and the periosteum (Fig 2.1). The endosteum is a thin layer of cell-rich tissue facing the marrow cavity. The periosteum, lining the outer surface of bone, is composed by two layers. The outer layer is more fibrous and its function is to connect bones at the joint. The inner layer is more vascularized and is rich on cells. The periosteum provides a large portion of the bone´s blood supply.

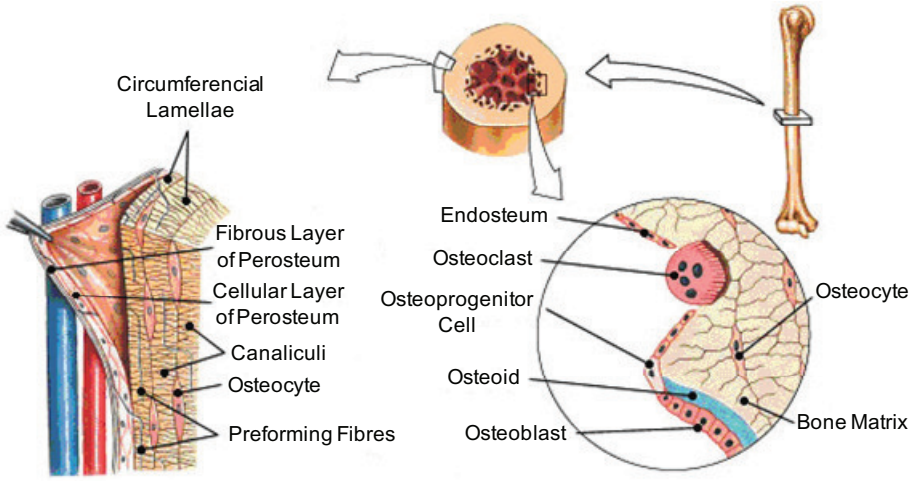

Fig 2.1. Schematic representation of the structure and cells of bone tissue (Martini 1998)

Bone tissue consists of bone cells, osteocytes, which are embedded within an organic extracellular matrix that is mineralized with inorganic salts (Fig 2.1). The chemical composition of mineralized bone is approximately 20% of water, 35% of organic molecules, and 45% of inorganic mineral salts by weight. Of the organic component;

nearly 90% is the structural protein type I collagen; and the remaining 10% is constituted by lipids, non collagenous proteins, peptides, glycoproteins, and various other molecules such as BMPs and osteocalcin. The principal constituents of the inorganic component are calcium phosphate and calcium carbonate, with small quantities of sodium, magnesium, and fluoride. The mineral component of bone exists mainly as carbonated apatite. Within this tissue there are pores that are filled primarily with vascular tissue and marrow. The non mineralized porous space is highly variable, ranging from less than 5% by volume in dense compact bone to more than 95% percent in porous cancellous bone.

The osteocytes reside in non mineralized spaced called lacunae. To remain viable, these cells must receive nutrients that diffuse from vascular canals. In mineralized compact bone, there are numerous canals in which blood vessels and nerves lie. A typical distance between blood vessels is approximately 200 to 300 μm which is small enough so as to allow all the osteocytes to be nourished by diffusive processes. The mineralized struts in cancellous bone, trabeculae, are generally less than 200 μm thick. The osteocytes in trabeculae receive nutrients from vessels in the neighboring marrow spaces. Osteocytes are extensively connected by a massive network of fine cell processes called canaliculi, which may aid the diffusion of nutrients. These canaliculi also provide a possible mechanism for osteocyte interaction and communication with other cells on the surface of the mineralized tissue.

Bone may be synthesized by intramembranous ossification, endochondral ossification, or appositional ossification. Intramembranous ossification is the synthesis of bone directly by osteoblasts. Osteoblasts synthesize extracellular organic matrix that then is progressively mineralized. As mineralization occurs, the osteoblasts become trapped within the tissue and thereby differentiate into osteocytes. Endochondral ossification is the gradual replacement of cartilage by bone and marrow cavities. In this process, chondrocytes become hypertrophied, next osteoprogenitor cells and blood vessels invade the spaces left, and osteoprogenitor cells differentiate into osteoblasts which synthesize extracellular matrix that then is calcified. Finally calcified cartilage is resorbed. The bone produced by endochondral ossification is called immature woven bone. This bone is rich in osteocytes and has small collagen fibrils that are oriented randomly. These two types of ossification are present during bone development. In the healthy adult bone appositional ossification takes place; progenitor mesenchymal cells located in the perosteum and the endosteum differentiate into osteoblasts that synthesize extracellular bone matrix (Carter and Beaupré 2001).

Bone tissue can be resorbed from mineralized surfaces by multinucleated cells called osteoclasts. In many of the surfaces where resoption occurs, bone is almost

immediately reformed by osteoblasts. The turnover of bone tissue by sequential osteoclastic and osteoblastic activity is called bone remodeling. Many cycles of bone remodeling in a bone region can occur during a person´s life time and allow tissue to be repaired from microdamage.

Different from bone remodeling, bone regeneration is a process initiated by tissue damage such as fracture or surgical cutting and drilling that causes a physical disruption of the mineralized tissue matrix, death of many types of cells, and the interruption of local body supply. Regeneration involves the formation of new tissue that implicate the proliferation and differentiation of pluripotential MSCs. In this case, intramembranous, endochondral and appositional ossification take place.

2.2.2. Cartilage

Three major types of cartilage are found in the human adult: Hyaline cartilage, elastic cartilage, and fibrocartilage. Hyaline cartilage is the most common; it is present at the connection between the ribs and the sternum, the nose, the conducting passageways of the respiratory tract, and the articular cartilage. Its matrix contains closely packed collagen fibers, making it tough but somewhat flexible. Elastic cartilage is present at the external flap of the outer ear, larynx, and epiglottis; it contains numerous elastic fibers that make it extremely resilient and flexible. Fibrocartilage is dominated by collagen fibers making the tissue extremely tough. It lies between the spinal vertebrae and between the pubic bones of the pelvis.

Cartilage cells (chondrocytes) are characterized by their production of the extracellular structural protein, type II collagen. In its mature stage, cartilage tissue has a relatively low density, less than 10% of the tissue volume, and the chondrocytes are confined to lacunae (Fig 2.2). The extracellular matrix is composed of about 70% of water, 20% of type II collagen, and 6% of proteoglycans, by weight, with the remainder consisting of other collagen types and non collagenous proteins.

The cell metabolism in cartilage is much lower than that in bone, and thus it can, and must, exist without internal vascular canals. The articular cartilage at the end of long bones, for example, is avascular. The chondrocytes within this tissue are kept viable primarily by the diffusion of nutrients from the adjacent synovial membrane and synovial fluid within the joint space. When the diffusion distances are large and the cartilage cells are undergoing rapid proliferation and matrix biosynthesis, therefore a greater supply of nutrients is required. Under such conditions, small branching cartilage canals containing arteries, arterioles, venules, and capillaries are formed.

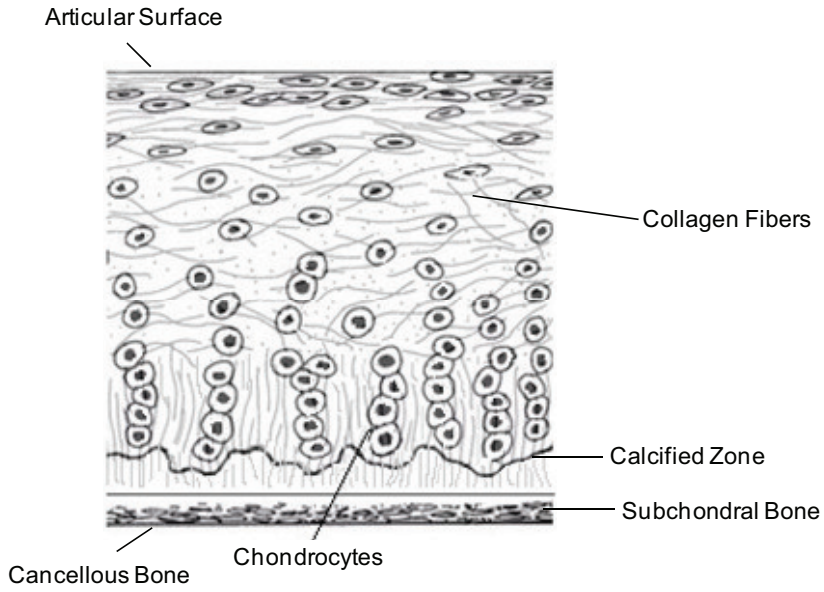

Fig 2.2. Schematic representation of the structure and cells of articular cartilage (Modified from Newman 1998)

2.2.3. Tendons and Ligaments / Fibrous Tissue

Tendons and ligaments consist of a tissue that is comprised of a dense network of collagen fibrils with relative few cells (Fig 2.3). Tendons are cords of dense regular connective tissue that attach skeletal muscles to bones, the collagen fibers run along the longitudinal axes of the tendon and transfer the pull of the contracting muscle to the bone. Ligaments are similar to tendons but connect one bone to another.

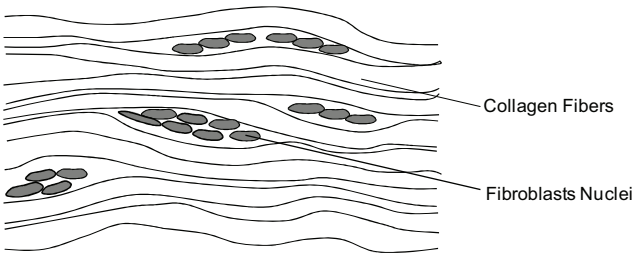

Fig 2.3. Schematic representation of the structure and cells of fibrous tissue

The predominant cells of these tissues are fibroblasts. Water accounts for 55% of the wet weight and type I collagen for about 38%. Other constituents include types III and IV collagen, elastin, glycoproteins, and other non collagenous proteins.

2.3. NUMERICAL STUDIES OF MECHANOREGULATION IN TISSUE DIFFERENTIATION

A key point in tissue differentiation is the capacity of pluripotential MSCs of the early granulation tissue to proliferate and differentiate into cells that form different types of tissue, for instance bone, cartilage and fibrous tissue (Fig 2.4). This differentiation is regulated by several chemical and physical factors in the cell environment. Among these factors, the mechanical stimuli play an important role.

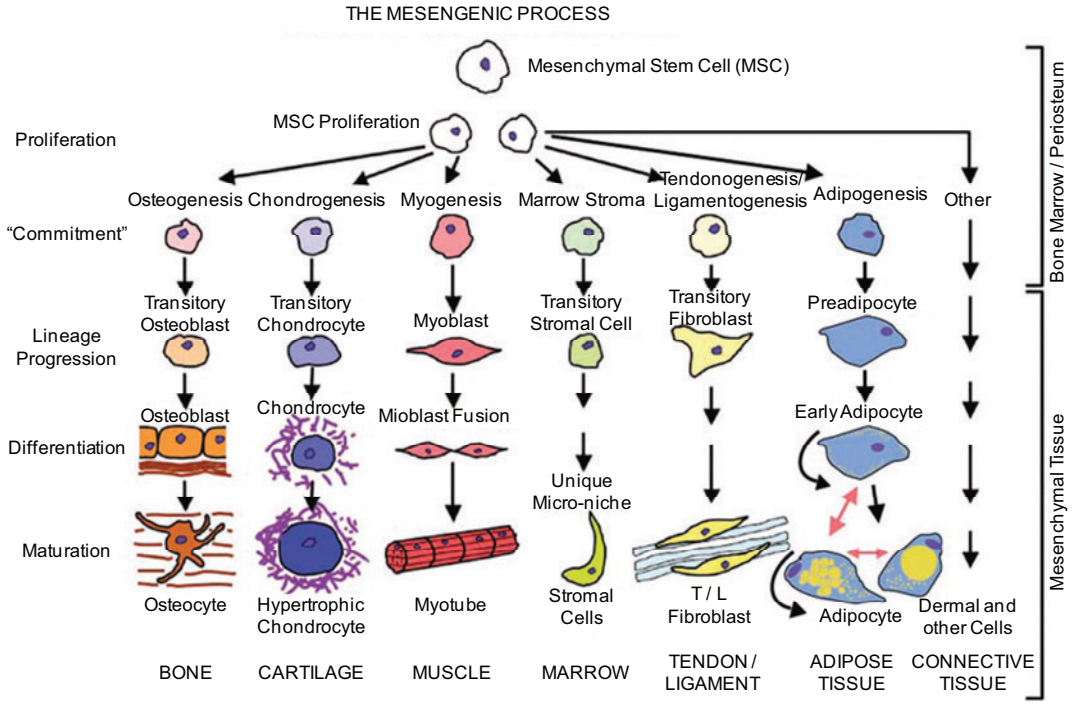

Fig 2.4. The mesengenic process (Caplan 2010).
MSCs can follow different differentiation pathways depending on external stimuli.

2.3.1. Initial Concepts Based on Clinical Observations

In 1941 Pauwels (Pauwels 1960 and Pauwels 1980) proposed that the effects of mechanical forces on tissue differentiation pathways occur through mechanical deformation of tissues. The local deformations in a tissue can be described by a strain tensor, which has first and second invariants representing dilatational and distortional strain components respectively. The first invariant represents a change in volume (caused by dilatational or hydrostatic stress D) and the second a change in shape (caused by distortional or shear stress S).

$$D = \frac{1}{3}\left(\sigma_I + \sigma_{II} + \sigma_{III}\right)$$

$$S = \frac{1}{3}\sqrt{\left(\sigma_I - \sigma_{II}\right)^2 + \left(\sigma_{II} - \sigma_{III}\right)^2 + \left(\sigma_{III} - \sigma_I\right)^2}$$

where σ_I, σ_{II} and σ_{III} are principal stresses.

Pauwels proposed that the combination of these variables determined the differentiation pathway from MSCs into fibrous, fibro-cartilaginous or cartilaginous tissue. Endochondral bone formation would occur in regions of low distortional and high dilatational strain (Fig 2.5). Pauwels´ theory was based on clinical observations; therefore he did not determine the specific stimuli for tissue formation.

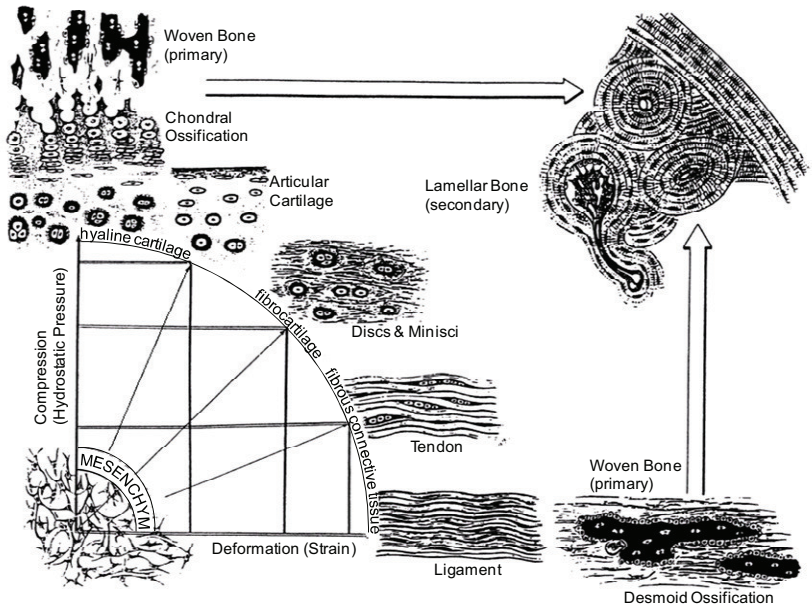

Fig 2.5. Concept of mechanoregulation of tissue differentiation proposed by Pauwels (Weinans and Prendergast 1996). MSCs differentiation is governed by hydrostatic pressure and strain.

In 1979 Perren postulated ''the interfragmentary strain theory'' (Perren 1979 and Perren and Cordey 1980). According to this theory, the interfragmentary strain ε was defined as the ratio of the relative displacement of fracture ends d versus the initial gap width G (Fig 2.6).

The magnitude of interfragmentary strain would determine the subsequent differentiation of fracture gap tissue. Interfragmentary strains above 100% would lead to non union. Strains between 10 and 100% would lead to form fibrous tissue. Strains between 2 and 10% would lead to cartilage formation and endochondral ossification. Strains under 2% would lead to direct bone formation.

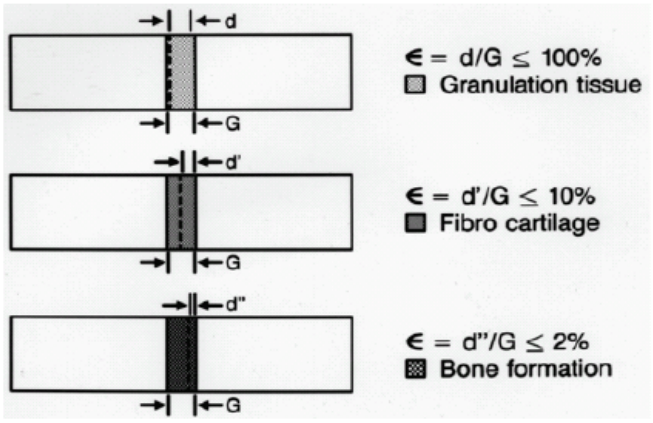

Fig 2.6. Interfragmentary strain theory proposed by Perren (Chao EYS and Inoue N 2003). Tissue differentiation is governed by the magnitude of interfragmentary strain.

2.3.2. Computational Simulations of Tissue Differentiation

Carter and co-workers introduced a semiquantitative theory to determine the contribution of the hydrostatic and the octahedral shear stresses in tissue differentiation within the context of fracture healing (Carter et al. 1988). Endochondral ossification was defined by an osteogenic index *I* combining the peak of cyclic hydrostatic stress *D* and the peak of cyclic octahedral shear stress S.

$$I = S + kD$$

where k is an empirical constant. Comparing the results with biological examples, the most predictive values were determined at $0.3 \leq k \leq 10$ (Carter and Wong 1988). With a good vascularity, low levels of intermittent hydrostatic stress and shear stress permit the direct formation of bone, cartilage is formed under high levels of compressive hydrostatic stress combined with low levels of shear stress, and fibrous tissue is formed under high levels of shear stress. Without a good vascularity, bone cannot form, even in a low-stress environment; instead, cartilage would form.

Later on, the octahedral shear stress was replaced with the octahedral or distortional strain history, and the hydrostatic stress with the hydrostatic stress history in order to emphasize that biological events at the tissue level are related to changes in cell shape and local matrix deformation and to include cyclic loading over time (Carter and Giori 1991) (Fig 2.7a). Additionally, an alternative diagram of mechanoregulation was developed considering that the magnitude of the maximum principal strain seems to be critical when intramembranous ossification occurs (Carter et al. 1988a) (Fig 2.7b).

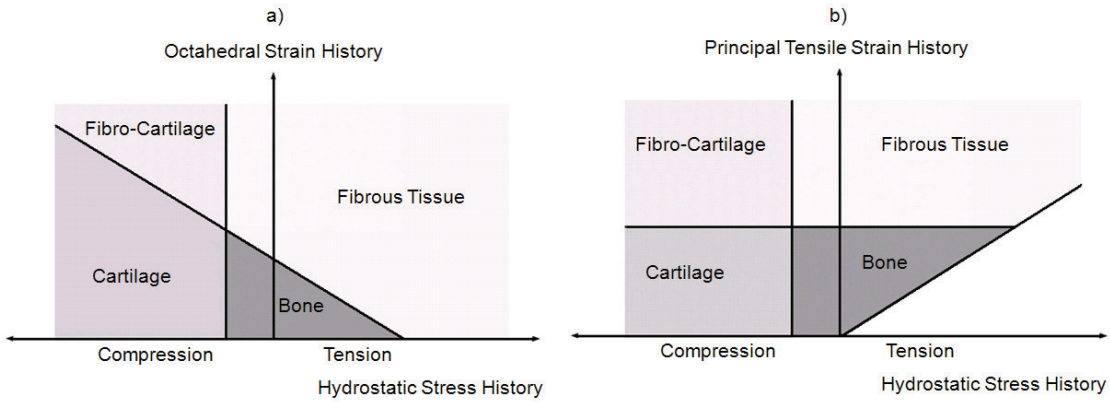

Fig 2.7. Concept of mechanoregulation of tissue differentiation proposed by Carter (Carter and Beaupré 2001). Tissue differentiation is governed by a) hydrostatic stress history and octahedral strain history, or b) hydrostatic stress history and principal tensile strain history.

Carter´s theories were tested using 2D plane stress linear elastic FE models of initial fracture varying axial and bending loads (Carter et al. 1988) and axisymmetric models (Carter et al. 1998a and Carter et al. 1998b). These FE analyses assumed homogeneity, isotropy and linear elasticity.

Claes and co-workers proposed that new bone formation in fracture healing mainly occurs along the edges of existing bone or calcified tissue and that the type of tissue formed depends on the local stress and strain magnitudes (Claes et al. 1998, Claes and Heigele 1999). Comparing their results of expected tissue type with cell culture experiments (Claes et al. 1998), they suggested that intramembranous bone formation occurs with strains lower than 5%. Compressive hydrostatic pressures greater than 0.15 MPa and strains smaller than 15% appeared to stimulate endochondral ossification. All other conditions apparently led to connective tissue or fibrous tissue (Fig 2.8).

Claes and co-workers used an axisymmetric FE model to calculate strains and stresses in callus. Connective tissues were described as hyperelastic and other tissues as linear elastic materials.

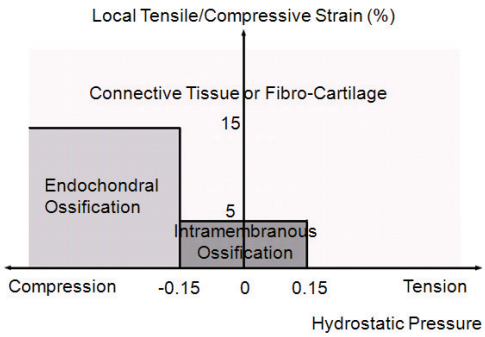

Fig 2.8. Concept of mechanoregulation of tissue differentiation proposed by Claes (Claes and Heigele 1999) Tissue differentiation is governed by hydrostatic pressure and local tensile/compressive strain.

Kuiper and co-workers developed a differentiation tissue theory using tissue shear strain and fluid shear stress as the mechanical stimuli regulating tissue differentiation and the strain energy as the mechanical stimulus regulating bone resorption (Kuiper et al. 1996, Kuiper et al. 2000a, Kuiper et al. 2000b) (Fig 2.9). They attempted to predict typical fracture healing patterns including callus growth. It was found that larger movements increased callus size and delayed bone healing.

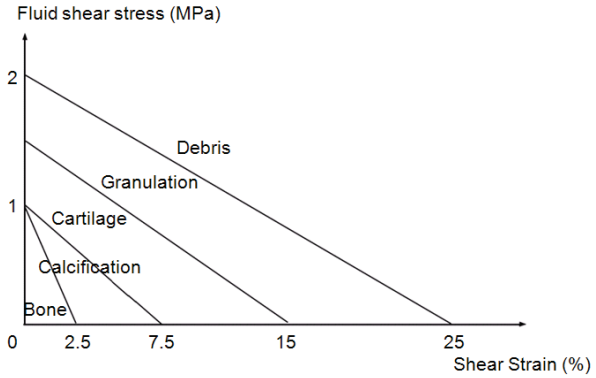

Fig 2.9. Concept of mechanoregulation of tissue differentiation proposed by Kuiper (Kuiper et al. 2000a). Tissue differentiation is governed by shear strain and fluid shear stress.

Kuiper and co-workers developed an axisymmetric FE model of a fracture applying the biphasic theory proposed by Mow et al. (1980). According to this theory, the material is considered to be a continuum mixture of a deformable solid phase and a fluid phase.

Based on studies of Prendergast and Huiskes (1996), Prendergast and co-workers proposed that the stress on cells is not only generated by the tissue matrix deformation but also by the drag forces of the interstitial fluid flow (Prendergast et al. 1997). They formulate the mechanoregulation index M as

$$M=\gamma/a + v/b$$

where γ is the octahedral shear strain, v is the interstitial fluid flow velocity, and a and b are empirical constants equal to 0.0375 and 3 µm/s respectively. If $M<1$ bone was differentiated, if $1<M<3$ cartilage was differentiated and if $M>3$ fibrous tissue was differentiated (Fig 2.10). They predicted tissue differentiation at implant/bone interfaces. Later on, Lacroix and co-workers use this concept to simulate tissue differentiation during fracture healing (Lacroix et al. 2002). A resorption field was added for low mechanical stimuli and the bone field region was divided into immature and mature woven bone to represent two mineralization stages of bone formation (Fig 2.10).

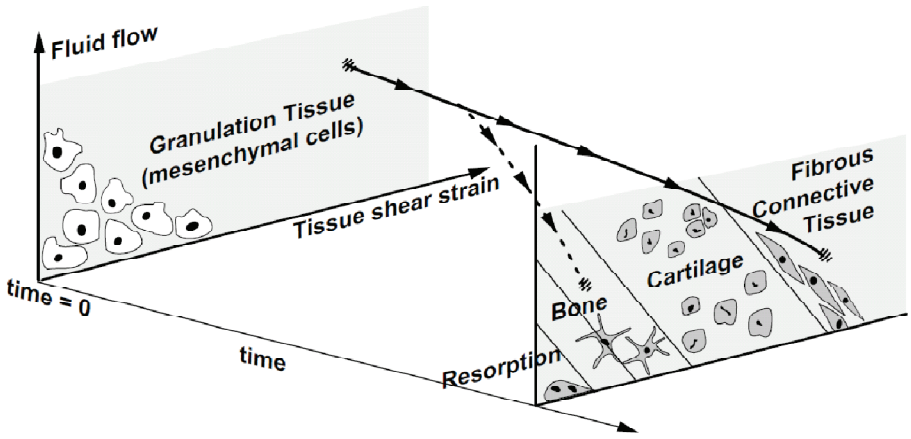

Fig 2.10. Concept of mechanoregulation proposed by Prendergast (Lacroix and Prendergast 2002). Tissue differentiation is governed by octahedral strain and relative fluid velocity.

Prendergast and co-workers as well as Lacroix and co-workers used the poroelastic formulation to simulate tissues. According to this formulation, developed by Biot (1941), tissue is considered as a porous elastic solid that is saturated by a pore fluid which flows relative to the deforming solid.

Prendergast and co-workers theory has been applied to study the time course of bone fracture healing (Lacroix and Prendergast 2002, Lacroix et al. 2002, Isaksson et al. 2006b) and to predict tissue differentiation at bone/implant interfaces (Liu and Neibur 2007), in bone chambers (Geris et al. 2004, Geris et al. 2008b, Khayyeri et al. 2009) and in scaffolds for bone tissue engineering (Kelly and Prendergast 2006, Byrne et al. 2007, Checa and Prendergast 2010, Khayyeri et al. 2010).

More recently, other theories have been developed. Ament and Hofer (2000) proposed a tissue regulation model based on a set of fuzzy logic rules derived from medical experiments, using the strain energy density as the mechanical stimulus that controls the process of cell differentiation. Bailon-Plaza and Van der Meulen (2001) studied the fracture healing process produced by growth factors. They used the finite differences method to simulate the sequential tissue regulation and the different cellular events, studying the evolution of the different cells that exists in the callus. Finally, Garcia and co-workers developed a continuum mathematical model that simulates the process of tissue regulation and callus growth, taking into account different cellular events (i.e., MSC migration and MSC, chondrocyte, fibroblast and osteoblast proliferation, differentiation and death), and matrix synthesis, degradation, damage, calcification and remodeling over time (Garcia et al. 2002). They also analyzed the evolution of the main components that form the matrix of the different tissues (i.e., different collagen types, proteoglycans, mineral and water) to determine mechanical properties and permeability according to the tissue composition (Doblare et al. 2004).

2.3.3. The Role of Angiogenesis

Normal bone tissue function depends on adequate supply of oxygen through blood vessels. Small blood vessels consist only of ECs while larger vessels are surrounded by mural cells (pericytes in medium-sized and smooth muscle cells in large vessels). Angiogenic sprouting is one of the mechanisms of blood vessel formation in the adult which consists in the formation of new blood vessels by the extensions of the existing vascular system (Carmeliet 2000) (Fig 2.11).

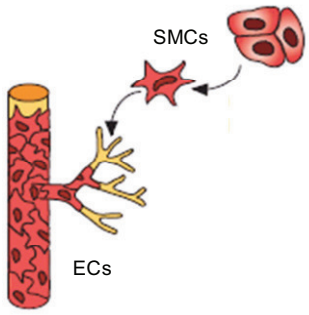

Fig 2.11. Schematic representation of angiogenic sprouting process (Carmeliet 2003)

The VEGF acts as modulator of angiogenesis. It is released by ECs, osteoblasts, patelet α-granules in the early stage of bone repair, and hypertrophic chondrocytes. VEGF activates receptors of ECs present in pre-existing blood vessels. Then, the activated ECs begin to release enzymes that degrade the basement membrane allowing extravasation of plasma proteins that lay down a provisional scaffold for ECs that migrate from the original (parent) vessel walls. ECs migrate in tandem, using adhesion molecules called integrins. Then they proliferate and form solid sprouts. These sprouts then form loops to become a developed vessel lumen. Angiogenic sprouting is different from splitting angiogenesis, because it forms entirely new vessels as opposed to splitting existing vessels. Sprouting occurs at a rate of several mm per day, and enables new vessels to grow across gaps in the vasculature.

In order to account for the role of angiogenesis during tissue differentiation, Checa and Prendergast (2009), proposed a mechanobiological model to simulate capillary network formation and its effect on tissue differentiation in a bone/implant interface. Using a lattice modeling approach, this model includes individual cell processes like proliferation, migration, differentiation and apoptosis. Briefly, vessels are formed by a sequence of ECs. Vessels growth direction, growth length and branching are defined as probabilistic functions based on the mechanical stimuli and on the presence of atrophied chondrocytes, which are supposed to release VEGF. MSCs can differentiate into osteoblasts, chondrocytes of fibroblasts based on the mechanoregulation concept

of Prendergast et al. (1997). When the mechano-regulatory stimulus corresponds to osteoblast differentiation, oxygen is accounted for; if an EC is closer than 100 μm, the MSC differentiate into osteoblast; otherwise, the MSC differentiate into chondrocyte. This model successfully predicts many features of angiogenesis and the tissue differentiation process observed during experimental studies (Checa and Prendergast 2009).

Another model that studies the effect of angiogenesis in tissue differentiation was developed by Geris and co-workers (Geris et al. 2008a). In this mathematical model, which is based on the concept of Bailon-Plaza and Van der Meulen (2001), fracture healing is described in 2D using a continuum system of diffusion equations, representing the spatiotemporal evolution of concentrations or densities of several cell types, extracellular matrix types and growth factors. Later on, Geris and co-workers included the effect of mechanical stimuli in their model (Geris et al. 2010).

2.4. COMPUTATIONAL STUDIES OF SCAFFOLDS FOR TISSUE ENGINEERING

FE models can contribute to the development of scaffolds for tissue engineering through the study of the stresses and strains distributions within the scaffold walls as well as the fluid flow within the interconnected pores. Because these stimuli distributions depend on the morphology of the scaffolds it is important to take into account their real architecture.

2.4.1. Characterization of Scaffolds using μCT Technique

μCT imaging is a non destructive and non invasive technique that allows a 3D reconstruction of the scaffold architecture (van Lenthe et al. 2007). The scaffold porosity, surface area, pore size, pore interconnectivity, pore distribution and wall thickness can be studied using this technique (Lin et al. 2003, Hiu-Yan et al. 2005, Filmon et al. 2002). Additionally, using μCT images, it is possible to follow tissue mineralization within the scaffolds cultured *in vitro* (Porter et al. 2007) or implanted *in vivo* (Jones et al. 2007).

Increasing the porosity and interconnectivity of the scaffold, the accessibility of the fluid flow and hence the accessibility of cells, nutrients and oxygen to the interior of the scaffold increased; however, the mechanical stability of the construct under

compressive loads decreased. FE models based on μCT have been used for the design of scaffold in order to optimize the relation between stiffness and porosity. For instance, Jaecques et al. (2004) presented an algorithm to develop appropriate scaffolds for bone regeneration in terms of mechanical properties of the material and its architecture. Van Cleynenbreugel et al. (2006) performed a study to quantify and evaluate some structural and biomechanical properties of different materials potentially suitable for being used as scaffolds.

2.4.2. Studies of Mechanical Stimuli

The specific mechanical stimuli at each specific point of the material have been studied using μCT based FE models. The effect of compressive loading in a macroporous CaP cement and in a porous glass ceramic scaffold (30% of porosity) was studied by Lacroix et al. (2006). Similar strain distributions under strain controlled loading were predicted for both materials; however, under load controlled loading the stress distribution varied between them. Parts of the scaffold underwent higher strains than others, suggesting that cell differentiation should be different from one part to another (Fig 2.12).

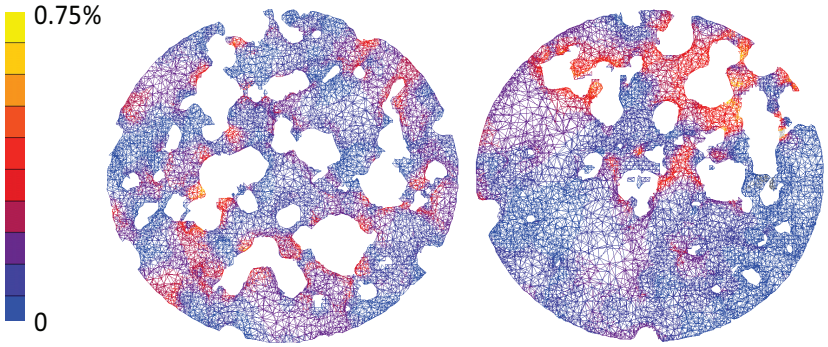

Fig 2.12. Octahedral shear strain distribution within two scaffolds studied by Lacroix and co-workers (modified from Lacroix et al. 2006). The strain distribution throughout the section is rather inhomogeneous.

Charles-Harris and co-workers determined the strain distribution within a section of a polylactic acid-glass scaffold for an applied compressive strain of 5%. Most of the scaffold underwent about 5% of strain though some pores were submitted to 15% of strain (Charles-Harris et al. 2007). Concentration of high strain values were predicted on the corner of the pores and on the thin walls.

Stops and co-workers performed a study of a collagen-glycosaminoglycan scaffold applying 1% of compressive unaxial strain (Stops et al. 2010a). Strains following a Gaussian distribution with mean value consistent to the applied strain were predicted. The maximum value of strain was about 30%.

Porter and co-workers computed the fluid shear stress on the material walls of a perfused trabecular bone scaffold using the Lattice–Boltzmann method (Porter et al. 2005). They predicted that flow through the microstructure of the scaffold was highly non-uniform. The highest values for local shear stresses were found on the surfaces of small channels in the scaffold (Fig. 2.13). Furthermore, comparing their *in silico* and *in vitro* results (Cartmell et al. 2003), shear stresses around $5x10^{-2}$ mPa were correlated with increases of cell proliferation, although an order of magnitude higher was required to obtain gene expression in osteoblasts adhered on scaffolds. Additionally, peaks of shear stresses of 57 mPa were associated with cell death within the scaffolds.

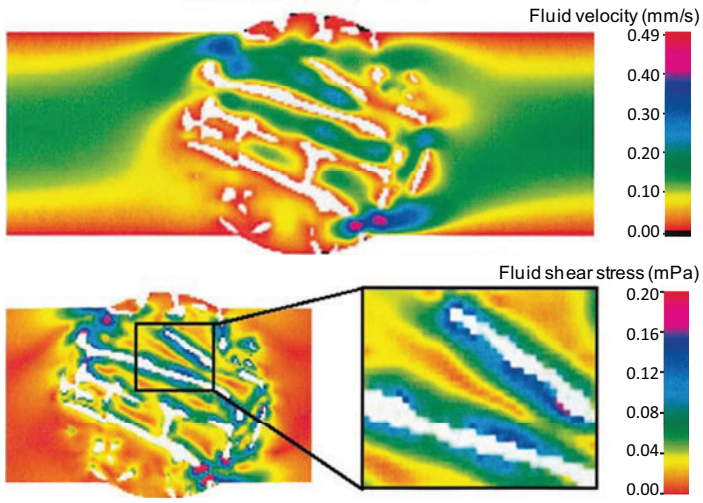

Fig 2.13. Velocity flow and local shear stress fields through a transversely perfused cylindrical trabecular bone scaffold computed by Porter et al. (2005). Flow through the scaffold was highly non-uniform.

Another perfusion fluid analysis was performed by Cioffi et al. (2006). Mean shear stress of 3.48 mPa was predicted when an inlet velocity of 53 μm/s was applied to a biodegradable polyestherurethane scaffold (77% of porosity). Maes and co-workers performed an analysis of fluid flow within two different scaffolds, one of titanium (77% of porosity) and the other of hydroxyapatite (73% of porosity). Square sections of 1 mm^3 were modeled applying a flow rate of 0.04 mL/min perfused through a 5 mm diameter scaffold corresponding to an inlet velocity of about 34 μm/s. Average wall shear stresses of 1.4 mPa and 1.1 mPa for the titanium and the hydroxyapatite scaffolds respectively were computed (Maes et al. 2009).

A polylactic acid-glass composite scaffold with a high porosity (95% of porosity) was studied by Milan et al. (2009) under two different mechanical conditions, a perfusion fluid flow and a dynamic compression. In the perfusion fluid flow simulation, the fluid achieved all the interconnected pores of the scaffold. The velocity increased 7.8 times the magnitude of the inlet fluid velocity in the center of the scaffold. The pressure drop between the inlet and the outlet side of the flow was uniform. In the compressive strain simulations, a heterogeneous strain distribution was predicted. Most of the

scaffold walls were only displaced without being significantly deformed, since strains of 400 times the magnitude of the total strain applied were predicted in some walls suggesting local material damage.

The comparison of the results between these scaffolds of different material and porosity show the effect of the morphology on the distribution of mechanical stimuli within the scaffold walls and pores which are the stimuli effectively transmitted to the cells.

2.4.3. Simulation of Tissue Differentiation

Studies using the mechanoregulation theory of Prendergast et al. (1997) have predicted tissue differentiation within scaffolds for tissue engineering. Kelly and Prendergast investigated the effect of mechanical loading on osteochondral defect healing (Kelly and Prendergast 2006) and the benefits of implanting a scaffold at the defect site (Kelly and Prendergast 2005). They predicted that increasing the stiffness of the scaffold up to 10 MPa, the amount of cartilage formation was increased and the amount of fibrous tissue formation in the defect was reduced, however when increasing the stiffness above this value the amount of cartilage formed was reduced. Reducing the permeability of the scaffold was also predicted to be beneficial for cartilage formation. Additionally, they demonstrated that the implantation of a scaffold at the defect site can significantly improve the healing of the defect. Kelly and Prendergast used diffusion equations to simulate the different cellular events, assuming that cells achieve a homogeneous distribution within the regenerating region.

The lattice concept was introduced in mechanobiological models in order to include the individual and random behavior of cells (Perez and Prendergast 2007). This concept was applied in tissue engineering by Byrne et al. (2007) to predict cell differentiation within a simplified scaffold subjected to compressive load (Fig. 2.14). Byrne and co-workers investigated the effect of important design properties, such as scaffold porosity, degradation rate and scaffold mechanical properties, on the tissue formation process inside a regular structured bone scaffold. In this study, they were able to identify optimal scaffold properties that would lead to the highest amount of bone formation. They showed that the rate of dissolution can either have a positive or negative effect on the amount of bone formation depending on the initial porosity and mechanical strength of the biomaterial. Dissolution of the scaffold increases the porous volume available for bone formation; however, it can also compromise the

structural integrity of the scaffold due to a reduction in stiffness and strength. These investigations assumed a well vascularized scaffold, with no limitations of oxygen and nutrient supply to the cells.

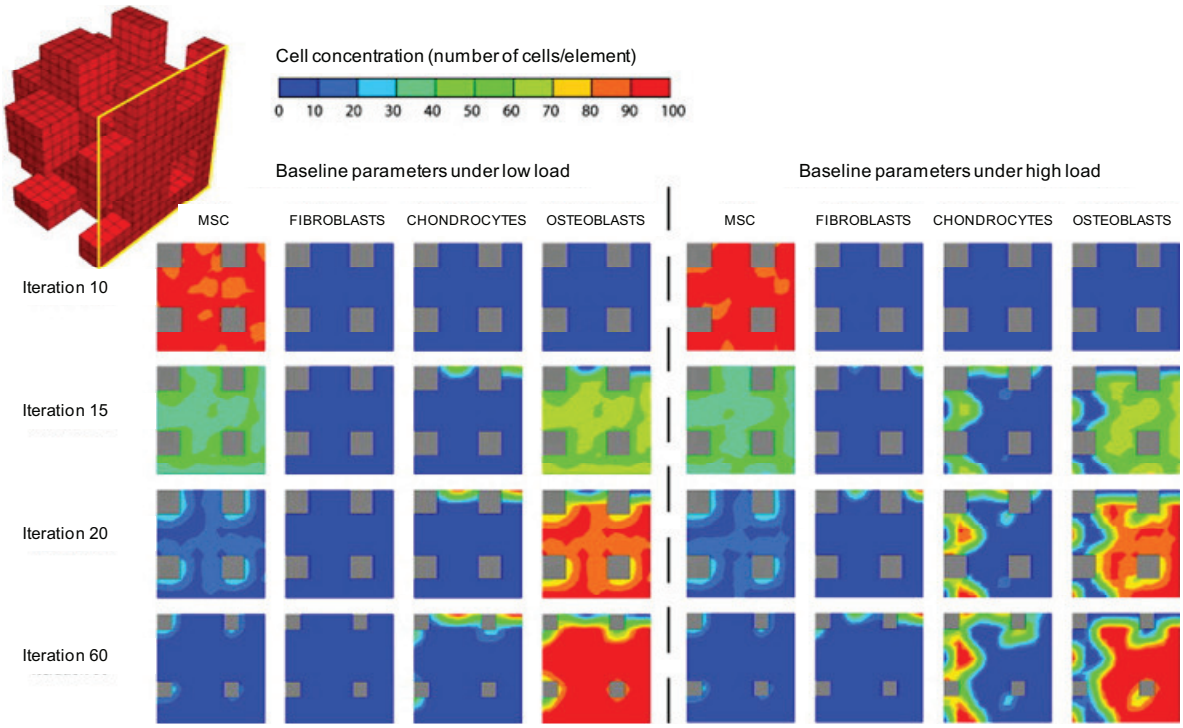

Fig. 2.14. Cell distribution in a simplified scaffold predicted by Byrne et al. (2007)

The concept of Prendergast et al. (1997) was also used by Stops et al. (2010b) to predict cell differentiation within a collagen-glycosaminoglycan scaffold subjected to mechanical strain and perfusion flow (Fig. 2.15). They used a Newtonian fluid formulation to compute fluid velocity. The mean velocity around the cells was accounted to compute the mechano-regulatory stimuli. They demonstrated that specific combinations of strains and inlet fluid flow cause dominant differentiation lineages. For instance, under 1% of strain and 1 μm/s of inlet fluid velocity most of cells differentiated into osteoblasts, while under 5% of strain and 1 μm/s of inlet fluid velocity most of cells differentiated into chondrocytes. Increasing fluid velocity increased the differentiation of fibroblasts.

Milan and co-workers predicted cell differentiation within a polylactic acid-glass composite scaffold for different rates and magnitudes of compressive load (Milan et al. 2010). They demonstrated that totally different distributions of tissue can be obtained according to the level and frequency of the applied load. Dynamic compressions of 0.5-1% at 0.0025-0.005 s^{-1} favored homogeneous mature bone tissue formation (Fig 2.15).

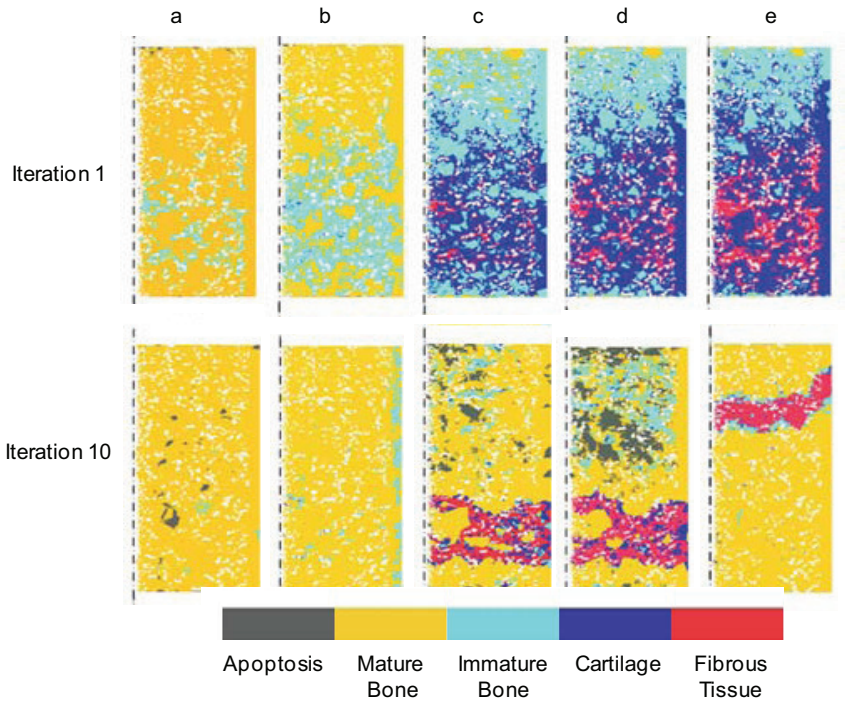

a 0.5% of compression at a strain rate of 0.0025 s−1
b 1% of compression at a strain rate of 0.005 s−1
c 5% of compression at a strain rate of 0.025 s−1
d 5% of compression at a strain rate of 0.005 s−1
e Ramp of force from 1 to 70 N at rates from 0.5 to 35Ns−1

Fig. 2.15. Tissue differentiation simulated by Milan et al. (2010) within a polylactic-acid-glass composite scaffold using different loading cases.

2.4.4. Simulation of Tissue Differentiation and Angiogenesis

The angiogenesis model of Checa and Prendergast (2009) was applied to a simplified scaffold for bone tissue engineering (Checa and Prendergast 2010), relating the number of cells initially seeded into the scaffold to the rate of vascularization and the penetration of the vascular network. The effect of the mechanical load magnitude applied to the scaffold on bone formation and capillary growth was also studied (Fig 2.16). They showed that the initial cell seeding conditions had a significant effect on the vascularization of the scaffold. A high number of cells initially seeded in the scaffold, resulted in limited penetration of the vascular network and peripheral formation of bone.

Khayyeri and co-workers applied also the angiogenesis model of Checa and Prendergast (2009) to simulate tissue differentiation in a collagen GAG scaffold implanted within a bone chamber (Khayyeri et al. 2010). They investigated the effect of the scaffold stiffness and determine that higher stiffness, holding pore structure constant, enhances bone formation.

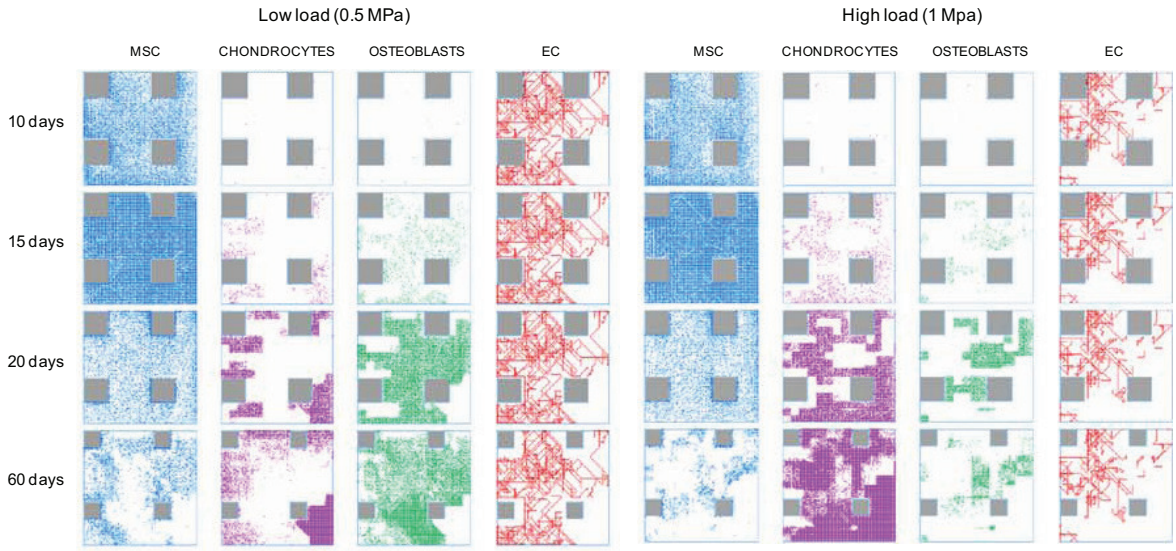

Fig. 2.16. Tissue differentiation and angiogenesis within a simplified scaffold simulated by Checa et al. (2010) using different loading cases. Case of uniform cell seeding density is shown.

2.4.5. Other Simulations

Some other remodeling theories have been proposed to mimic bone growth within scaffolds implanted *in vivo*. Adachi and co-workers proposed a method for the design of porous scaffold microstructure by three dimensional computational simulation of bone tissue regeneration (Adachi et al. 2006). According to this method the rate of scaffold degradation is assumed to be proportional to the water content diffused from the surface to the bulk material. The new bone formation on both bone and scaffold surfaces is driven by the rate between trabecular surface remodeling and mechanical stimulation. Using the voxel FE method, these two phenomena were solved at the same time frame, predicting bone regeneration in the bone scaffold system.

Sanz-Herrera and co-workers proposed a method using the asymptotic homogenization theory to evaluate the effective behavior of porous scaffolds in terms of mechanical properties and permeability (Sanz-Herrera et al. 2009). Bone growth into the scaffolds was estimated considering a macroscopic effective stress and the mechanoregulation stimulus.

2.5. CONCLUSION

The principal concepts that predict tissue differentiation and angiogenesis in the process of bone regeneration were summarized. State of the art of *in silico* studies of

the mechanical stimuli distribution and the mechanoregulation of tissue differentiation within scaffolds was presented. μCT based FE models have demonstrated that the micro-mechanical stimuli within scaffolds can be different than the mechanical stimuli applied to the scaffold showing the importance of modeling the real architecture of the scaffolds. Using the mechanoregulation concept of Prendergast and co-workers (1997) to study the mechanoregulation of tissue differentiation, optimal scaffold design properties have been determined.

CHAPTER 3
Scaffold Reconstruction

3.1. INTRODUCTION

The aim of biomaterial scaffolds is to serve as a support structure for cells so that they can proliferate and differentiate. Therefore, from a morphological point of view, (1) the scaffolds should have sufficient surface area in order to give the cells enough space to proliferate and generate new tissue, (2) the pores should be well interconnected in order to allow the flow of culture medium with cells, nutrients and oxygen to achieve all regions of the scaffold and (3) the scaffold should support mechanical loads and translate them into appropriate mechanical stimuli so that cells can follow a specific differentiation pathway (Lanza et al. 2000, Ratner et al. 2004).

CaP scaffolds do not have a regular structure because of the hand made process of fabrication. Since cells are attached to the scaffold surfaces and the stimuli transmitted to them are related to the scaffold morphology, a computational reconstruction that represents the real architecture of the construct is required in order to determine the specific mechanical stimuli at each point of the structure. The 3D computational reconstruction of the real architecture of the CaP scaffolds can be obtained from μCT images. Using this technique, high resolution transversal images of the scaffolds are obtained and then superimposed to give a 3D reconstruction.

Meshes for FE models can be built from the 3D computational reconstructions of the scaffolds. The most used method to obtain FE meshes from μCT images is the voxel method that consists on obtaining hexahedral elements from the voxels (Van

Rietbergen et al. 1996 Viceconti et al. 2004); these meshes can be smoothed to represent better irregular geometries using the marching cube method. Nevertheless, an irregular geometry, as in the CaP scaffolds case, is better represented by triangles or tetrahedrons than by squares or cubes since a less number of elements and nodes are necessary to obtain the same surface accuracy. Commercial software can be used to obtain not only the computational reconstruction from the μCT images but also to develop the tetrahedral FE meshes.

The main objective of this chapter is to obtain a computational reconstruction of a CaP scaffold using the software Mimics (Materialise, Belgium), in order to:

1) Analyze the most important structural properties i.e. porosity, pore size distribution, pore interconnectivity and specific surface area.

2) Build tetrahedral-element meshes of the solid and the pore phase that represent the real architecture of the scaffold for FE studies.

3.2. MATERIALS AND METHODS

3.2.1. Materials

Scaffolds of 6 mm diameter and 12 mm height of two biodegradable and porous materials: (1) cement based on CaP and (2) glass ceramic type Na_2O-CaO-P_2O_5-TiO_2, were used. These scaffolds were elaborated by the biomaterials group at the UPC.

For the preparation of the CaP cement scaffolds, on the one hand a mix of $CaHPO_4$ and $CaCO_3$ is heated at 1400°C, after it is quickly cooled in air, and then it is grounded until obtaining a powder of average grain size 6.21 μm. Then 2% in weight of rushed hydroxyapatite is added. On the other hand powder of albumen is dissolved in water generating a solution of 12% in weight. This solution is mixed to form a foam. Finally, the CaP powder is diluted in distilled water (0.35 mL/g) and it is mixed with the foam of albumen. This mix is introduced in moulds of Teflon that are immersed in a solution of Ringer at 37 °C during 7 days (Almirall et al. 2004).

For the preparation of the glass ceramic scaffolds, particles of glass type Na_2O–CaO–P_2O_5–TiO_2 are grounded until obtaining a grain size that varies between 0.1 and 100 μm. Next this powder is mixed homogeneously with foamed egg white. This mix is introduced in moulds of Teflon and heated to remove the egg white and sintering the glass particles (Avila et al. 2005).

3.2.2. Micro Computer Tomography

One scaffold of each material was scanned using a µCT X-Tek HMX225 (Digisens) with a resolution of 7.8 µm x 7.8 µm x 12.2 µm. 501 images of each scaffold were obtained (Fig 3.1)

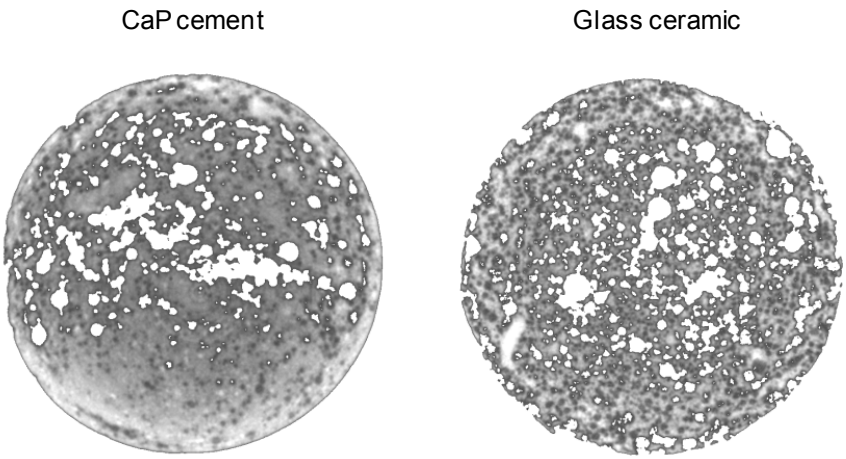

Fig 3.1. µCT images of the CaP cement and glass ceramic scaffolds. 6 mm diameter.

3.2.3. 3D Reconstructions.

Using the program Mimics (Materialise Software, Belgium), the µCT images were superimposed and the 3D geometries of the scaffolds were reconstructed (Fig 3.2).

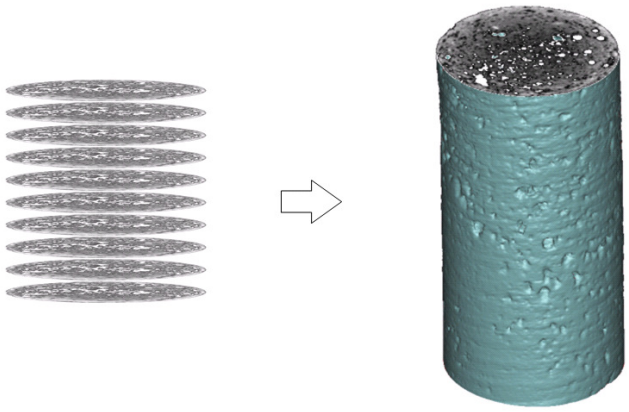

Fig 3.2. Schematic representation of scaffold 3D reconstruction µCT images

In the studied materials, grey pixels corresponded to the solid phase, and white pixels corresponded to the pores. In Mimics pixels can be grouped by tones of grey, the 3D sets of pixels are called masks. Two masks were initially generated, one for the solid material phase and another for the pores (Fig 3.3).

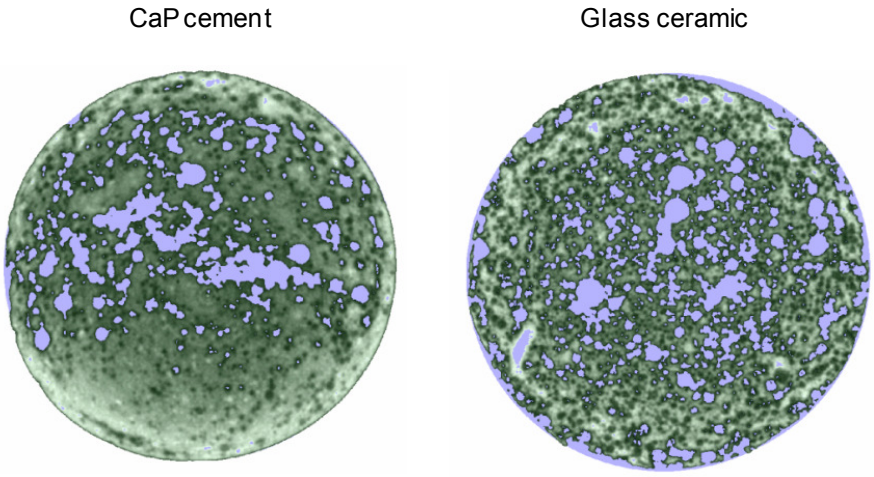

Fig 3.3. Masks built to separate the scaffold phases. Solid phase in green and pores in blue. 6 mm diameter.

Then two new masks were built in order to separate closed or non interconnected from interconnected pores. In order to do that, first the connected region of the initial pore mask was selected, forming the interconnected pore mask; second the interconnected pore mask was subtracted from the pore mask, the resulting mask corresponds to the closed pores.

3.2.4. Structural Characterization

The porosity Φ was computed as the volume percentage of the pore volume over the scaffold apparent volume.

$$\phi = \frac{\text{Pore volume}}{\text{Aparent volume}} \times 100\ \%$$

The interconnectivity I was computed as the volume percentage of the interconnected pore volume over the scaffold apparent volume.

$$\text{I} = \frac{\text{Interconnected pore volume}}{\text{Aparent volume}} \times 100\ \%$$

The specific surface area SA was computed as the ratio between the pore surface area and the scaffold apparent volume.

$$\text{SA} = \frac{\text{Surface area}}{\text{Aparent volume}}$$

The pore shape and the pore size distribution were visually investigated since in Mimics (Materialise Software, Belgium) there is not a developed tool to quantify them.

3.2.5. Meshing

Surface meshes of triangles that enclose the masks can be built in Mimics (Materialise Software, Belgium). The quality of these meshes, which in the scaffold case corresponds to its precision in representing the real surface of the material, is related to the total number of triangles. A higher number of triangles is translated into a higher precision but also into a higher computational cost. The mesh quality is controlled with the number of pixels accounted to build the surface mesh and the number of iterations carried out in the process of automatic meshing.

In order to determine the parameters to obtain an optimal surface mesh (best possible surface representation using a minimal possible number of triangles), surface meshes of the solid phase were performed using the three qualities predetermined by the program (low, medium and high). The total volume enclosed by each mesh was computed and compared to the total volume of the mask in order to quantify the error. The CaP cement scaffold was used.

Volume meshes of tetrahedral-elements built from the surface meshes can be built in Patran (MSC. Software, CA-USA). The meshes of the solid faces were made directly meshing the domains closed by the surface meshes. The meshes of the interconnected pores were made creating cylindrical surface meshes that surround the scaffold surface meshes (without touching them) and meshing the domains enclosed between the scaffold and the cylindrical surface meshes.

3.3. RESULTS

A total porosity of 18% was computed for the CaP cement scaffold, of which 16% corresponded to interconnected pores and 2% to closed pores. For the glass ceramic scaffold a total porosity of 23% was computed, corresponding to 21% of interconnected pores and 2% of closed pores. Specific surface areas of 4.87 mm^2/mm^3 and 6.85 mm^2/mm^3 were computed for the CaP cement and the glass ceramic, respectively (Table 3.1).

Table 3.1. Scaffold structural properties measured from µCT reconstructions

Property	CaP cement	Glass ceramic
Porosity	18 %	23 %
Interconnectivity	16 %	21 %
Specific Surface Area	4.87 mm^2/mm^3	6.85 mm^2/mm^3

The distribution of the pores and the pore interconnectivity throughout the scaffold was more uniform within the glass ceramic scaffold than within the CaP cement one. In the glass ceramic scaffold, interconnected pores were found through all the structure. On the contrary, regions without pores and regions with high concentration of closed pores were observed in the CaP cement scaffold (Fig 3.4).

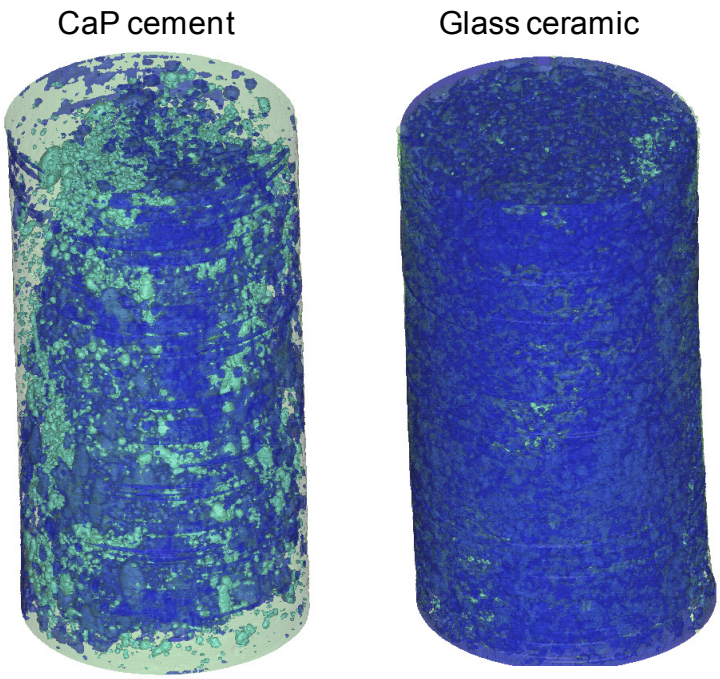

Fig 3.4. 3D reconstruction of the scaffolds. 6 mm diameter and 12 mm height.
Interconnected pores are shown in dark blue, closed pores in light blue and the solid phase in green.

The irregular distribution of the pores was confirmed studying transversal sections of the scaffolds. Extensive regions without pores were observed at the upper and lower extremes of the CaP cement scaffold, and the pores seemed to be concentrated at the center of the scaffold. There was not well interconnectivity between the pores and the exterior of the scaffold. In the glass ceramic scaffold, a large quantity of interconnected pores was observed throughout the whole structure (Fig 3.5).

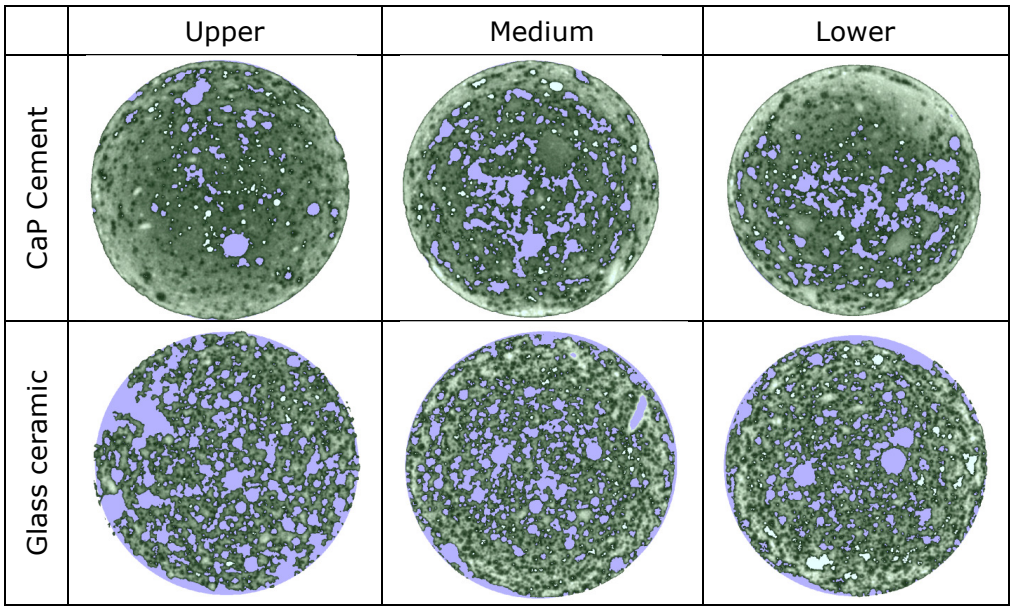

Fig 3.5. Pore distribution and interconnectivity observed through the scaffolds.
Interconnected pores are shown in blue, closed pores in white and the solid phase in green.

The pore shape seemed to be spherical when observing the transversal sections of both scaffolds; however, in the longitudinal sections stretched shapes were observed being more similar to ellipses that to spheres. The distribution of the pore size was not uniform in any case (Fig 3.6). In the CaP cement scaffold, significant variations on the pore size were observed from one region to another; larger pores were found in the lower than in the upper half of the scaffold. Due to the irregular pore size distribution, it is difficult to estimate visually an average pore size; pores between 15 μm and 1.37 mm of length approximately were observed. In the glass ceramic scaffold, pores between 22.5 μm and 2.33 mm of length were found; most pores had an approximated size between 184 and 533 μm (Fig 3.6).

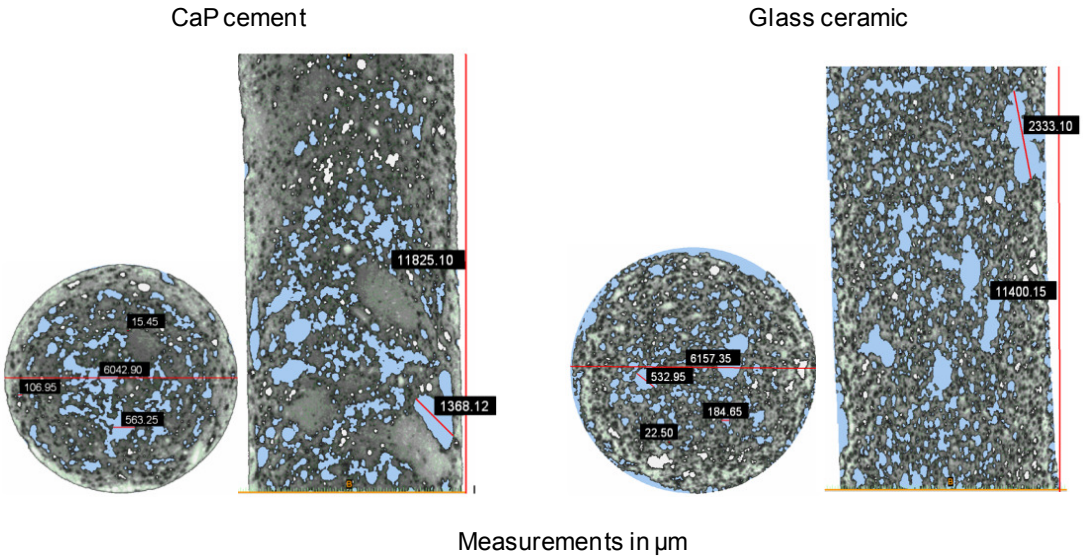

Fig 3.6. Pore size and form observed through the scaffolds.
Interconnected pores are shown in blue and close pores in white.

Generating surface meshes, when the total number of triangles was decreased, the mesh separated from the scaffold surface and the total volume within the mesh increases, information about small pores and thin walls as well as pore interconnectivity was lost (Fig 3.7). The higher quality mesh had more than three times the number of triangles than the medium quality mesh; nevertheless the difference in volume between them was only 3%. The medium quality mesh had 3.5 times the number of triangles than the low quality mesh with a difference of 7% in volume (Table 3.2).

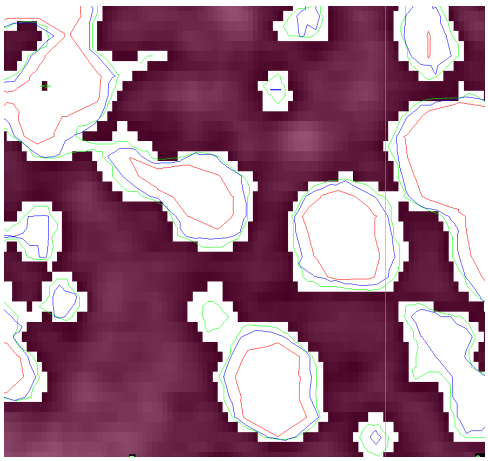

Fig 3.7. Comparison between surface mesh qualities. Outline of the meshes of the solid phase are shown in a transversal section of the CaP cement scaffold (high quality in green, medium in blue and low in red).

Table 3.2. Comparison between surface mesh qualities in terms of mesh size and % of error.

Mesh quality	**Number of triangles x 10^6**	**Volume (mm^3)**	**(Mesh vol-mask vol)/ mask volume**
Mask		278.45	0%
High	25.99	292.63	5.09 %
Medium	8.22	301.30	8.20 %
Low	2.32	321.33	15.40 %

Selecting the medium quality surface mesh, a volume mesh larger than 137 million tetrahedrons for the solid phase and 26 million for the fluid phase would be generated. Because computer resources were not sufficient to obtain meshes and to model the whole scaffolds, smaller samples of 1 mm diameter and 2 mm height were used for the FE models presented in next chapters. These samples were selected arbitrarily, close to the center of the scaffolds, trying to obtain sections where the pores were well interconnected (Fig 3.8). The section of the CaP cement scaffold had 32.9% of pore interconnectivity and the one of the glass ceramic scaffold had 27.5%.

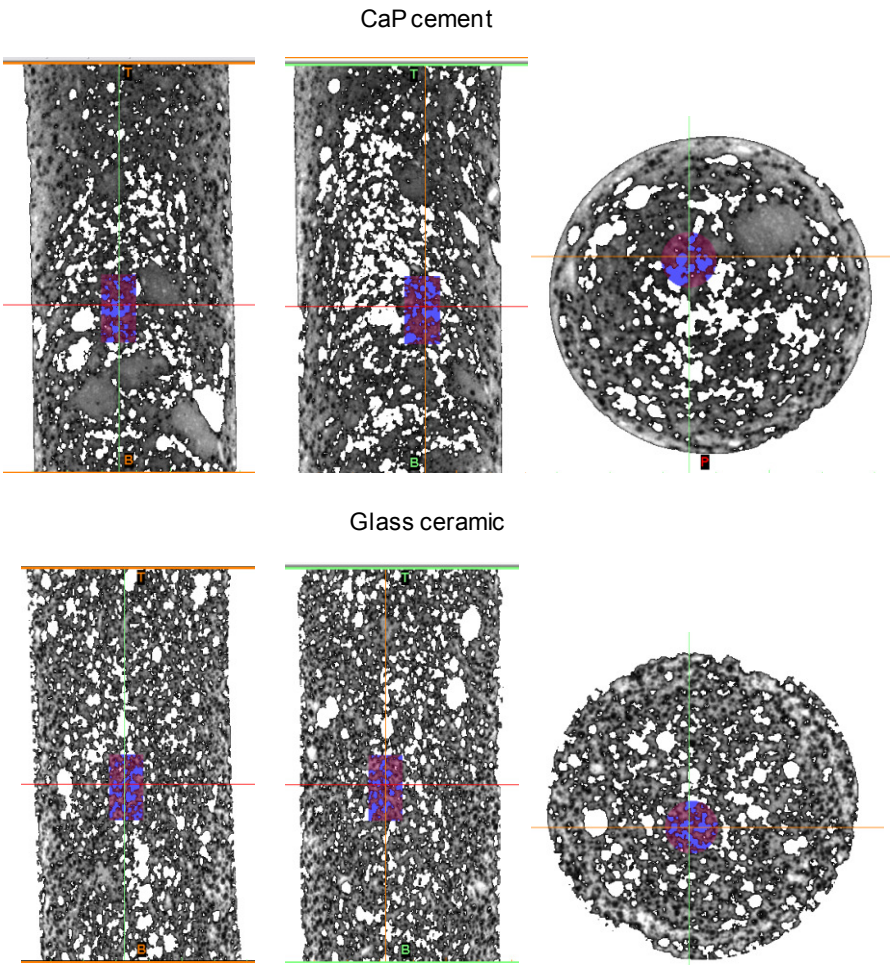

Fig 3.8. Reduced sections of the scaffolds used to build the meshes for the FE models.

Meshes for the solid and the fluid phase for the reduced samples were built in Patran (MSC software, CA-USA). The meshes of the fluid phase were made using external cylinders, top and bottom sides of these cylinders represented the tubes of a perfusion chamber when the scaffold is subjected to perfusion fluid flow. The lateral elements were deleted by hand in Mentat (MSC software, CA-USA) (Table 3.3, Fig 3.9).

Table 3.3. Number of tetrahedral elements of the reduced section FE meshes.

Material	**Solid tetrahedrons x10^3**	**Fluid tetrahedrons x10^3**
CaP cement	636.18	174.71
Glass ceramic	711.35	124.10

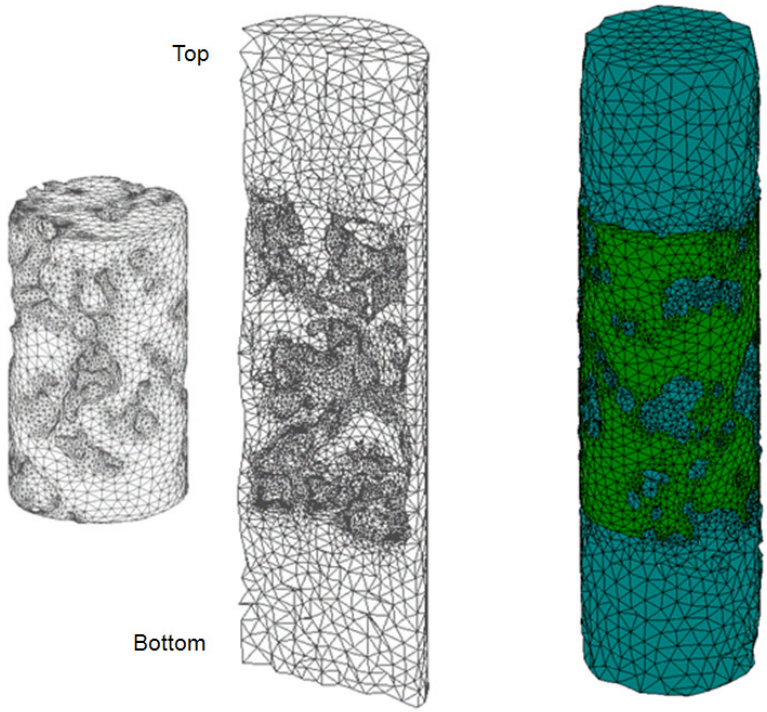

Fig 3.9. Tetrahedral element meshes for the CaP cement scaffold. The solid phase is shown in green and fluid phase in blue.

3.4. DISCUSSION

Computational reconstructions allowed calculating the porosity, the pore interconnectivity, and specific surface area of the scaffolds in addition to examine the distribution, the interconnectivity and the shape of the pores within the scaffold in a non destructive manner. The computed macroporosity of the scaffolds were 18% for the CaP cement and 23% for the glass ceramic. Since the resolution of μCT was 7.8 x 7.8 x 12.2 μm^3, pores smaller than these dimensions cannot be detected; however, taking into account that the main objective of this thesis is to simulate tissue differentiation and that the mean size of a MSCs cell is 10 μm and the minimum pore diameter required for osteoinduction is 100 μm (Karageorgiou and Kaplan 2005), the porosity error generated by non detected closed pores does not affect the prediction of tissue differentiation.

The specific surface areas computed were 4.87 mm^2/mm^3 for the CaP cement scaffold and 6.85 mm^2/mm^3 for the glass ceramic scaffold. These values were similar to values found by Van Cleynenbreugel and co-workers (2006) for scaffolds of hydroxyapatite (7.02 mm^2/mm^3) and titanium (4.25 mm^2/mm^3). However the specific surface area of

trabecular bone varies between 13.12 and 23.73 mm^2/mm^3 (Hildebrand et al. 1999). This suggests that the values computed for the scaffolds can be too low for cell adhesion, proliferation and differentiation.

Carrying out a visual evaluation of the pores within the scaffold it was possible to capture differences that were not captured only measuring the porosity. For instance, the difference between the computed CaP cement and glass ceramic porosities was only 2%; however, there was a significant difference in the pore distribution within these scaffolds. In the glass ceramic scaffold, pores were homogeneously distributed within the whole scaffold, as opposed to the CaP cement scaffold, where both large areas without porosity and regions with large pores were observed.

From a morphological point of view, the glass ceramic scaffold seemed to be more appropriate than the CaP cement scaffold for tissue engineering, because it had higher porosity, interconnectivity and specific surface area than the CaP cement scaffold. The flow of medium could be more homogeneous and hence cells, oxygen and nutrients could result better distributed within the scaffold, additionally there was more space for cells to seed, migrate, proliferate and synthesize new tissue.

Different quality surface meshes that simulate the real morphology of the scaffolds were obtained. Because the difference in volume between the high and the medium quality meshes was only 3% respect to the mask volume, and three times the number of elements was needed to build a high quality mesh than a medium quality mesh, the medium quality meshes were used to build volume meshes. Meshes generated in low quality are not recommended since information about small pores and pore interconnectivity can be lost.

The main difficulty when building the meshes of tetrahedral elements were the cross triangles and free edges generated on the thin walls. These mistakes in the automatic meshing process had to be fixed manually. However, despite of the tedious process of fixing the meshes, the obtained meshes of tetrahedral element represent better amorphous structures than hexahedral element meshes using a smaller number of elements and nodes.

Computer limitations still hinder the use of automatic and large sample mesh analysis and this is certainly a challenge in the future (Viceconti et al. 2004). Computer resources are not sufficient to obtain meshes of the whole scaffolds, so smaller samples of material were used for the models. The studied volume corresponded to $1/6^3$ th of the total scaffold volume; therefore meshes larger than 137 million elements for the solid models and 26 million elements for fluid models would have been

necessary to analyze the complete scaffold, assuming constant number of elements per unit of volume through the scaffolds. Moreover only one sample of each material was modeled. In spite of these limitations, the sections modeled are sufficient to observe the relation between the distribution of the mechanical state and the architecture of the studied scaffolds.

The possibility of generating FE models that simulate the real morphology of the scaffolds, allows analyzing its mechanical properties in addition to determine the specific mechanical stimuli that cells would perceive in each point of the material. Given that the μCT method does not destroy the scaffolds, comparison of results obtained in *in vivo* or *in vitro* studies with computations obtained in *in silico* studies using specific samples can be possible.

3.5. CONCLUSION

3D computational reconstructions using μCT images, allow examining carefully the internal structure of the scaffolds. Information of the total porosity, the pore interconnectivity, the pore size, the pore distribution within the material, and the specific surface area was obtained by a non destructive manner. This information can contribute to the biomaterials development for tissue engineering, where the structural and mechanical properties are of great importance.

CHAPTER 4
Micro FE Study of a Tissue Engineering Scaffold

4.1. INTRODUCTION

Mechanical loads are applied to scaffolds in order to transmit mechanical stimuli to the cells attached to the surface walls. When compressive loads are applied, stress and strain are generated on the scaffold solid phase. When a perfusion fluid is applied, the fluid medium flows through the interconnected pores generating hydrostatic pressure and fluid shear stress at the material surface. The distribution of these mechanical stimuli depends on the morphology of the scaffolds.

The main goal of this chapter is to build μCT based FE models of CaP cement and glass ceramic scaffolds in order to achieve detailed information of

1) the stress and strain in the solid phase caused by a compression load, and

2) the interstitial fluid velocity, pressure and surface shear stress within the pores at the initial stage of a bioreactor cell culture.

It is hypothesized that the non uniformity of the scaffolds architecture creates areas with high strain, stress and fluid flow distribution relevant to explain the influence of mechanical stimuli on cells at a microscopic level. Separated model were developed. Linear elastic solid formulation was used to model the compressive load and

Newtonian fluid formulation to model the perfusion fluid flow. Because tissues formed within scaffolds have been simulated as poroelastic materials, in addition to the models described above, a poroelastic formulation was used to model the perfusion fluid flow in order to compare results with the Newtonian fluid formulation.

4.2. SOLID MODEL

4.2.1. Model Definition

For the simulation of an unconfined compressive load, a constant displacement equivalent to an uniaxial strain of 0.5% was applied on the nodes of the upper side of the meshes fixing the nodes of the lower side (Fig 4.1). Linear isotropic materials were used due to the linear elastic behavior of the materials for this strain level (Lacroix et al. 2006), see Table 4.1. Major principal stress, major principal strain and octahedral shear strain were computed. Meshes of the solid phase built in Chapter 3 were used. FE models were developed in Marc–Mentat (MSC Software, CA-USA). The analyses were solved using MSC Marc 2005. For constitutive equations see Appendix A.

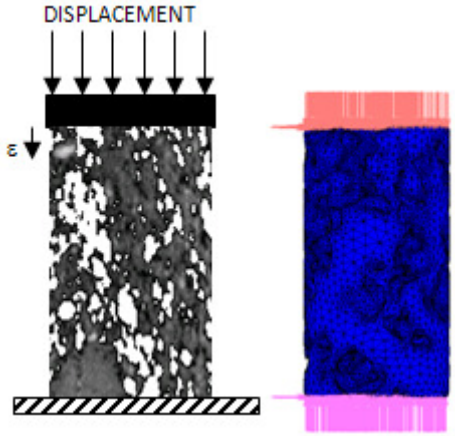

Fig 4.1. Compressive strain model definition. Boundary conditions and FE mesh.

Table 4.1. Material properties used in the compressive load FE model

Sample	Young's modulus (MPa)	Poisson's ratio
CaP cement	147	0.3
Glass ceramic	455	0.3

4.2.2. Results

The distributions of major principal stress were similar to the distributions of major principal strain due to the isotropic properties of both materials CaP cement and glass ceramic (Fig 4.2). None of these stimuli distribution was homogeneous. There were more elements under compression (values of stress and strain lower than zero) than under tension (values of stress and strain higher than zero).

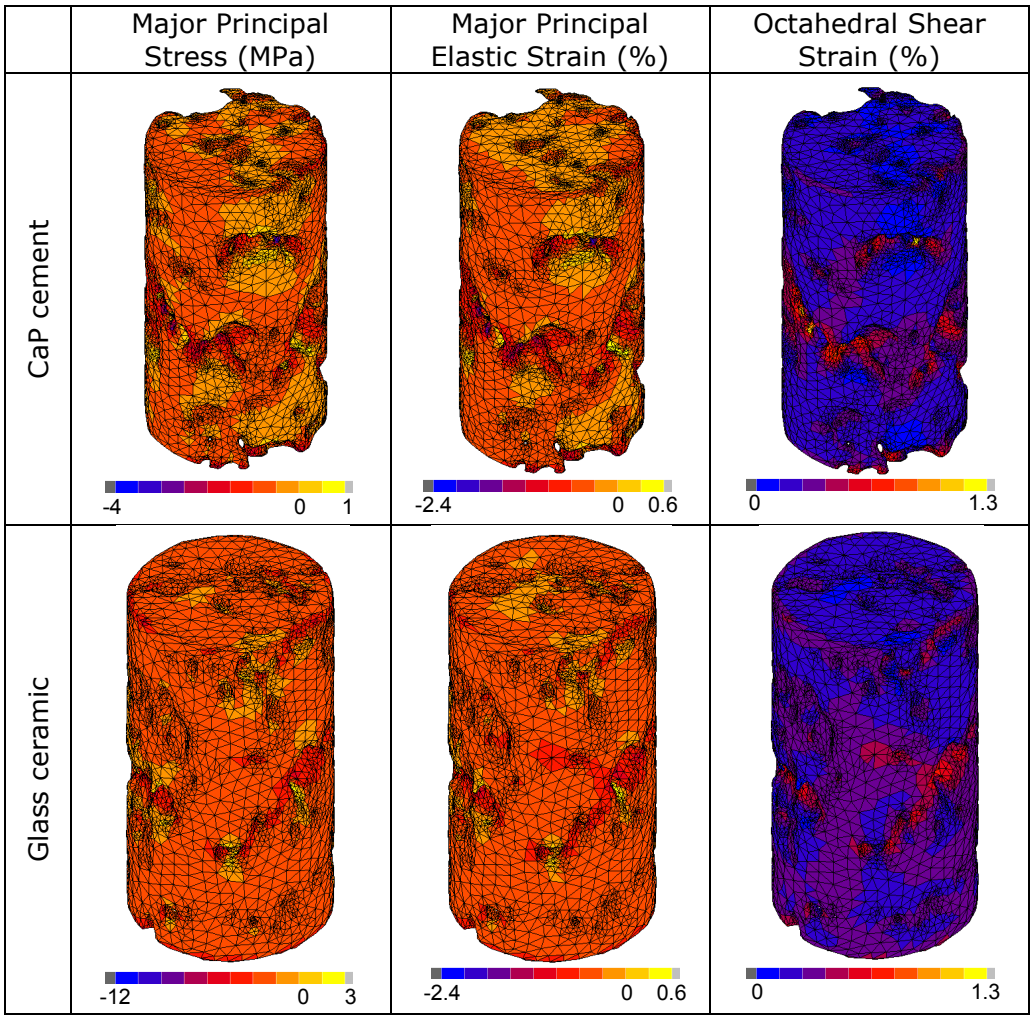

Fig 4.2. Stimuli distribution within the scaffold walls under compressive strain. Views of the scaffolds.

The maximal value of stimuli under compression (-4 and -12 MPa for CaP cement and glass ceramic respectively) were higher than maximal value of the stimuli under tension (1 and 3 MPa for CaP cement and glass ceramic respectively). The magnitude of the stress was in general three times higher for the glass ceramic than for the CaP cement, because of the higher Young's modulus of the material. The magnitude of the

major principal strain ranged between -2.4 and 0.6%. The magnitude of octahedral shear strain ranged between 0 and 1.3% for both materials (Fig 4.2).

The maximal values of tensile strain within the material matrix were located at the thinner walls (Fig 4.3). The thicknesses of the inner walls depended on the proximity between the pores or the proximity between them and the external surface of the scaffold. The irregular distribution of pore location and pore size generated an irregular distribution of strain. Therefore, in a same pore one side had low values of deformation while another side had high values of deformation. In the same way one side can be under compression while another side can be under tension. Additionally, each pore of the samples had different values and different distribution of surface strain.

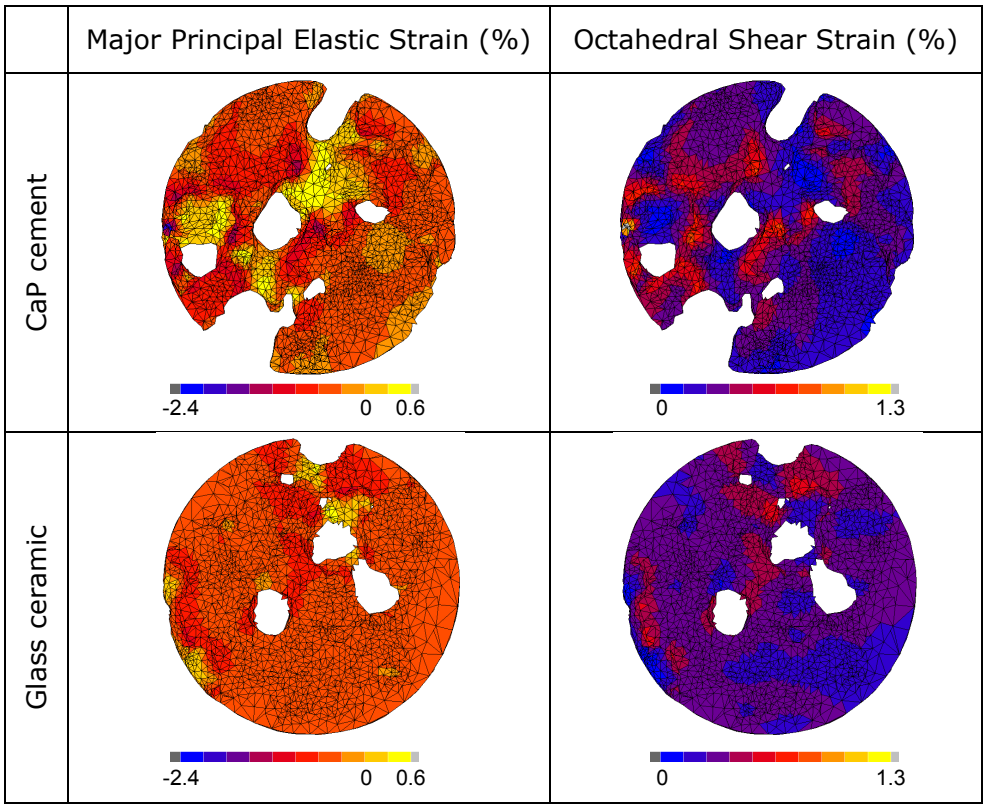

Fig 4.3. Stimuli distribution within the scaffold walls under compressive strain. Transversal sections.

At the surface nodes, the major principal strain and the octahedral shear strain followed a Gaussian distribution with values of deformation between -1.6 and 0.6% for the major principal strain and between 0 and 1% for the octahedral shear strain (Fig 4.4). The frequency of nodes under compression was higher for the glass ceramic

sample than for the CaP cement one which had more regions under tension. The octahedral shear strain was lower for the CaP cement than for the glass ceramic.

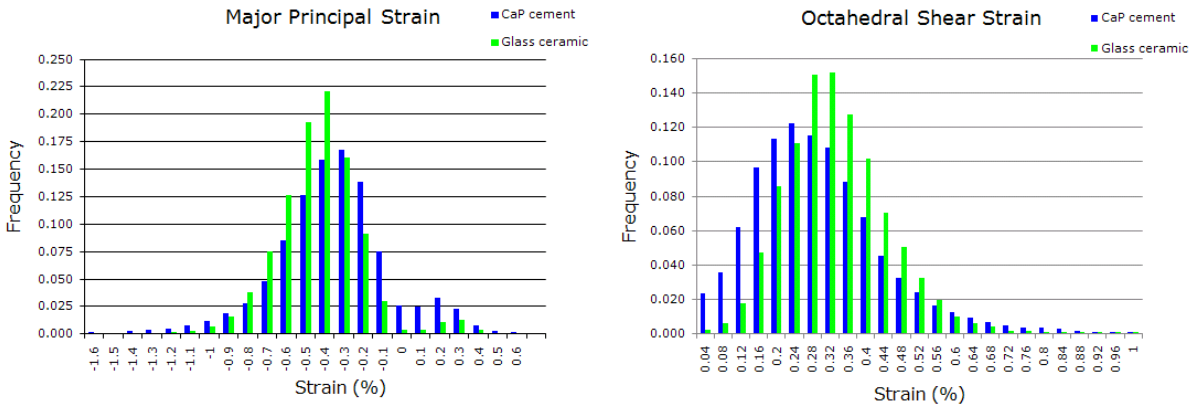

Fig 4.4. Histograms of stimuli under compressive strain. Only nodes at the scaffold walls were reported.

4.3. FLUID MODEL

4.3.1. Model Definition

For the simulation of the interstitial fluid flow, inlet fluid velocity was fixed on the nodes of the entrance side of the meshes (side A), nil fluid velocity was fixed on the nodes of the walls simulating a confined perfusion system, and the outlet fluid pressure was set as zero on the nodes of the exit side (side B) (Fig 4.5). Steady state Newtonian fluid analyses were performed. Fluid density and viscosity were similar to the cell culture medium (DMEM) at 37°C (Bacabac 2005), see Table 4.2. Fluid flow, fluid pressure and fluid shear stress were computed. Meshes for the fluid phase obtained as described in Chapter 3 were used. FE models were built in Marc–Mentat (MSC Software, CA-USA). The analyses were solved using Marc (MSC Software, CA-USA). For constitutive equations see Appendix B. An inlet fluid velocity of 10 μm/s was set by trial and error in order to obtain results of fluid shear stress that can be correlated with cell activity (Porter et al. 2005).

Table 4.2. Fluid properties used in the perfusion fluid FE model.

Sample	Viscosity (mPa·s)	Density(Kg/m^3)
CaP Cement	1.45	1 x 10^3
Glass	1.45	1 x 10^3

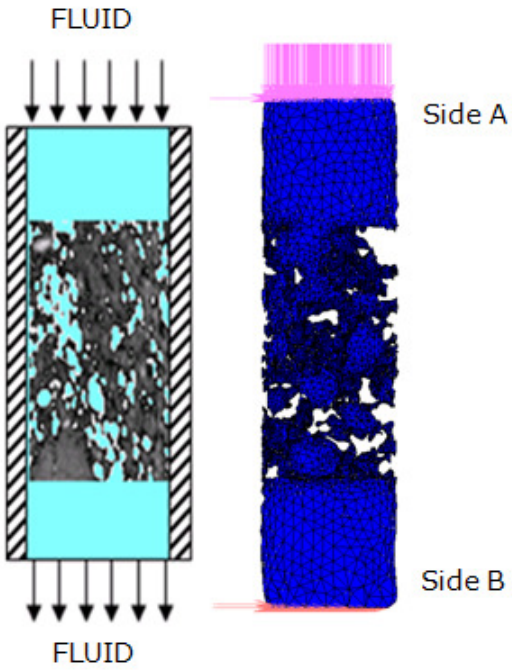

Fig 4.5. Perfusion fluid model definition. Boundary conditions and FE mesh.

A parametric study was performed on the fluid models to study the influence of fluid viscosity as cell proliferation and differentiation progress, the influence of inlet fluid velocity and, the influence of fluid flow direction. Three levels of fluid viscosity, three levels of inlet fluid velocity and two levels of inlet fluid flow directions were used to make up 18 different models for each material, see Table 4.3. Wilcoxon tests with significant level of 0.001 were used to verify statistical differences between variables when the fluid models conditions were changed.

Table 4.3. Levels of fluid viscosity and inlet velocity used for the parametric study of the perfusion fluid.

Material	Viscosity (mPa·s)	Inlet Velocity (µm/s)	Inlet Side
CaP cement Glass ceramic	0.7 1.45 2.1	1 10 100	A B

4.3.2. Results

The fluid velocity distribution into the pores showed that the fluid flow did not reach all interconnected pores of the samples. Moreover, high changes of fluid velocity were observed; there were regions where the fluid velocity was almost nil, and zones where the fluid velocity increased up to 100 times the inlet velocity (Fig 4.6). Maximal values

were around 1000 times the inlet fluid velocity (12.76 and 14.89 mm/s for the CaP cement and the glass ceramic respectively for 10 μm/s of inlet velocity), see Table 4.4.

The fluid shear stress distribution was consistent with the fluid velocity distribution, since the shear stress is a function of the velocity gradient. Regions where the magnitude of fluid shear stress was high corresponded to regions where the magnitude of fluid velocity was high. Most values of fluid shear stress were around 0.05 mPa and maximal values were around 40 mPa (Fig 4.6).

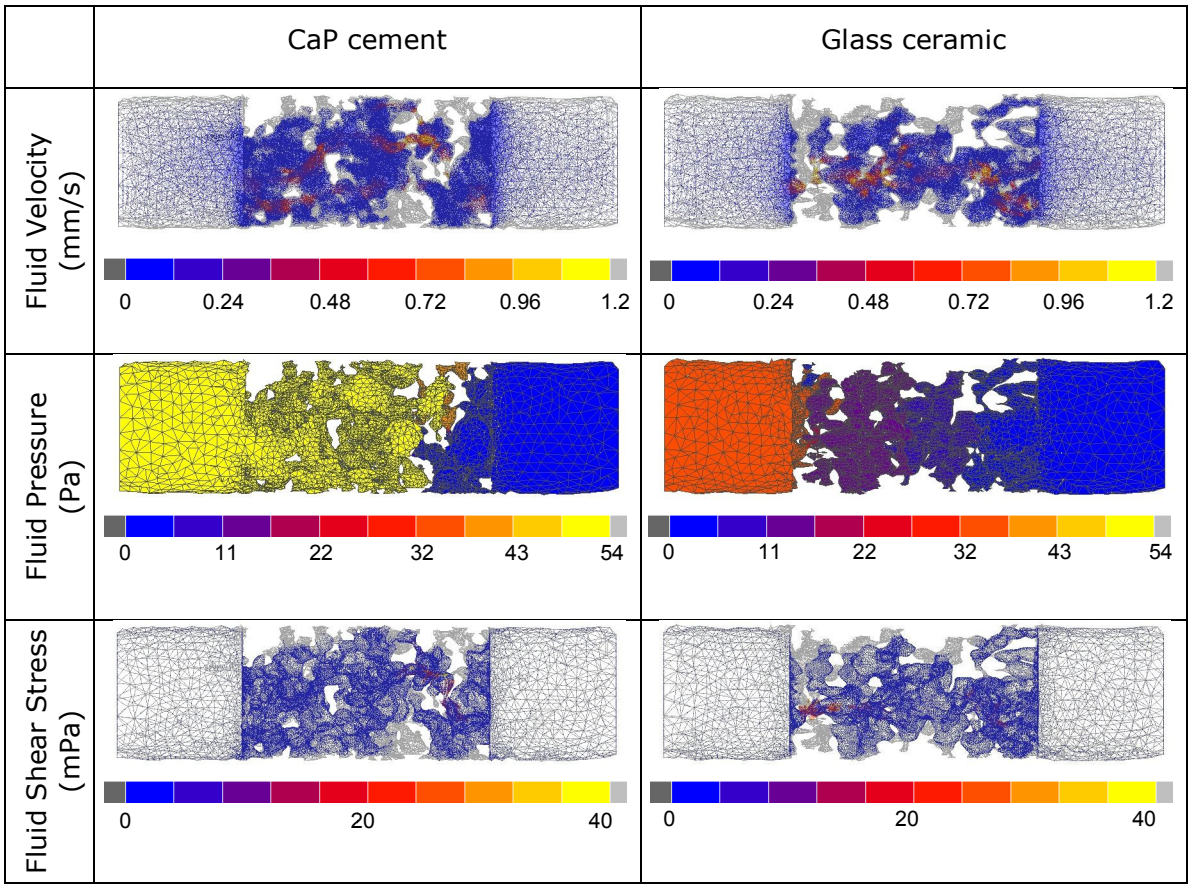

Fig 4.6. Stimuli distribution within the scaffold pores under perfusion fluid flow.

The maximum fluid pressure was higher for the CaP cement sample than for the glass ceramic; however, the maximum fluid shear stress was higher for the glass ceramic sample than for the CaP cement. The maximal fluid velocities were around the same magnitude (Table 4.4).

Table 4.4. Maximum values of fluid velocity, fluid pressure and fluid shear stress.

Sample	Inlet side	Fluid Velocity (mm/s)	Fluid Pressure (Pa)	Fluid Shear Stress (mPa)
CaP	A	12.76	54.00	37.58
cement	B	12.56	53.17	37.01
Glass	A	14.89	37.64	46.55
ceramic	B	14.51	36.67	45.05

The fluid pressure drop from the inlet to the outlet of the pores of both samples was not gradual, abrupt changes of fluid pressure were present between regions. Those sudden changes of fluid pressure were due to the low interconnectivity between some porous regions. If the fluid flowed between two pores through an area with small transversal section, the fluid velocity and the shear stress increased quickly and the fluid pressure fell rapidly (Fig 4.7). Each pore of the samples had different values of fluid velocity, fluid pressure and fluid shear stress, depending mainly on its position within the scaffold, its size and its interconnectivity with other pores.

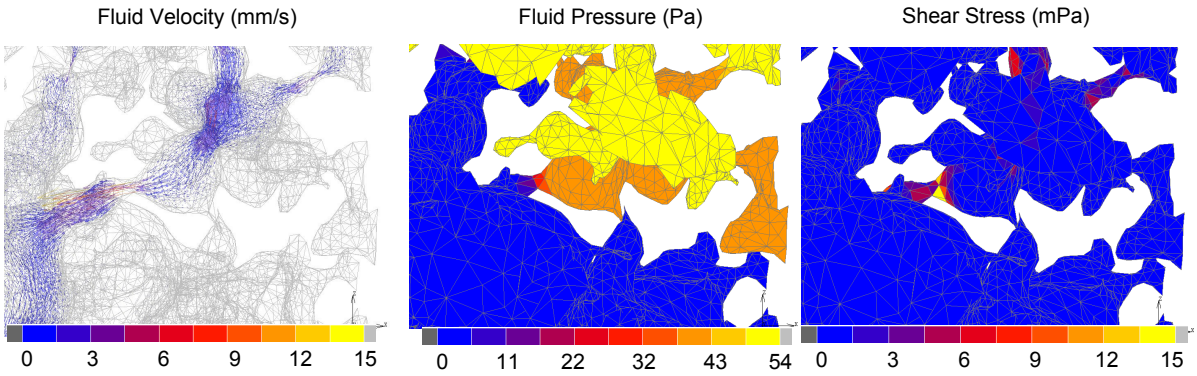

Fig 4.7. Detailed view of the fluid flow within the CaP cement sample.

Minor differences between the fluid velocity and fluid shear stress distributions in a cross section at the center of the CaP cement and the glass ceramic scaffolds were detected. However, the magnitude of the pressure was much lower for the glass ceramic than for the CaP cement (Fig 4.8). This difference was caused because of the abrupt changes of pressure which in the CaP cement case occurred close to the exit side and in the glass ceramic case occurred close to the inlet side (Fig 4.6).

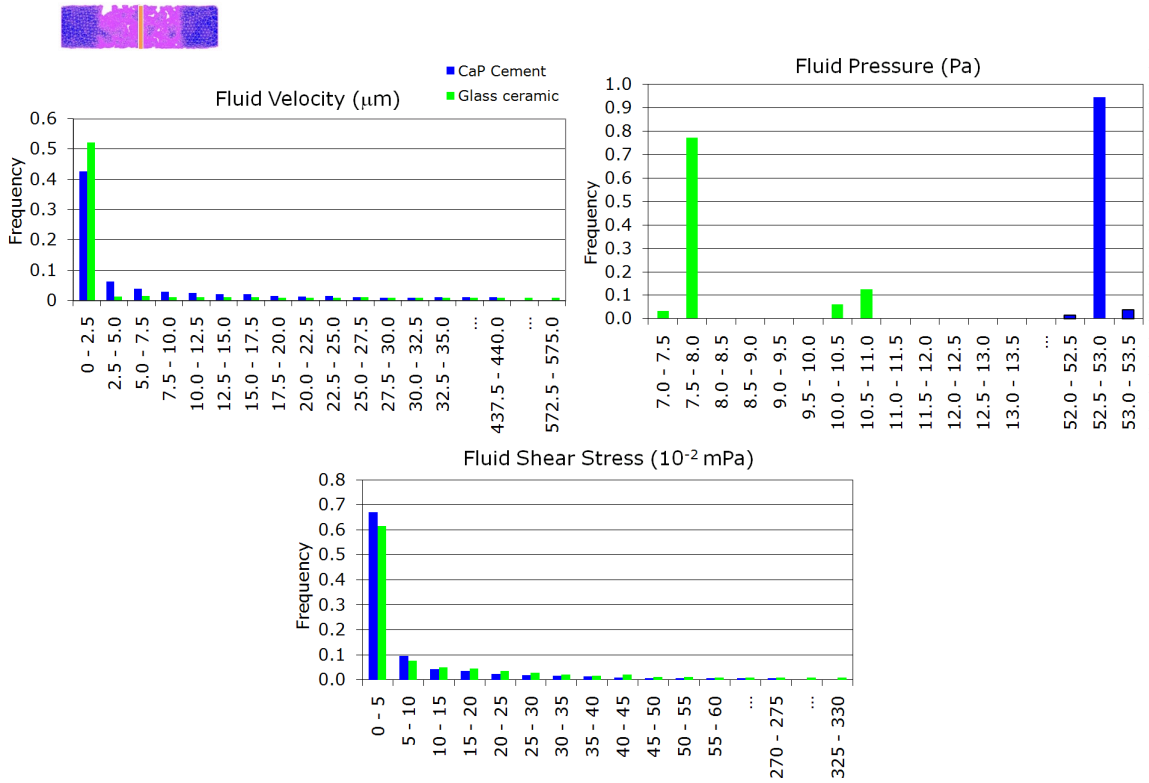

Fig 4.8. Histograms of stimuli under perfusion fluid flow. Only nodes in a transversal section in the center of the scaffolds were reported.

Parametrical study

There was hardly any difference in the fluid penetration for different levels of inlet fluid velocity, fluid viscosity or inlet side of the mesh. When the fluid flow inlet side was changed (from side A to side B), for constant inlet velocity and constant fluid viscosity, statistically significant differences in the magnitudes of the fluid velocity, fluid pressure and fluid shear stress at each specific node were found.

When the inlet fluid velocity was changed (from 1 to 100 μm/s), for constant fluid viscosity and constant inlet fluid side, the magnitude of fluid velocity, fluid pressure and fluid shear stress at each node of the mesh changed proportionally to the inlet fluid velocity. For instance, in the case of the CaP cement scaffold using a viscosity of 1.45 mPa·s, an increase of the inlet fluid velocity from 10 to 100 μm/s, increased 10.04, 10.01 and 9.98 times the maximum values of fluid velocity, pressure and shear stress, respectively (Table 4.5).

When the fluid viscosity was changed (from 0.7 to 2.21 mPa·s), for constant inlet fluid velocity and inlet fluid flow direction, statistically non significant differences in the magnitudes of the fluid velocity were found for the cases of low inlet fluid velocity (1 and 10 μm/s). However, statistically significant differences were found when the

inlet fluid velocity was 100 μm/s. The variation of the fluid pressure and fluid shear stress was proportional to the change of fluid viscosity. For instance, in the case of the CaP cement scaffold, when using an inlet velocity of 10 μm/s, an increase of the fluid viscosity from 1.45 to 2.1 mPa·s, caused no change in the maximum value of fluid velocity and increased 1.45 times the maximal values of fluid pressure and fluid shear stress (Table 4.5).

The interaction between inlet fluid velocity and fluid viscosity did not affect the results. When they were changed at the same time, the magnitude of fluid velocity, fluid pressure and fluid shear stress at each node changed proportionally to the product of inlet fluid velocity and fluid viscosity (Table 4.5).

Table 4.5. Effect of fluid viscosity and inlet fluid velocity on the maximum values of fluid velocity, fluid pressure and fluid shear stress.

		Fluid Velocity ratio			**Fluid Pressure Ratio**			**Fluid Shear Stress ratio**		
Material	**Viscosity (mPa·s)**	**Inlet velocity (μm/s)**								
		1	**10**	**100**	**1**	**10**	**100**	**1**	**10**	**100**
CaP cement	**0.7**	0.10	1.00	10.06	0.05	0.48	4.86	0.05	0.48	4.80
	1.45	0.10	1.00	10.04	0.10	1.00	10.01	0.10	1.00	9.98
	2.1	0.10	1.00	10.03	0.14	1.45	14.49	0.14	1.45	14.46
Glass ceramic	**0.7**	0.10	1.00	9.82	0.05	0.48	4.85	0.05	0.48	5.26
	1.45	0.10	1.00	9.95	0.10	1.00	10.01	0.10	1.00	10.39
	2.1	0.10	1.00	9.97	0.14	1.45	14.49	0.14	1.45	14.81

$$Fluid\ Velocity\ Ratio(v,\mu) = \frac{Maximum\ Fluid\ Velocity(v,\mu)}{Maximum\ Fluid\ Velocity(10\ \mu m/s, 1.45 mPa \cdot s)}$$

$$Fluid\ Pressure\ Ratio(v,\mu) = \frac{Maximum\ Fluid\ Pressure(v,\mu)}{Maximum\ Fluid\ Pressure(10\ \mu m/s, 1.45 mPa \cdot s)}$$

$$Fluid\ Shear\ Stress\ Ratio(v,\mu) = \frac{Maximum\ Fluid\ Shear\ Stress(v,\mu)}{Maximum\ Fluid\ Shear\ Stress(10\ \mu m/s, 1.45 mPa \cdot s)}$$

Even though solid and fluid analyses were performed separately, it was possible to observe the distribution of these stimuli at the surface nodes of the scaffolds since the meshes were congruent and the nodes were consistent. Each point at the surface of the scaffold had a different combination of solid shear strain and fluid shear stress (Fig 4.9).

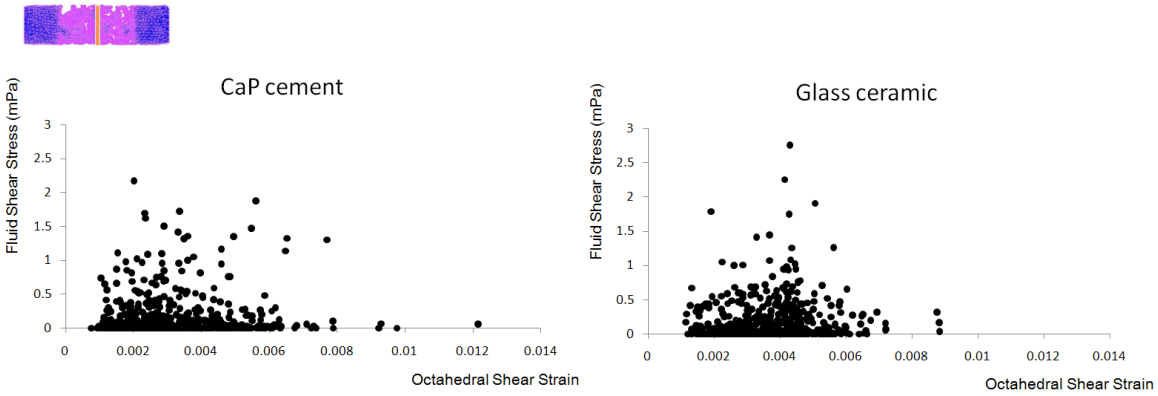

Fig 4.9. Fluid shear stress and octahedral shear strain at the scaffold walls. Only nodes in a transversal section in the center of the scaffolds were reported.

4.4. POROELASTIC MODEL

4.4.1. Model Definition

A fluid flow within the interconnected pores of the CaP cement scaffold was simulated using a poroelastic formulation. Because it is not possible to apply a constant inlet velocity, a gradient of pressure between side A and side B was simulated. Therefore, a fluid pressure of 57 Pa was fixed on the nodes of the entrance side of the meshes and a fluid pressure of zero on the nodes of the exit side of the meshes, consistently to the results obtained for the simulation using the Newtonian fluid formulation. For material properties see Table 4.6. Fluid velocity and fluid pressure were computed. Analysis was performed in Abaqus (Simulia, RI-USA). For constitutive equations see Appendix C.

Table 4.6. Material Properties used in the fluid flow FE model. Poroelastic formulation.

Material Properties	**Culture Medium**
Young´s modulus (MPa)	0.2
Poisson´s ratio	0.167
Permeability (m^4/Ns)	10^{-7}
Bulk modulus grain (MPa)	2300
Bulk modulus fluid (MPa)	2300

4.4.2. Results

Consistent to the results obtained using the Newtonian fluid formulation, nil fluid velocity were predicted in regions with low pore interconnectivity, while peaks of fluid velocity and abrupt drops of pressure were predicted in other zones. High velocities of around 3 mm/s were predicted in some regions.

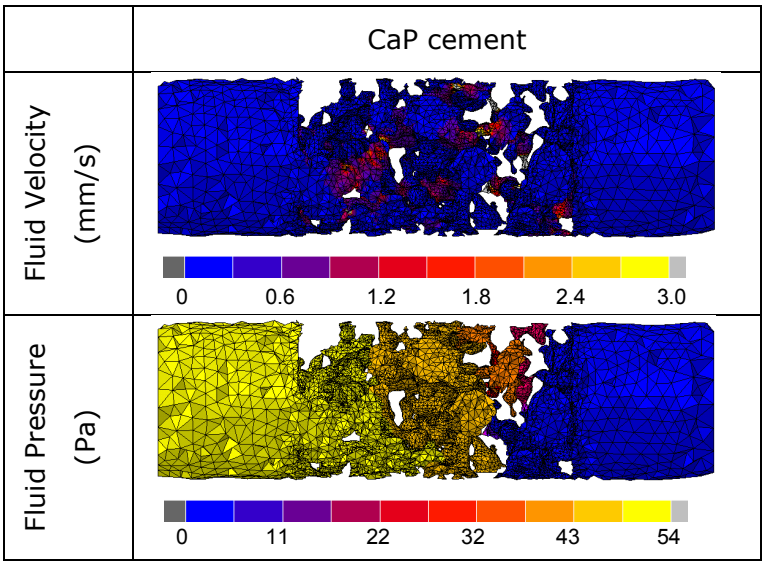

Fig 4.10. Stimuli distribution within the scaffold pores under fluid flow. Poroelastic formulation.

4.5. DISCUSION

Stress and strain distributions within the solid phase, and fluid velocity, pressure and shear stress distributions within the pores were heterogeneous because of the morphology of the studied scaffolds. The wall thickness, pore size, and the pore shape are not uniform, and the pores are not totally interconnected. Therefore mechanical stimuli will be different according to the sample used and the specific point observed within the scaffold.

Uncoupled mechanical studies of both solid material phase and fluid flow were performed for the same samples of material. This simplified approximation does not consider the influence of forces generated by the fluid flow on the solid phase and vice versa. Nevertheless, since the major principal strain, the fluid pressure and the fluid shear stress were less than 2%, 54 Pa, 40 mPa respectively, it is assumed that the solid fluid interaction can be neglected. Moreover, fluid surface tension forces are neglected in the fluid models causing an error of 4% in the fluid pressure (calculated using the surface tension of the medium and the measured contact angle). However,

fluid velocity and fluid shear stress are not influenced because the inlet velocity is imposed as a boundary condition.

Biological conditions were not included in the models and cell migration, proliferation and differentiation were not simulated. Nonetheless conclusions about mechanical stimuli on cells at the initial cell stimulation can be done based on the mechanical analysis of the scaffolds. Solid models showed that different values of principal stress and strain can be present in a specific pore. Obtained values of compressive and tensile strains are of the same order of magnitude of values associated with cell proliferation and differentiation by Meyer et al. (2006) ($2x10^{-3}$ strain). This suggests that some regions of these scaffolds are viable for cell activity. As shown by the fluid analysis, pore interconnectivity is not sufficient to guarantee that fluid flow will reach all internal walls of the scaffold. Besides each region in the pores will have a different combination of fluid pressure, fluid velocity, and fluid shear stress. Cells will be transported into the scaffolds by means of the interstitial fluid flow; therefore they may not reach the pores where the fluid flow does not penetrate. Abrupt changes of fluid velocity, fluid pressure, and fluid shear stress will be perceived by cells during the migration process. Once cells are seeded in the scaffold, they could attach to specific areas of a pore, according to the mechanical stimuli of each point. When simulating a physiological fluid flow within the scaffold it was found that the fluid flow could increase between 100 and 1000 times. This clearly could not have been predicted using a continuum model that does not account for the discretized pore structure. This result therefore shows that the mechanical stimuli through fluid flow sensed by the cells can be much higher than the one applied macroscopically on the scaffold. Cowin (2002) proposed the bone paradox to explain that strains applied to whole bone are much smaller than the strains that are necessary to cause bone signaling. A similar result is obtained in this study applied on direct fluid flow stimuli. This study shows that the gradient of pressure is small compared to the gradient of fluid flow. Thus, cells may be more sensitive to fluid flow than to fluid pressure. This corroborates some of the *in vitro* experiments on the effect of fluid flow (Fassina et al. 2005). Finally, it is difficult to make comparisons of *in vitro* and *in silico* results when sample specific models are not used.

The parametric study of the fluid showed that the mechanical stimuli increase linearly and independently with increments of the fluid inlet velocity and fluid viscosity for low levels of fluid velocity. Nevertheless those increments are not linear for high levels of fluid velocity. As a result, the inlet fluid velocity necessary to stimulate cells properly can be interpolated from the parametric study, but not extrapolated. For higher levels of fluid flow, new analyses should be done. A Newtonian fluid in steady state has been

simulated in this study, however when cells start being stimulated by fluid shear stress, they start producing nitric oxide and prostaglandin $E_{2.}$ These substances increase the viscosity of the fluid and consequently the magnitude of fluid shear stress. Therefore, for a constant inlet velocity for a long period of time, the magnitude of shear stress will increase over time. This aspect should be considered when simulating tissue differentiation. Finally, according to the levels of fluid shear stress correlated with cell proliferation and differentiation by Cartmell et al. (2003) and Porter et al. (2005) an inlet fluid velocity of 10 μm/s is appropriate for cell proliferation and differentiation in some regions of the studied scaffolds. However maximum values of fluid shear stress could be associated with cell death in other regions.

Using a poroelastic formulation it is possible to model a perfusion fluid flow. Qualitatively, similar results were obtained when a Newtonian formulation was used; abrupt drops of pressure and peaks of fluid velocity were predicted because of the irregular morphology of the pores. However the magnitudes of the velocity were different. High values of fluid velocity were around 1.2 mm/s in the simulation using a Newtonian formulation while they were around 3 mm/s in the simulation using the poroelastic formulation. These magnitudes depends on the parameter used, specifically the value of permeability. The appropriate magnitude of permeability necessary to model a perfusion fluid flow depends on the microstructure of the pore domain. Using the correct value of permeability equivalent results can be obtained using a poroelastic of a Newtonian fluid formulation; however, using the poroelastic formulation an inlet fluid velocity cannot be simulated and fluid shear stress at the scaffold walls cannot be computed.

4.6. CONCLUSION

This study provides detailed information about mechanical stimuli within the internal walls of two biomaterial scaffolds with different morphology caused by mechanical loading on the extra cellular matrix and interstitial fluid flow. This information was obtained by μFE models of the real shape of the solid material phase and the pores. Different conditions of stress, strain, and fluid flow were found within the scaffolds according to the architecture of the samples suggesting that cells would be exposed to different stimulations. In particular velocities of around 100-1000 times the inlet velocity were found in some regions of the samples. Such kind of studies combined with *in vitro* studies should contribute in the future to the understanding of cell mechanotransduction and therefore to the process of tissue differentiation.

CHAPTER 5
Study of Cell Seeding

5.1. INTRODUCTION

In vitro perfusion studies have shown that by dynamically seeding cells into scaffolds, an even cell distribution and high cell density throughout those porous constructs can be achieved (Cartmell et al. 2003, Wendt et al. 2003). These studies investigated different medium inlet velocities and correlated them with cell distribution and density at a macroscopic level. Specifically, they demonstrated that under low fluid flow cells seed mainly on the bioreactor tubes and they do not penetrate the scaffolds. However *in vitro* it is difficult to determine the specific mechanical stimuli transmitted to the cells during the seeding process taking into account the scaffold morphology.

Models developed in Chapter 4 predicted different levels of fluid velocity and fluid shear stress within the scaffold according to the inlet fluid velocity and the pore interconnectivity. The objective of this chapter is to study the possible relation between cell seeding and the mechanical stimuli affecting each point at the scaffold surface. It is hypothesized that the specific locations of the cells throughout a scaffold at the initial state of a cell culture, achieved by dynamic perfusion seeding, can be predicted using the shear stress affecting the cells locally. Cells will adhere in points within certain range of fluid shear stress [a, b], and the specific locations can be predicted with a probabilistic function $p=f(\tau)$ where p is the nodal probability of locating a cell and τ is the fluid shear stress.

Three probabilistic cell seeding models were proposed:

In the first model, each point on the surface of the material with a value of shear stress higher than zero has a constant probability P for locating a cell (Fig 5.1).

$$p = P \quad 0 < \tau < \infty$$

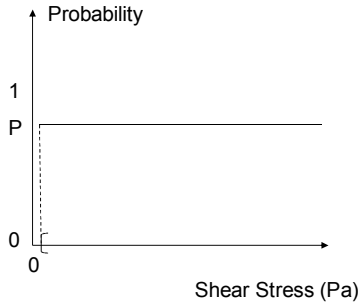

Fig 5.1. Function of probability used to simulate cell seeding.
Constant probability independent on the fluid shear stress.

In the second model, each point on the surface of the material with a value of fluid shear stress within a certain range has a constant probability P for locating a cell (Fig 5.2).

$$p = P \quad 0.057 < \tau < 57$$

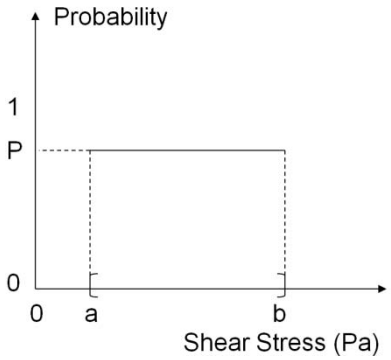

Fig 5.2. Function of probability used to simulate cell seeding.
Constant probability within a range [a,b] of fluid shear stress.

In the third model, the probability of the nodes within this range is not constant but is a Gaussian distribution with mean μ and variance σ (Fig 5.3).

$$p = N(\mu,\sigma) \quad 0.057 < \tau < 57$$

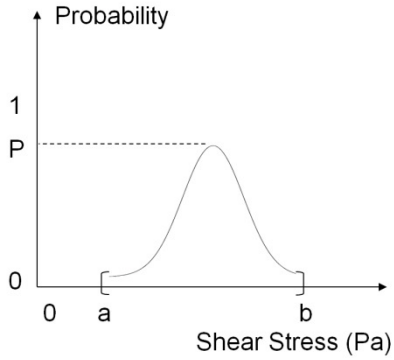

Fig 5.3. Function of probability used to simulate cell seeding.
Gaussian probability within a range [a,b] of fluid shear stress.

5.2. METHODS

A 2D FE mesh based on a longitudinal section of the CaP scaffold was used in order to simplify the model and to be able to observe directly the relation between pores morphology and cell seeding (Fig 5.4). A section of 1 mm width and 1.33 mm height was used. A mesh of 1333 8-node square elements of the pores was built manually. A perfusion fluid flow was simulated. A constant velocity was imposed to the nodes at the inlet side, nil velocity was set at the nodes in the interface between solid and fluid (scaffold walls), and pressure equal to zero was fixed at the nodes of the exit side. The distribution of fluid shear stress at the nodes corresponding to the scaffold walls was computed. The mesh was built in Marc-Mentat (MSC Software, CA-USA) and the models were solved in Marc (MSC Software, CA-USA).

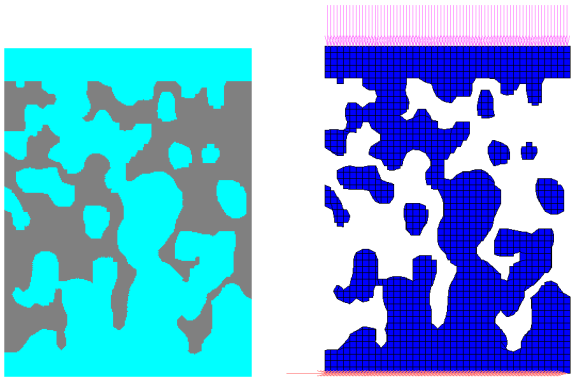

Fig 5.4. 2D section of the scaffold used for the cell seeding study, fluid flow domain in blue and solid material in grey. FE mesh and boundary conditions.

Two independent numbers were generated for each node at the scaffold walls. The first one was its probability of locating a cell which was assigned according to the magnitude of shear stress and the functions described below. The second one was a random number between zero and one. Then, if the random number was lower than the value of probability assigned, the node was assumed to be occupied for a cell, else the node was assumed to be empty. Models using inlet fluid velocities of 1, 10 and 100 μm/s were performed and functions of probability described above were applied.

5.3. RESULTS

Fluid velocity and fluid pressure distribution when an inlet velocity of 1 μm/s was applied are shown in Fig 5.5. Maximal velocities and pressures were around 23 μm/s and 15 Pa respectively.

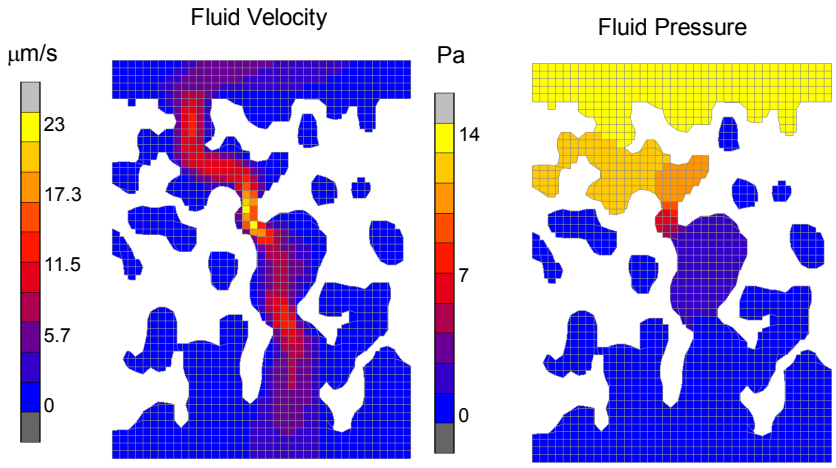

Fig 5.5. Fluid velocity and fluid pressure distributions within the section used for the cell seeding study.

The distribution of fluid shear stress at the scaffold pores was irregular due to the irregular morphology. There was not an inlet fluid velocity that caused fluid shear stresses in all pores within the assumed physiological range [0.057, 57] mPa; there were always nodes with magnitude of mechanical stimuli lower or higher than this range (Fig 5.6). The percentage of nodes whose fluid shear stress was out of the range varied according to the inlet fluid velocity; when 1 μm/s was applied, 48% of the surface nodes had a mechanical stimuli lower than 0.057 mPa and 14% higher than 57 mPa. When the inlet fluid velocity was increased to 10 μm/s, these

percentages changed to 38% and 29%. When the inlet fluid velocity was increased to 100 μm/s the percentage of nodes under low stimuli was reduced to 32% and the percentage of nodes under high stimuli was increased to 47% (Fig 5.6).

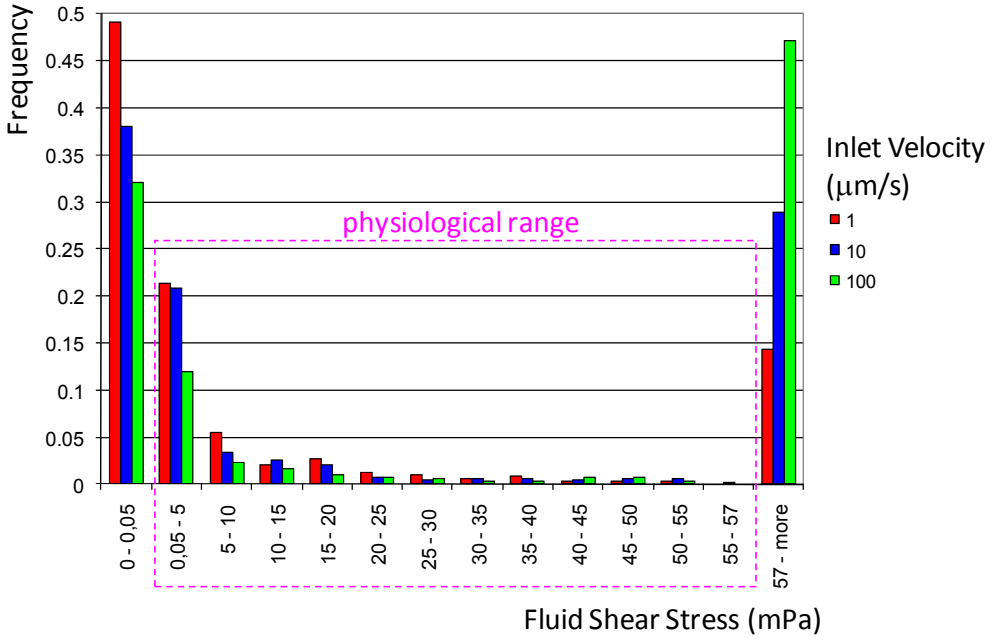

Fig 5.6. Histograms of fluid shear stress at the scaffold walls comparing different inlet velocities.

Not only the total percentage of nodes out of the physiological range changed but also the location of points stimulated by shear stress within that range (Fig 5.7). When the inlet fluid velocity was low (1 μm/s), only the walls that connect the pores from the top to the bottom directly were affected by stimuli within the physiological range. The walls that were not in that trajectory had low fluid shear stress even if they were well connected (point A). When the fluid velocity was increased (10 μm/s), the fluid flow had more accessibility and the fluid shear stress in those regions became within the physiological range (point A). However, if the fluid inlet velocity was further increased (100 μm/s), the fluid shear stress in the narrow regions started being above the physiological range (point B). There were also scaffold walls that were not very well interconnected and the fluid shear stress was below the physiological range independently of the simulated inlet fluid velocity (point C).

According to the probability function used to simulate cell seeding, predicted cell locations varied. By definition, when the probability was independent of the fluid shear stress, cells were distributed randomly within the whole pore structure. According to the probability used, a different number of cells were predicted (Fig 5.8).

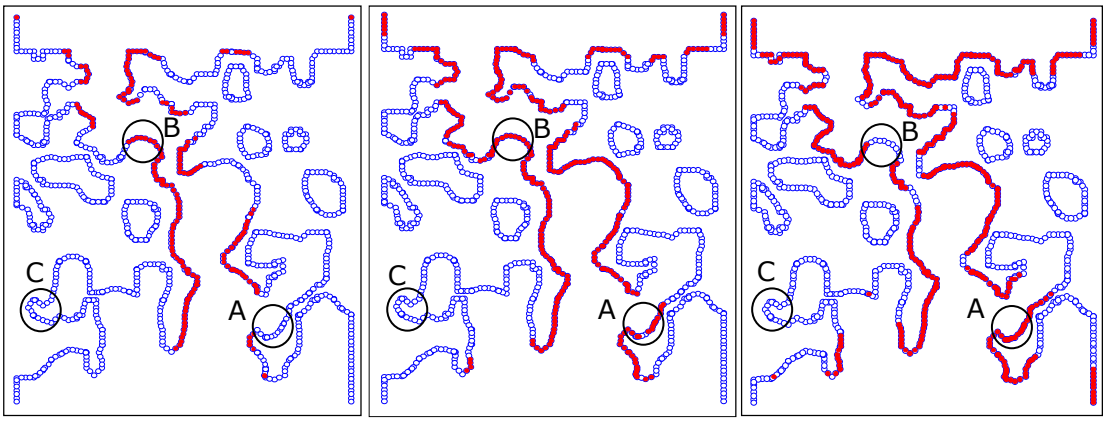

Inlet velocity = 1 μm/s Inlet velocity = 10 μm/s Inlet velocity = 100 μm/s

Fig 5.7. Walls locations under the physiological range of shear stress for different inlet velocities. Cells are shown in red and empty points in blue.

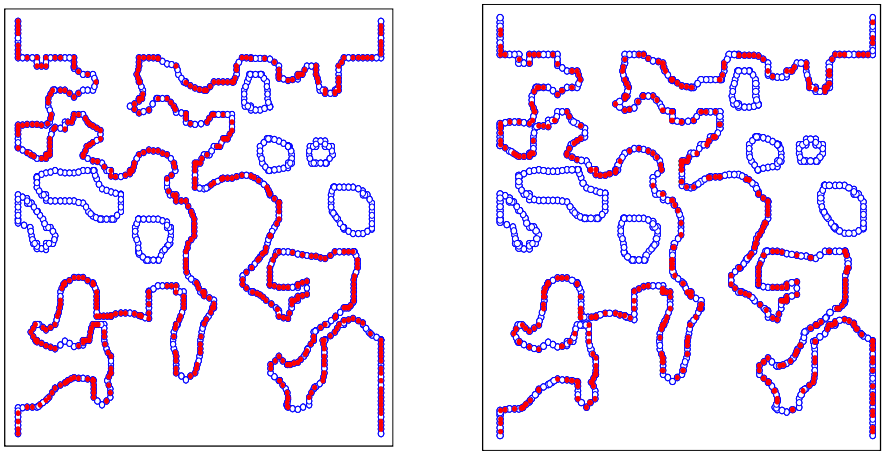

p= 0.7 p= 0.5

Fig 5.8. Cell distribution at the scaffold walls. Constant probability 0.7 independent on the fluid shear stress. Cells are shown in red and empty points in blue.

When the applied probability function was dependent on the fluid shear stress, the number of cells predicted and their location were related to the fluid inlet velocity and the pore morphology (Fig 5.9). When a constant probability within the physiological range was used, the location of cells were predicted consistently to the feasible regions described before (Fig 5.7) and the total number of cells depended on the value of probability used (p=0.7). When a Gaussian function was used, by definition, cells were more concentrated at the regions affected by magnitudes of fluid shear stress around 28.5 mPa and a lower number of cells were predicted at regions affected by fluid shear stress around the limits of the physiological range (Fig 5.9).

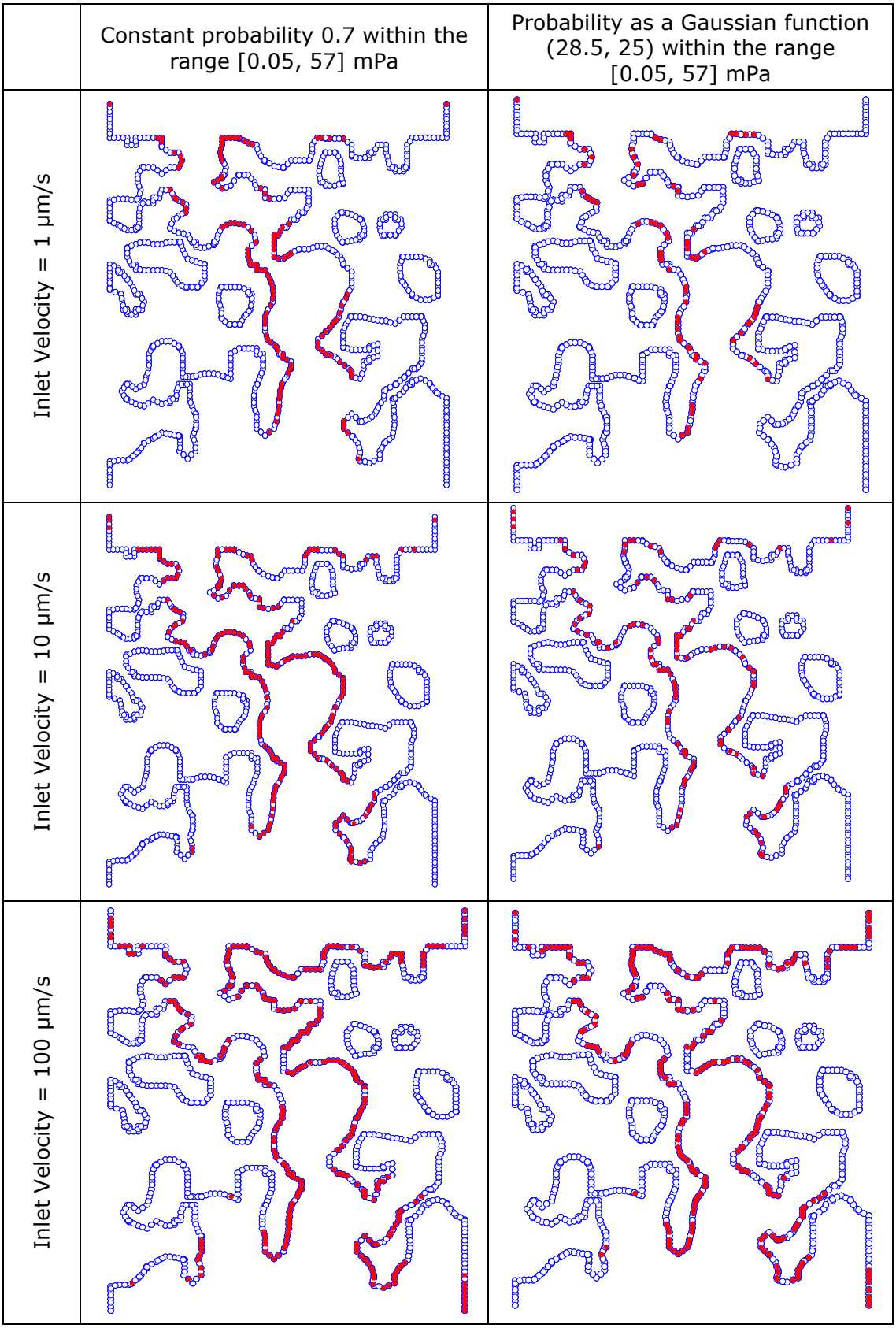

Fig 5.9. Cell distribution at the scaffold walls. Constant probability 0.7 and Gaussian probability within the physiological range of fluid shear stress. Cells are shown in red and empty points in blue.

5.4. DISCUSSION

Probabilistic functions were used to predict possible cell locations within a scaffold subjected to perfusion. Models in 2D were used as a simplification to analyze the effect that could have the fluid shear stress in the seeding process. Probabilistic functions including the mechanical stimulus as a parameter captured the fact that in scaffolds with irregular pore distribution, cells were not distributed homogeneously. Cells were predicted neither within pores poorly interconnected, nor in narrow regions with high fluid flow. However, these models did not capture the fact that cells accumulate in the bioreactor tubes at the entrance of the scaffold when the fluid inlet velocity is low (Wendt et al. 2003).

It was assumed that the medium flows throughout the interconnected pores transporting cells, oxygen and nutrients, therefore no cells were predicted in regions where the fluid flow was too low. Cell migration and oxygen diffusion were not considered. However, oxygen can diffuse to regions near the flow and cell can migrate to those regions. The assumed physiological range used for the probabilistic functions was based on results of cell activity within a specific scaffold of hydroxiapatite (Cartmell et al. 2003, Porter et al. 2005); however, the range of fluid shear stress that cells can support can change according to the material surface. Neither this range nor the probabilistic functions were validated; however, the presented seeding models illustrate qualitatively the correlation between scaffold morphology and fluid shear stress. If a different range of physiological stimuli were used, the distribution of shear stress and hence the distribution of cells within the scaffold pores will change according to the inlet fluid velocity. For a specific scaffold, there is a specific inlet velocity that causes the maximum percentage of surface with mechanical stimuli within a specific range. Additionally, cells location after an *in vitro* seeding could be controlled selecting a specific inlet fluid velocity in order to optimize the space available for cells to proliferate.

5.5. CONCLUSION

The proposed probabilistic models can be used to predict regions in the scaffold feasible for cell seeding in terms of fluid shear stress. Those regions are related to the inlet fluid velocity. There is a specific velocity for each scaffold (depending on its morphology) that maximizes the pore regions with mechanical stimuli within a specific range of fluid shear stress.

CHAPTER 6
Study of the Mechanoregulation of Tissue Differentiation

6.1. INTRODUCTION

Compressive loads and perfusion fluid flow can be used *in vitro* in order to increase cell proliferation and differentiation. The distributions of stress and strain at the scaffold walls under the effect of compressive loading and the distribution of fluid velocity and fluid shear stress at the scaffold pores under perfusion fluid flow were computed in Chapter 4. It was demonstrated that the micro mechanical stimuli transmitted to the cells can be several orders of magnitude different than the macro mechanical stimuli applied to the scaffold depending on the porosity, the interconnectivity and the wall thickness. The initial mechanical loads necessary to generate a specific level of stimuli were determined; nevertheless, the presence of cells and new differentiated tissue within the constructs can generate changes in the mechanical stimuli distribution over time.

Tissue differentiation within scaffolds for tissue engineering has been investigated in some *in silico* studies based on the mechanoregulation concept of Prendergast et al. (1997) (Kelly and Prendergast 2006, Byrne et al. 2007, Checa and Prendergast 2010). In these studies *in vivo* mechanical loads are simulated. According to the mechanoregulation theory developed in Prendergast et al. (1997), the octahedral shear strain of the solid phase and the interstitial fluid flow velocity driven by the pore

deformation are used as mechano-regulatory stimuli. Even thought it has been demonstrated that these stimuli are the most appropriate to explain the mechanisms of tissue differentiation during bone fracture healing (Isaksson et al. 2006a), the mechanism of tissue differentiation within a scaffold can be different (Sikivitsas et al. 2001, Potier et al. 2010). In native tissue, osteocytes are believed to be the mechano-sensory cells. Since they are buried in the bone extracellular matrix, they are stimulated by tissue deformation and interstitial fluid velocity. Then, osteocytes transmit signals to MSCs, osteoblasts and osteoclasts so that they can differentiate, synthesize or resorb bone tissue. In a scaffold, MSCs are initially attached to the material walls and are expected to differentiate and synthesize new tissue. They can be stimulated directly by the deformation of the material caused by compressive loads and/or by the fluid shear stress generated by fluid flow within the pores.

The effect of a compressive strain and a perfusion fluid flow on cell differentiation within a scaffold has been investigated by Stops et al. (2010b). In this study individual cells were simulated and the mean velocities around each cell were used as mechano-regulatory stimuli to simulate cell differentiation. However, the variation on the fluid velocity and on the shear strain distributions that can be caused because of tissue formation were not accounted for.

The objectives of this study are:

1) to propose a new method that allows simulating tissue differentiation when a scaffold is subjected to *in vitro* mechanical loading (compressive load and perfusion fluid flow).

2) to investigate tissue differentiation and the dynamics of the mechanical stimuli transmitted to the cells when extracellular matrix starts to form in a scaffold of irregular morphology.

The mechanoregulation concept of Prendergast et al. (1997) was modified in order to consider the effect of a perfusion flow shear stress instead of the effect of interstitial fluid velocity using fluid viscosity to simulate tissue growth. It was hypothesized that the mechanical stimuli transmitted to the cells allow the formation of different types of tissue within different regions of the scaffold according to the morphology of the pores.

6.2. SIMULATION BASED ON OCTAHEDRAL SHEAR STRAIN AND FLUID SHEAR STRESS

6.2.1. Methods

a) Sample

A cylindrical section of 1 mm diameter and 0.6 mm height of the glass ceramic scaffold described in Chapters 3 and 4 was used, see Fig 6.1. This section has 174015 and 24907 tetrahedral elements of 10 nodes for the solid and the pore phases respectively.

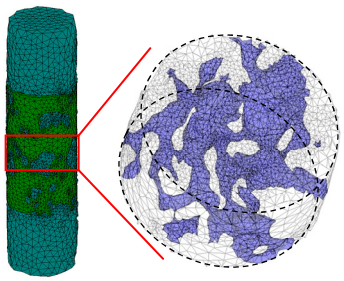

Fig 6.1. Section of the scaffold used for the simulations of tissue differentiation. Pore mesh in blue and solid phase mesh in grey

b) FE models

As described in Chapter 4, two separate FE analyses were performed in Marc (MSC Software, CA-USA) in order to compute the mechanical stimuli. In the first model, a compressive strain equivalent to 0.5% of total deformation was simulated using the whole mesh (including solid and the pore phases). The bottom nodes of the scaffold were fixed. A constant displacement was applied in the top nodes. Octahedral shear strains were computed using a solid linear elastic formulation.

$$\gamma_{oct} = \frac{2}{3}\sqrt{(\varepsilon_I - \varepsilon_{II})^2 + (\varepsilon_{II} - \varepsilon_{III})^2 + (\varepsilon_{III} - \varepsilon_I)^2}$$

where ε_I, ε_{II}, and ε_{III} are the principal strains.

In the second model, a steady state perfusion flow through the interconnected pores of the scaffold was simulated. Constant fluid velocity or constant fluid pressure was

applied in the nodes at the inlet side and nil pressure was applied in the nodes at the outlet side of the mesh. Non slip boundary condition was applied at the nodes of the walls of the scaffold. Fluid shear stresses were computed using the Newtonian fluid formulation.

$$\tau = \mu \nabla v = \frac{\sigma_I - \sigma_{III}}{2}$$

where μ is the fluid viscosity, ∇v is the gradient of fluid velocity, and σ_I and σ_{III} are the maximum and minimum principal fluid stresses respectively. In order to simulate an alternating fluid flow, two directions of fluid flow were modeled separately switching the boundary conditions between the inlet and the outlet sides. For each element, only the maximum value of stimuli within the values computed in these two models were accounted for in the mechanoregulation algorithm: $\tau=\max(\tau_{side1}, \tau_{side2})$. Solid and fluid interaction was neglected due to the high stiffness of the ceramic scaffold.

c) Mechanoregulation

It was assumed that cells could differentiate within a certain range $[\tau_1, \tau_2]$ of fluid shear stress. If the fluid shear stress was lower than τ_1 it was assumed that the fluid flow could not transport cells, nutrients and oxygen to this region and therefore no differentiation was predicted. If the fluid shear stress was higher than τ_2, cells were detached from the surface and underwent apoptosis. This range of fluid shear stress was assumed to be [0.01 60] mPa, based on studies of Porter et al. (2005). These studies correlated values of 0.05 mPa with cell proliferation and peaks of 57 mPa with cell apoptosis. It was also assumed that if the octahedral shear strain at the walls of the scaffold was higher than 0.225, necrosis could occur. This value was arbitrarily imposed as twice the value for fibrous tissue differentiation. Based on these assumptions and using fluid shear stress instead of fluid velocity in the mechanoregulation theory of Prendergast el al. (1997), the mechano-regulatory stimulus *S* was computed as

$$S = \frac{\gamma_{oct}}{a} + \frac{\tau}{b}$$

were γ_{oct} is the octahedral shear strain obtained in the compressive load model, τ is the maximum fluid shear stress obtained from the alternating perfusion fluid flow

model and *a* and *b* are constants equal to 0.0375 and 10 mPa·s respectively. If $\tau \leq 0.01$ or $S > 6$ no tissue formation was predicted. If $0.001 < S \leq 1$ bone tissue was predicted, if $1 < S \leq 3$ cartilage was predicted, if $3 < S \leq 6$ fibrous tissue was predicted (Fig 6.2).

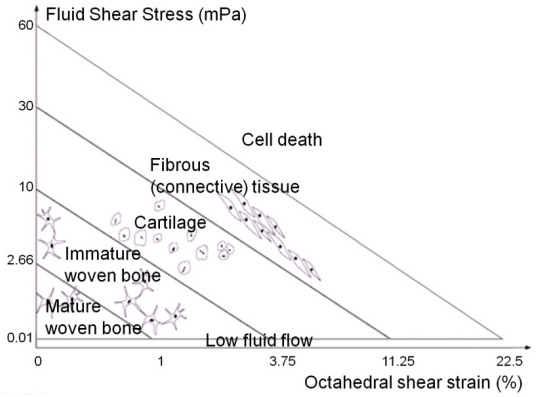

Fig 6.2. Mechanoregulation diagram regulating tissue differentiation. The mechano-regulatory stimulus is computed using octahedral shear strain and fluid shear stress.

d) Material properties

The effect of extracellular matrix maturation over time within the scaffold pores was simulated changing the material properties of each element of the pore mesh according to the mechano-regulatory stimuli predicted at the element. The material properties of a specific element were computed as an average of the properties of the tissues predicted in the last 10 iterations. In the compressive strain model, because a solid linear elastic formulation was used, the material properties considered were the Young´s modulus and the Poisson´s ratio (Table 6.1).

Table 6.1. Material properties of tissues for the compressive strain model

Property	Culture Medium	Mature Bone	Immat. Bone	Cartilage	Fibrous Tissue	Glass ceramic
Young´s Modulus (MPa)	0.2	6000[a]	1000[a]	10[a]	2[a]	455[b]
Poisson´s Ratio	0.499	0.3[a]	0.3[a]	0.475[c]	0.475[c]	0.33[b]

a Lacroix et al. 2002
b Lacroix et al. 2006
c Carter and Beaupré 2001

In the fluid flow model, the viscosity was used to simulate tissue formation. Briefly, if a cross section of a cylindrical domain is modeled as a poroelastic material, the average flow through this section according to the Darcy´s law is defined as

$$Q = K\left(-\frac{dP}{dx}\right)$$

where K is the coefficient of permeability of the material and dP/dx is the gradient of pressure. If the same section is modeled as a Newtonian fluid flow, the equivalent average flow according to the Newton equation is

$$Q = \frac{1}{\mu_T}\left(\frac{R^2}{8}\right)\left(-\frac{dP}{dx}\right)$$

where μ_T is the tissue viscosity and R is the radius of the cross section.

Therefore, the tissue viscosity can be defined as

$$\mu_T = \frac{1}{K}\left(\frac{R^2}{8}\right)$$

For more detail in the description of these equations see Appendix D. Following this equivalence and taking into account that the structure of the scaffold pores is more complex than a cylinder section, the viscosities used to simulate bone, cartilage, and fibrous tissue were assumed to be inversely proportional to their coefficient of permeability when they are simulated as poroelastic materials:

$$\mu_T \sim \frac{c}{K}$$

where μ_T is the tissue viscosity, K is the tissue coefficient of permeability, and *c* is a constant of proportionality that depends on the micro-morphology of the tissues and the scaffold (Table 6.2).

Table 6.2. Material properties of tissues for the perfusion fluid flow model

Property	Culture Medium	Mature Bone	Immat. Bone	Cartilage	Fibrous Tissue
Permeability (10^{-14} m^4/Ns)	$4x10^6$	37	10	0.5	1
Viscosity (10^{-3} Pa·s)	1	1·*c*	3.7·*c*	74·*c*	37·*c*

Because it is not possible to determine analytically the magnitude of c, a parametrical study varying it from 1 to 10^5 was performed. This maximum value was chosen from the comparison of mean velocities computed for constant gradients of pressure using Newtonian fluid flow and poroelastic formulations at the interconnected pore mesh. Briefly, pressure gradients of 0.3, 3 and 30 Pa were modeled using different values of permeability for the poroelastic formulation and using 1 mPa·s of viscosity for the Newtonian fluid flow formulation. Mean velocity within the pore domain was computed (Fig 6.3). For a gradient of pressure between 3 and 30 Pa, the permeability equivalent to model a fluid flow with viscosity μ=1 mPa·s ranges between 3×10^{-8} and 4×10^{-8} m^4/Ns.

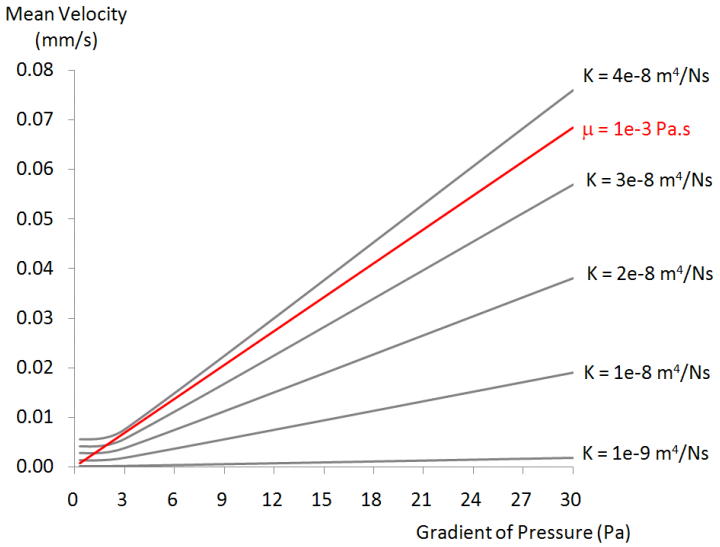

Fig 6.3. Comparison between Poroelastic and Newtonian fluid formulation. Mean fluid velocities computed for different gradients of pressure and different levels of permeability.

e) Solution procedure

The simulation of material properties change was performed for each element of the interconnected pore mesh. Since material degradation was not simulated, the mesh domain did not vary during the simulation. For every iteration, the mechano-regulatory stimulus *S* was computed from the FE models, the type of tissue equivalent to *S* was determined, and the mechanical properties were updated. The algorithm was stopped when the system stabilized or when the pattern of the results repeated (50 iterations) (Fig 6.4).

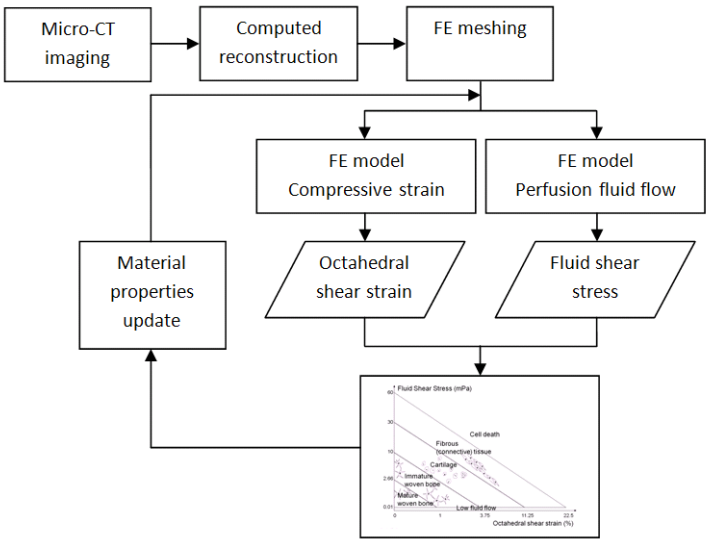

Fig 6.4. Schematic representation of the algorithm used to simulate tissue differentiation based on octahedral shear strain and fluid shear stress.

f) Simulations for parametrical study

In order to study the effect of modeling tissue as a Newtonian fluid, a parametric study was performed. Two types of boundary conditions for the perfusion fluid flow (constant inlet velocity of 10 μm/s and constant inlet pressure of 3 Pa) and six levels of the constant of proportionality c were used to perform 12 different simulations (Table 6.3).

Table 6.3. Simulations for the parametrical study changing boundary conditions and fluid viscosity.

Simulation	**1**	**2**	**3**	**4**	**5**	**6**	**7**	**8**	**9**	**10**	**11**	**12**
Boundary Condition	V	V	V	V	V	V	P	P	P	P	P	P
Constant c	1	10	10^2	10^3	10^4	10^5	1	10	10^2	10^3	10^4	10^5

V = Constant inlet Velocity
P = Constant inlet Pressure

6.2.2. Results

The stimuli distribution predicted over time within the pores of the scaffold was heterogeneous presenting a significant sensitivity to the constant of proportionality used to define the tissue viscosity and to the fluid boundary conditions.

a) Effect of tissue viscosity

In the cases of constant fluid velocity used as boundary condition, when low values of tissue viscosity were used the stimuli equivalent to bone stabilized in 82% of the pore volume for c = 1 and in 78% for c = 10 (simulations 1 and 2). When increasing the magnitude of tissue viscosities, c = 10^2, the stimuli distribution started being instable, the percentage of pore volume equivalent to bone formation decreased to 35% and stimuli corresponding to fibrous tissue and cell death were predicted in 12 and 35% of the pore volume respectively (simulation 3). For high values of tissue viscosity, c ≥ 10^3, cycles where the magnitude of the stimuli increased and decreased were observed (simulations 4-6). At the end of simulation 6 the percentage of pore volume equivalent to bone oscillated around 11%, to cartilage around 5%, to fibrous tissue around 4%, and to cell death around 50% (Fig 6.5).

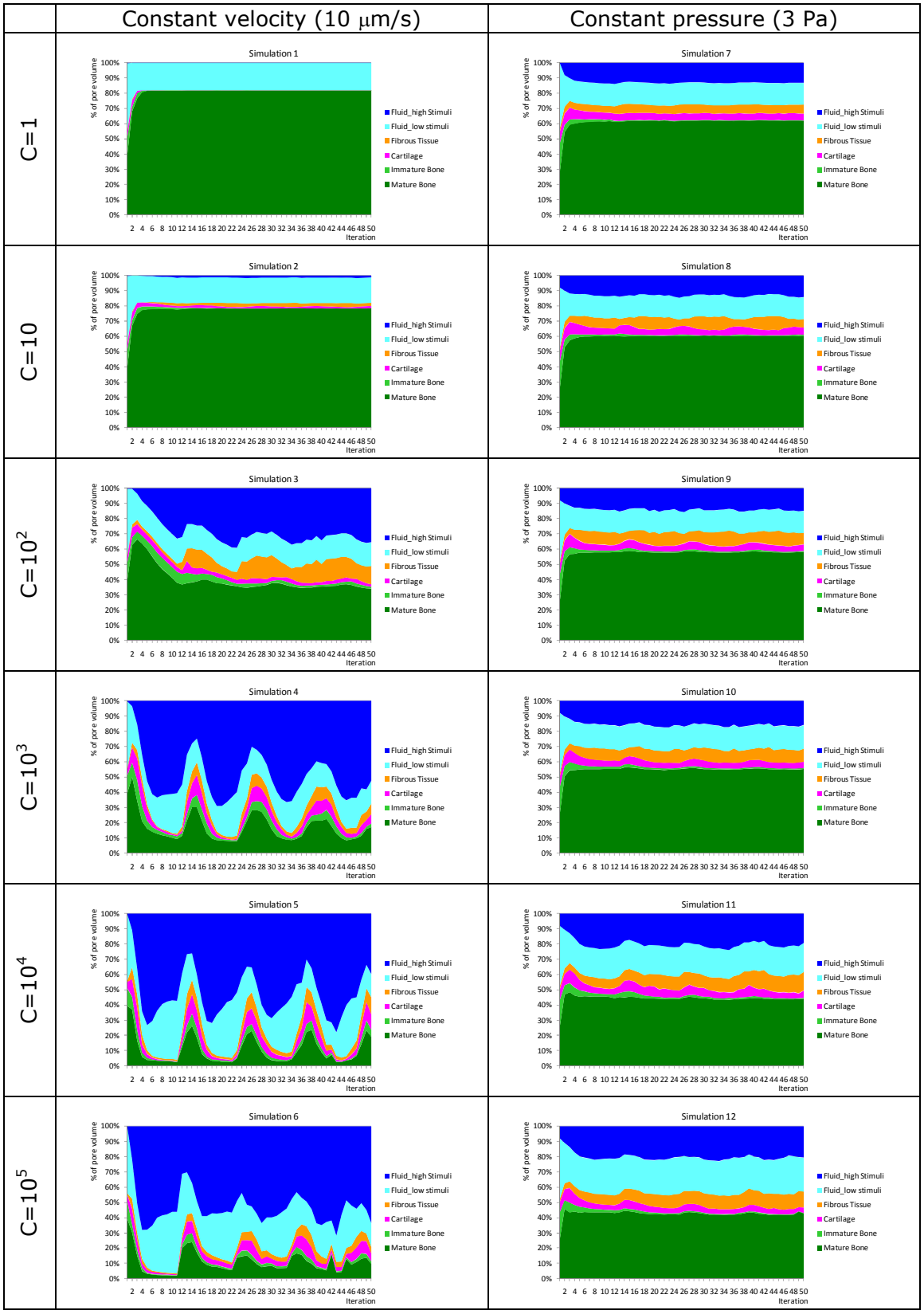

Fig 6.5. Distribution of mechano-regulatory stimuli over the simulations.

In the simulations with constant pressure used as an inlet boundary condition, for lower values of tissue viscosity, c = 1, the stimuli equivalent to bone, cartilage, fibrous tissue and cell death predicted at the end of the simulation was 62, 4, 6 and 14% of the pore volume respectively (simulation 7). When the tissue viscosity was increased, stimuli oscillations were predicted although the variation in the magnitude of stimuli was less marked (simulations 8-12). At the end of simulation 12, 42% of pore volume was equivalent to bone, 4% to cartilage, 10% to fibrous tissue, and 20% to cell death (Fig 6.5).

b) Effect of fluid boundary conditions

At the beginning of the simulations, the scaffold pores were assumed to be filled with culture medium so the stimuli predicted in most of the walls were equivalent to bone formation (50%). Therefore the material properties started to change linearly from fluid medium to the properties of the predicted tissue at each element. As a result, the fluid velocity distribution changed. When a constant inlet velocity was simulated, the fluid velocity distribution presented lower magnitudes where tissue was predicted and higher magnitudes where fluid medium was predicted (Fig 6.6). The mechano-regulatory stimuli increased up to the range of cell death in some regions due to the high fluid shear stresses, consequently the material properties were set back to the properties of fluid flow. Because the simulation was not stopped at this point, oscillations where the mechanical stimuli increased and decreased were predicted. See simulation 1-6 in Fig 6.5.

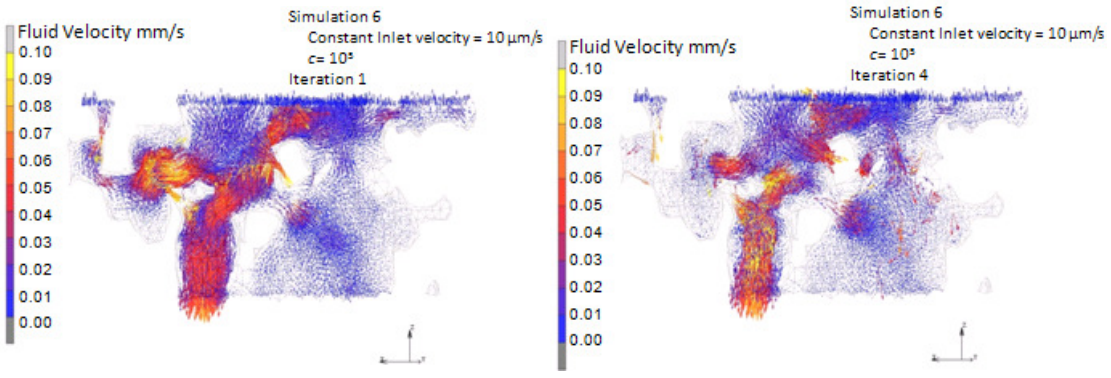

Fig 6.6. Fluid velocity distribution at iterations 1 and 4. Simulation using constant velocity and c = 6.

The fluctuations of fluid velocity over the simulation because of the mechanical properties variation within a pore were observed in Fig 6.7. The discontinuity in the standard deviation demonstrated the generation of peaks of fluid velocity. The fluid

flow distribution changed with the change of fluid flow inlet side. In the case of the specific pore showed in Fig 6.7 the velocity was higher when the inlet side was side B.

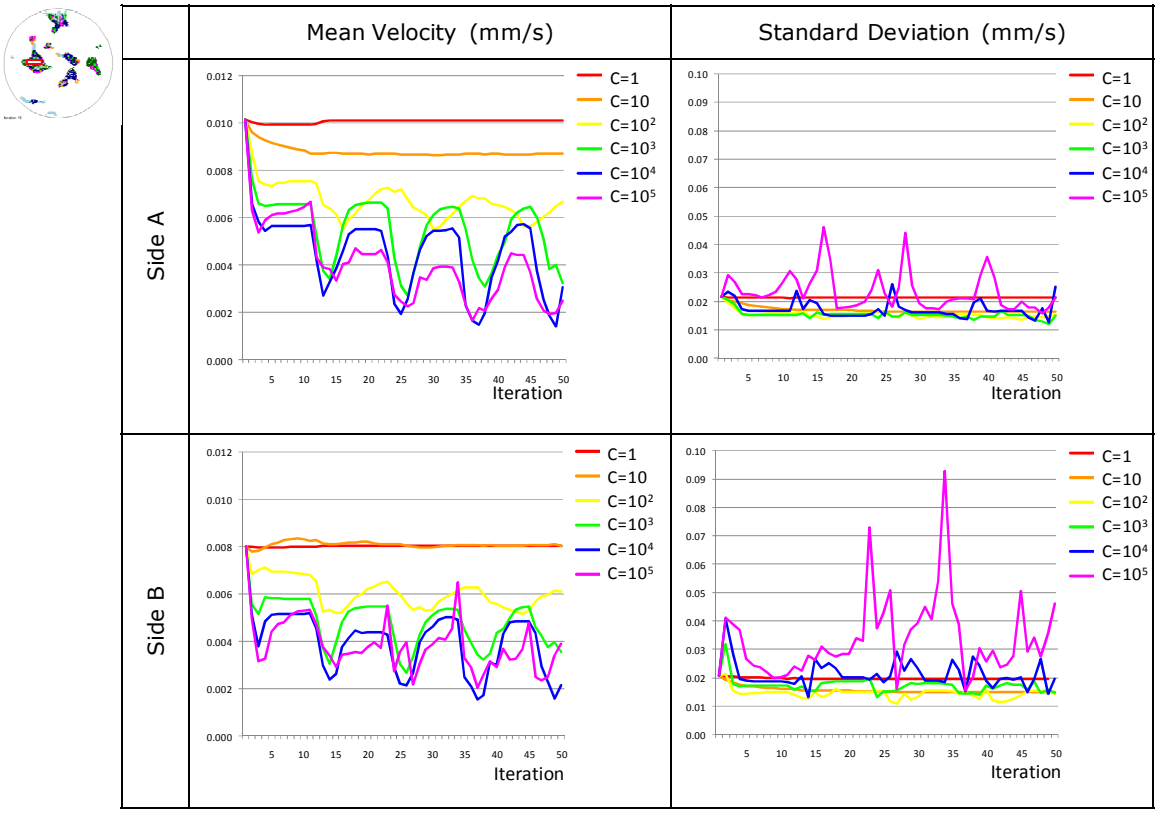

Fig 6.7. Effect of constant c on the fluid velocity oscillations over the simulation. Simulations using constant velocity.

The pattern of mechanical stimuli was different when a constant inlet pressure was used. In these cases, when some regions of the scaffold were assumed to be filled with tissue, the total fluid flow decreased (Fig 6.8) and the stimuli in most of the pore volume remained constant, see simulations 7-12 in Fig 6.5. The oscillations in the mean fluid velocity within a pore in the center of the scaffold, as well as the effect of the constant *c*, were less marked (Fig 6.9)

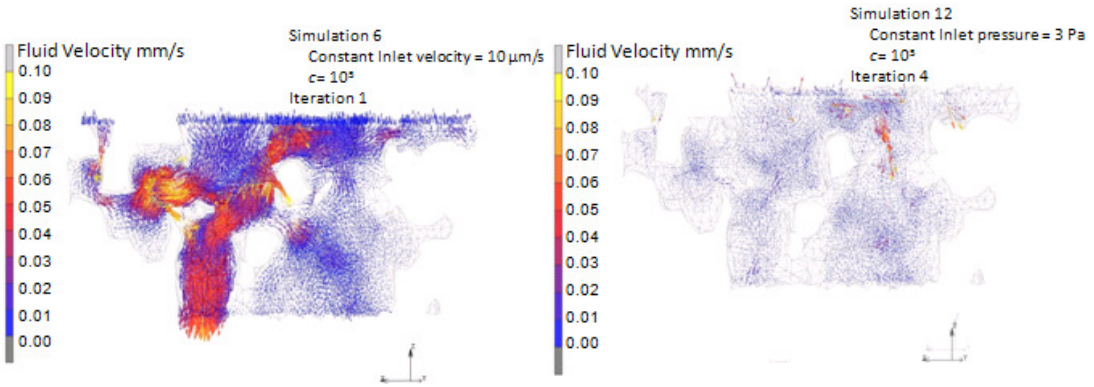

Fig 6.8. Fluid velocity distribution at iterations 1 and 4. Simulation using constant pressure and c = 6.

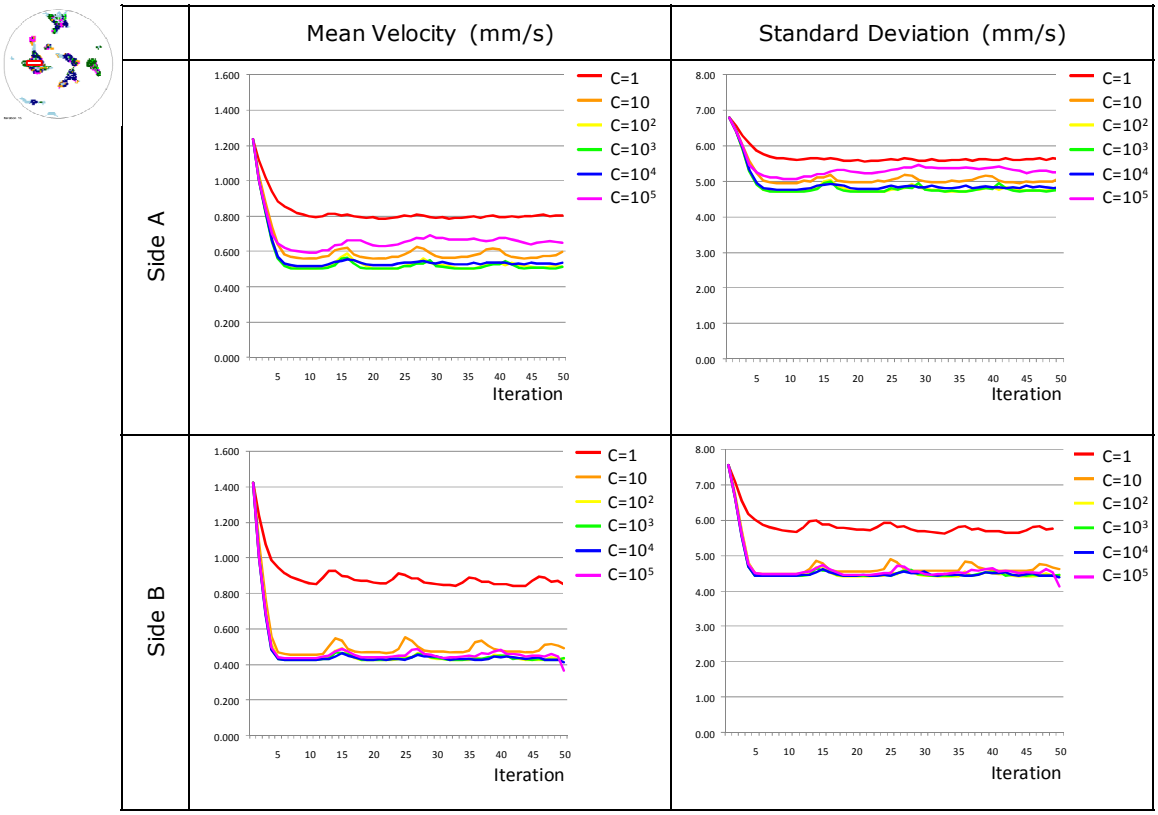

Fig 6.9. Effect of constant c on the fluid velocity oscillations over the simulation. Simulations using constant pressure.

c) Effect of compressive strain

The octahedral shear strain within the pores of the scaffold became homogeneous in regions were tissue was predicted, due to the increase of the Young´s modulus. For instance, at the beginning of simulation 6 (case with constant inlet velocity and maximal values of tissue viscosity), values of octahedral shear strain between 0.6% and 3% were predicted within the large pores, while at iteration 4 the magnitude of octahedral shear strains within most of pores were lower than 0.6% (Fig 6.10).

The stiffness of the sample over the simulation varied consequently with the variation of predicted tissue within the scaffold. When tissue was predicted the effective scaffold Young´s Modulus increased, according to the properties of the predicted tissues. However, in the simulations where tissues did not stabilized, the effective scaffold Young´s Modulus oscillated in concordance to the tissue predicted (Fig 6.11).

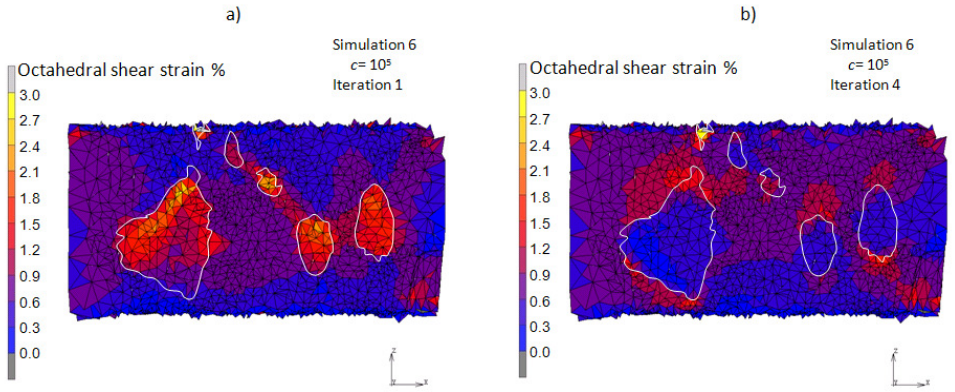

Fig 6.10. Octahedral shear strain distribution at iterations 1 and 4.
Simulation using constant velocity and c = 6

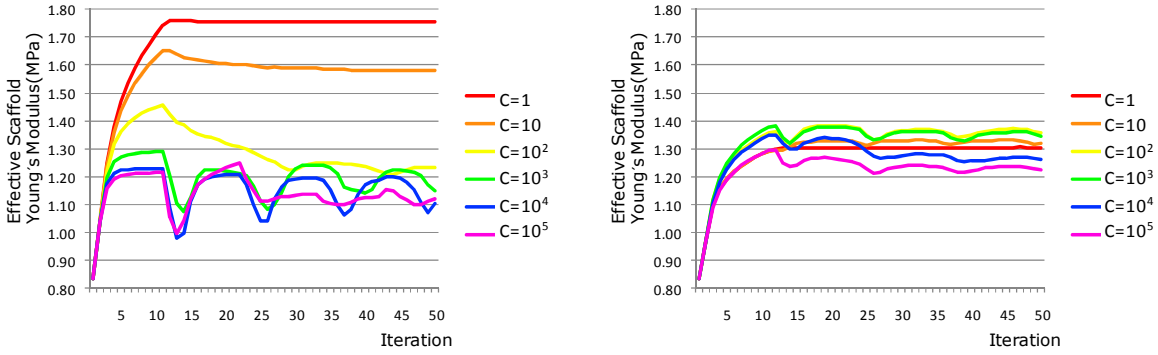

Fig 6.11. Effect of constant c on the scaffold stiffness over the simulation.

d) Effect of scaffold morphology

There was not a clear relation between pore size or pore location and the corresponding stimuli predicted (Fig 6.12). The stimuli predicted in some regions that were not well interconnected were constantly in the range of low stimuli. The stimuli predicted in the pores better interconnected changed according to the different conditions used in the simulations. When low viscosities were used (simulations 1, 2, 7 and 8), bone stimuli were predicted in most of the pore space. When the viscosities were increased, the results depended on the boundary conditions as stated before. For the case of constant velocity (simulations 3-6), the stimuli fluctuated between bone, cartilage, fibrous tissue and cell death in most of pore volume. For the case of constant pressure (simulations 9-12), bone was predicted in the walls of the pores while the stimuli fluctuated between fibrous tissue and cell death in the center of the pores.

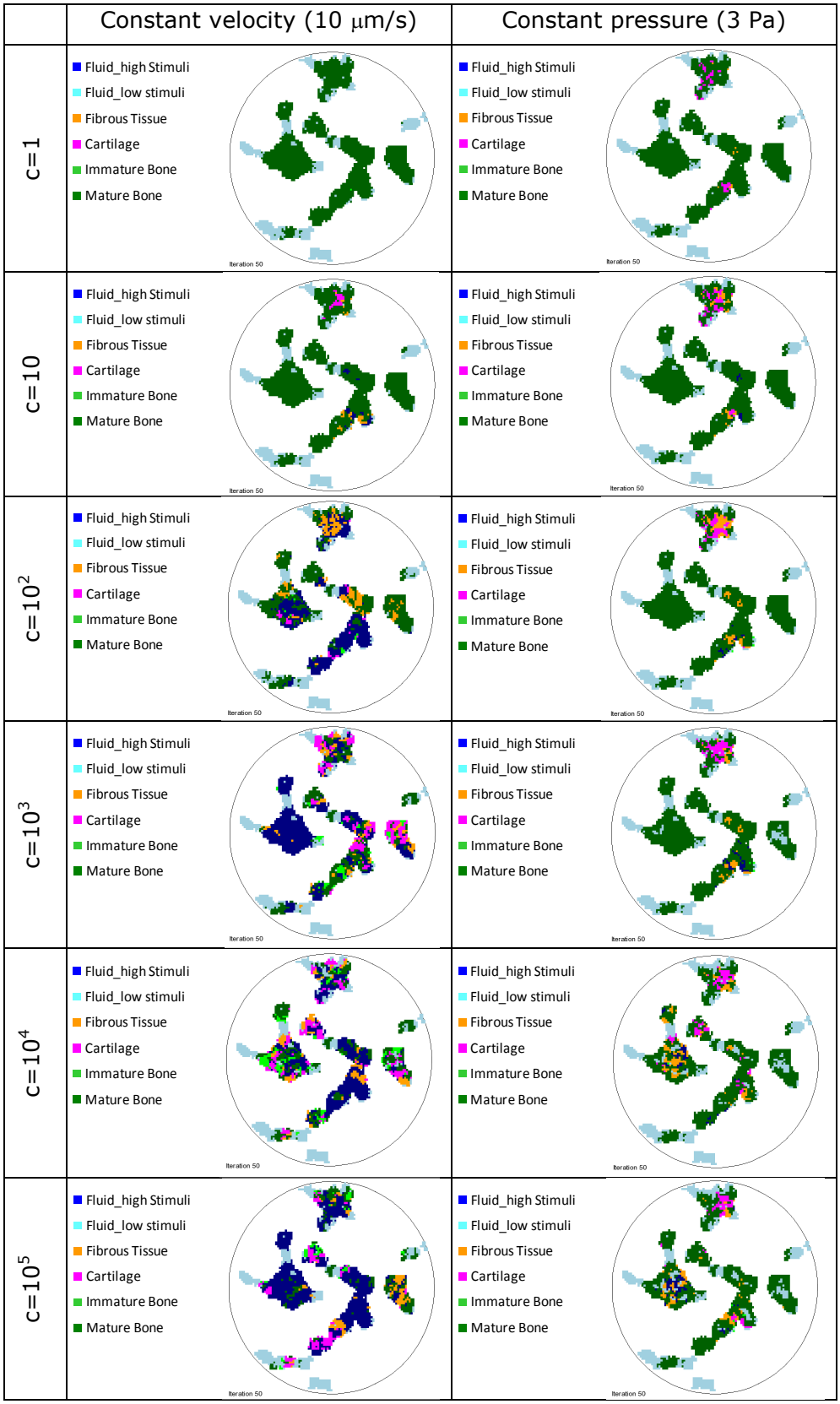

Fig 6.12. Distribution of tissue in a cross section of the scaffolds at the end of the simulations.

e) Effect of number of iterations used for the rule of mixtures

For both cases of inlet fluid boundary conditions (constant velocity and constant pressure) the frequency of the cycles was 11 iterations (Fig 6.5). This frequency was associated to the number of iterations used to compute the mechanical properties each iteration, which in this case was 10. To verify this statement the number of iterations used to compute the material properties was changed to 5 and to 15 iterations, obtaining cycles of 6 and 16 iterations respectively (Fig 6.13).

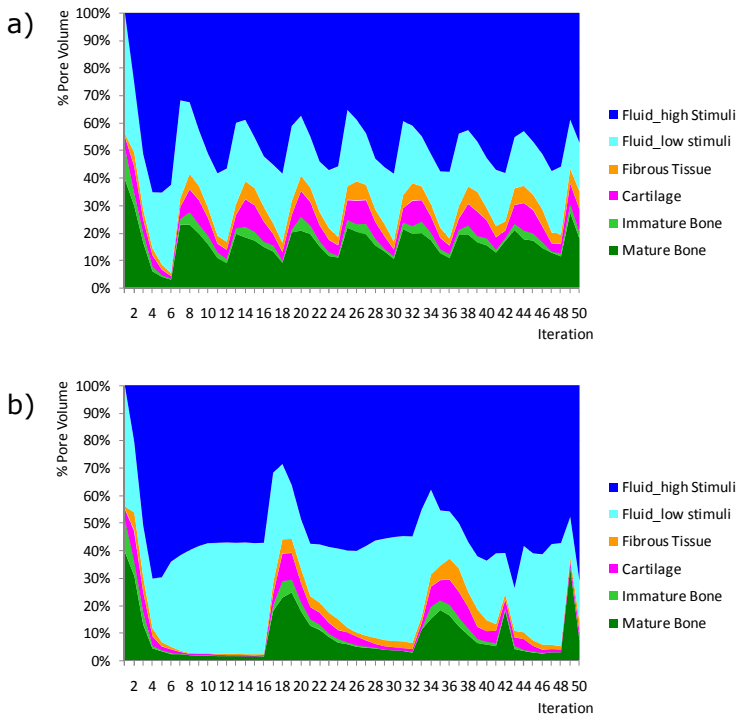

Fig 6.13. Distribution of mechano-regulatory stimuli over the simulations using a) 5 and b) 15 iterations to compute material properties. Simulation using constant velocity and c = 6.

f) Effect of low and high stimuli regions

To verify the effect of the low and high stimuli regions added to the mechanoregulation concept, two additional simulations were performed, one without the low stimuli region and another one without the high stimuli region, using the boundary conditions and material properties of simulation 6. The low stimuli region did not have an effect in the distribution of tissue predicted. The high stimuli region had an obvious effect. Without this region fibrous tissue was predicted in most of the scaffold pore volume instead of stimuli fluctuations (Fig 6.14).

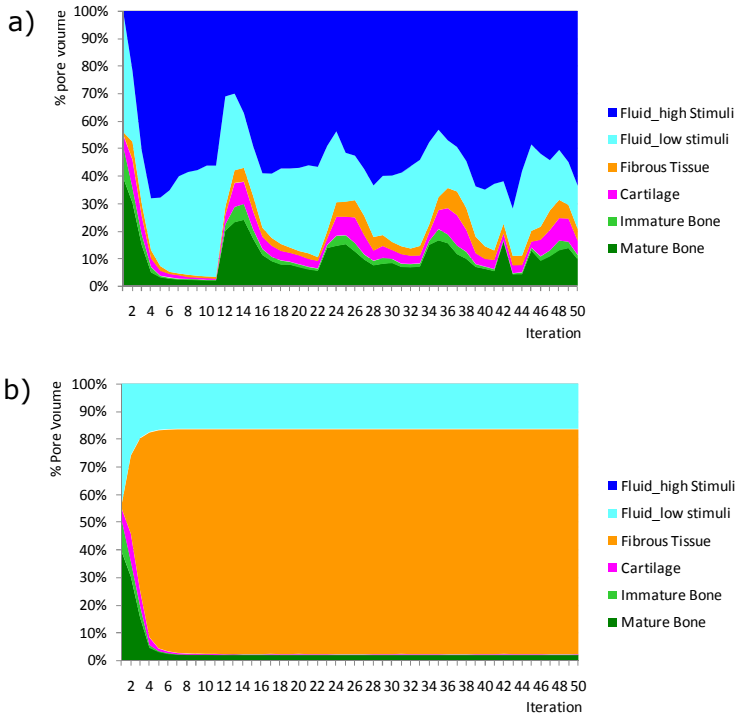

Fig 6.14. Distribution of mechano-regulatory stimuli over the simulations without a) low stimuli and b) high stimuli regions. Simulation using constant velocity and c = 6.

6.3. SIMULATION BASED ON OCTAHEDRAL SHEAR STRAIN AND FLUID VELOCITY

6.3.1. Methods

With the aim of determining the effect of the modifications performed to the methodology proposed by Prendergast et al. (1997), an additional simulation using this methodology was performed (Fig 6.15). FE analyses were performed in Abaqus (Simulia, RI-USA) in order to compute the mechanical stimuli. A compressive strain equivalent to 5% of deformation and a gradient of pressure of 3 Pa between the inlet and the outlet sides of the mesh were simulated using a poroelastic formulation. The inlet and the outlet sides were switched in order to simulate an alternating fluid flow. Octahedral shear strain and fluid velocity were computed. The mechano-regulatory stimulus S was computed as

$$S = \frac{\gamma_{oct}}{a} + \frac{v}{b}$$

where γ_{oct} is the octahedral shear strain, *v* is the maximum fluid velocity, and *a* and *b* are constants equal to 0.0375 and 3 μm/s respectively. The maximal level of stimuli for tissue formation were included, so if S > 6 no tissue is formed. Young´s modulus, Poisson´s ratio, coefficient of permeability and bulk modulus were used to simulate tissue growth (Table 6.4).

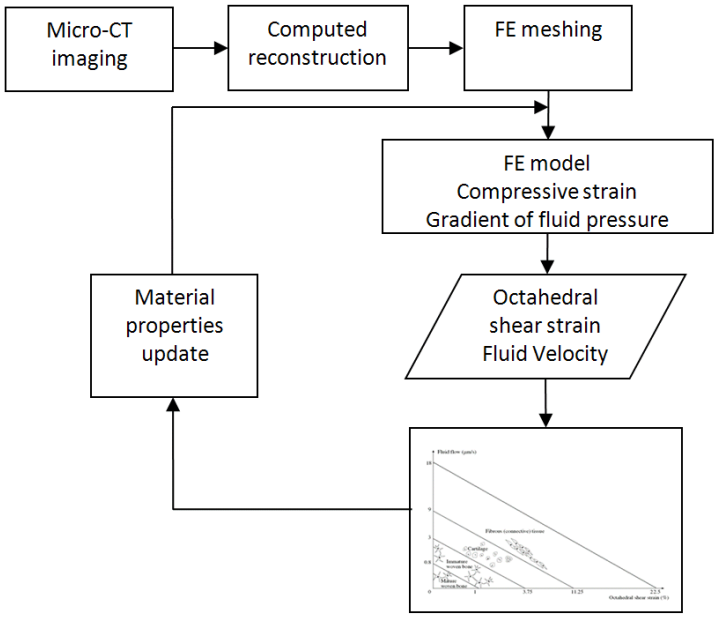

Fig 6.15. Schematic representation of the algorithm used to simulate tissue differentiation based on octahedral shear strain and fluid velocity.

Table 6.4. Material properties of tissue for the FE models using a poroelastic formulation.

	Culture Medium[a]	**Mature Bone[a]**	**Immat. Bone[a]**	**Cartilage[a]**	**Fibrous Tissue[a]**	**Glass Ceramic**
Young´s modulus (MPa)	0.2	6000	1000	10	2	455[b]
Poisson´s ratio	0.167	0.3	0.3	0.167	0.167	0.33[b]
Permeability (10^{-14} m^4/Ns)	$4x10^6$	37	10	0.5	1	1
Bulk modulus grain (MPa)	2300	13920	13920	3700	2300	13920
Bulk modulus fluid (MPa)	2300	2300	2300	2300	2300	2300

a Lacroix et al. 2002
b Lacroix et al. 2006

6.3.2. Results

When the fluid velocity computed with a poroelastic formulation was used, the stimuli stabilized through the simulation (Fig 6.16). In the first iteration, stimuli equivalent to bone, cartilage, and fibrous tissue were predicted in 15, 13 and 4% of the pore volume respectively, and stimuli in the range of cell death were predicted in 68% of the pore volume. After 11 iterations, the percentage of pore volume where stimuli

corresponding to bone was predicted increased up to 32%, and after 30 iterations the stimuli distribution remained constant. At the end of the simulation, 34.5% of the pore volume corresponded to bone stimuli, 1% to cartilage and 64.5% to cell death. Stimuli equivalent to bone tissue were predicted in regions that were not well interconnected. In these regions the fluid velocity was not induced by the gradient of pressure but rather by the compression of the solid that drove the movement of fluid. Stimuli corresponding to cell death were predicted in the well interconnected pores. In these regions the fluid velocity was induced by the gradient of pressure and consequently the fluid velocity and the mechano-regulatory stimuli were too high to allow tissue formation. No regions with low stimuli were predicted (Fig 6.16).

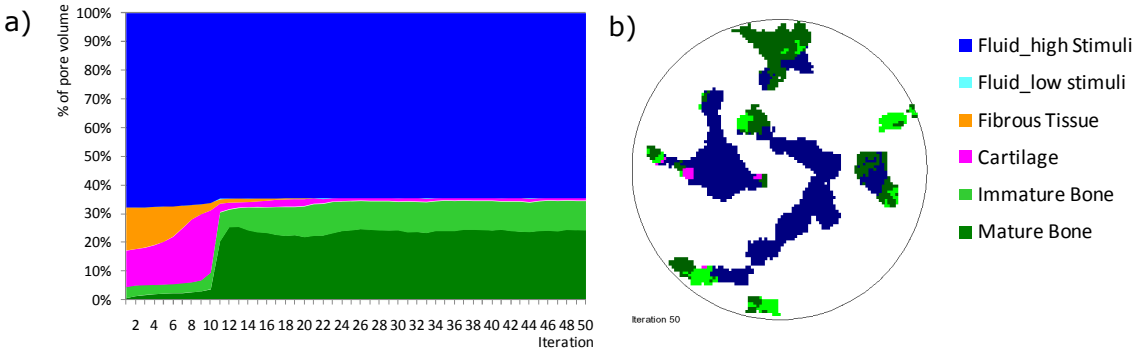

Fig 6.16. Mechano-regulatory stimuli distribution when using octahedral shear strain and fluid velocity. a) Stimuli distribution over the simulation and b) Stimuli distribution in a cross section of the scaffold at the end of the simulation.

6.4. DISCUSSION

The objective of this study was to propose a new method that allows to investigate the time course of the mechanical stimuli within a scaffold subjected to *in vitro* conditions. The hypothesis that different types of tissues were going to be predicted in different regions of the scaffold according to its morphology was not confirmed. It was expected that after a certain number of iterations, the mechanical stimuli became stable and that according to the pore size and the wall thickness, different tissues would form. Nevertheless, when constant inlet velocity was imposed to the scaffold, the mechanical stimuli became stable only in simulations with low tissue viscosity. In the cases of high tissue viscosity, when tissue was formed and the pores were blocked, the mechanical stimuli within the pores increased up to the level of cell death. Then tissue was resorbed and mechanical stimuli corresponding to bone was predicted. Because the simulation was not stopped, oscillations of stimuli over time were

predicted. Although the hypothesis was not confirmed, the proposed method captured the discontinuity of the fluid velocity and the mechano-regulatory stimuli within the scaffold pores and can be useful to improve the understanding of the mechanoregulation and hence the design of scaffolds and bioreactors.

Modifications were performed to the mechanoregulation theory of Prendergast et al. (1997). Fluid shear stress instead of fluid velocity was used as mechano-regulatory stimulus and regions where tissue could not be formed due to low fluid flow and high stimuli were included. The use of fluid shear stress instead of fluid velocity has a significant effect on the tissue distribution at the end of the simulations. This effect can be observed comparing the simulation performed using Prendergast et al. (1997) methodology with the simulations performed using the proposed methodology applying equivalent boundary conditions (constant fluid pressure). In both cases stimuli stabilized in most of the pore volume. However stimuli within the range of tissue formation were predicted in the well interconnected pores when fluid shear stress was used; while stimuli within the range of cell death were predicted in these pores when fluid velocity was used. The range of shear stress used in this study was based on a cell culture within a scaffold subjected to perfusion fluid flow (Cartmell et al. 2003 and Porter et al. 2005) and was corroborated by studies of Raimondi et al. (2006). The difference between the results obtained using different mechanical stimuli confirms the necessity to develop more long term *in vitro* and *in silico* studies using sample specific scaffolds in order to determine the stimuli that better describe cell behavior.

The maximum level of mechano-regulatory stimulus for tissue formation was already included in Stops et al. (2010b). In this case (fluid velocity was used as mechano-regulatory stimuli) the final distribution of tissue was not sensitive to this value. However, in this study the oscillations between tissues and cell death are generated by this limit; without it, stimuli within the majority of the pore volume would stabilize in the range of fibrous tissue. The region of low fluid shear stress where tissue is not differentiated had a minor effect on the overall results of the simulations. However, without this minimum level of stimuli, bone would be predicted in regions where low stimuli had been computed, and the low interconnected pores could not be identified.

Uncoupled mechanical studies of solid and fluid phases were performed. As described in Chapter 4, since the strain and the fluid pressure are lower than 0.5% and 3 Pa, respectively, solid fluid interaction was neglected. Additionally, tissues were simulated as linear elastic solids (in the compressive load models) and as Newtonian fluids (in the fluid flow models) instead of as poroelastic materials. In the fluid flow models, the magnitude of the viscosity was used to model tissues, and fluid shear stress was used

as a mechano-regulatory stimulus. Because the shear stress is a function of both the viscosity and the gradient of velocity, the constant c had a significant effect on the results. In the simulations of constant inlet velocity, fluctuations of mechanical stimuli over time appeared for high levels of c. In the simulations of constant inlet pressure, the percentage of volume where bone tissue was predicted decreased when c was increased. Additionally, the number of iterations of the stimuli fluctuation was related to the number of iterations used to compute the material properties, that was fixed to 10 (Lacroix et al. 2002). The simulations performed were not validated, therefore determining the right level of tissue viscosity necessary to simulate tissue formation and the time necessary for tissue maturation is still a challenge. In spite of this important limitation, the simulations illustrated the mechanoregulation of tissue differentiation over time in a scaffold subjected to perfusion fluid flow, showing that the system become unstable once tissue mineralized.

The use of a Newtonian fluid formulation in addition to be computationally less expensive than the poroelastic formulation, allowed simulating the perfusion flow controlling the inlet velocity and computing fluid shear stress. It has been previously demonstrated that the simulation of this mechanical stimulus is critical since peaks of fluid flow can be generated due to the micro-morphology of the scaffold. This formulation was also used by Stops et al. (2010b) to predict tissue differentiation; however, due to the high porosity (95%) of the scaffold used in their study, the fluid velocity distribution was uniform and consequently the mechanoregulation was less sensitive to the perfusion fluid flow than to the compressive load. In this study, mechanoregulation within the scaffold was more sensitive to the fluid shear stress than to the octahedral shear strain. When tissue was differentiated and began to fill the scaffold pores, the distribution of octahedral shear strain became uniform, while the distribution of fluid shear stress did not.

The fact that MSCs need to maintain their 3D form in order to differentiate into chondrocytes (Glowacki et al. 1983) was not considered in this study. It was assumed that MSCs could differentiate into osteoblasts, chondrocytes and fibroblasts, even though the studied scaffold had pores large enough to allow cells to spread and to lose their 3D form. Since stimuli equivalent to cartilage formation represented less than 6% of the scaffold pore volume, this limitation did not have a significant influence on the obtained results. Nevertheless, this aspect should be accounted if this methodology is used to predict chondrogenesis. Additionally, *in vitro* experimental techniques do not lead to mature bone yet, therefore in the mechanoregulation concept the mature bone zone could be replaced by immature bone. Because minor

changes in the results would happen with such a change, this aspect was neglected in order to avoid more changes in the initial mechanoregulation concept.

This study presented a novel methodology to determine the dynamics of stimuli within a scaffold due to the formation of new tissue. The obtained results demonstrated the discontinuity of the stimuli over time within a scaffold applying constant fluid flow when tissue is formed determining the effect of the pore obstruction on the fluid flow. Studies performed using the mechanoregulation theory of Prendergast et al. (1997) did not capture this discontinuity. Since Byrne et al. (2007) used a poroelastic formulation only modeling a compressive load; the perfusion fluid was not investigated. Stops et al. (2010b) used a Newtonian fluid formulation, although they did not take into account the variation in the fluid velocity at each specific point within the scaffold due to tissue formation.

A modification of the mechanoregulation concept of Prendergast et al. (1997) was used to determine tissue differentiation at each specific location of the scaffold pores according to the local mechanical stimuli. Although this overall concept has been successfully applied to predict tissue differentiation *in vivo* regenerative processes; it has not been extensively used to simulate tissue differentiation in vitro where the mechanism of MSC differentiation can be different than in vivo. Because no other mechanoregulation theory has been used to predict the effect of mechanical loading on cell differentiation in *in vitro* bioreactors, and because the theory proposed by Prendergast et al. (1997) has been demonstrated to be most suitable *in vivo* (in particular for the fluid flow contribution (Isaksson et al. 2006)), this concept was used in this study. Further studies under controlled environment and scaffold structures need to confirm whether such approach can be used qualitatively in any tissue engineering application and whether the mechanoregulation thresholds regulating cell differentiation are valid quantitatively *in vitro*.

Limited studies have reported information of *in vitro* perfusion cultures of MSCs on CaP scaffolds. Holtorf et al. (2005) observed an increment in the total number of cells in the first 4 days and the formation of a thin layer of bone in the pore walls within the first 8 days. Although new bone was differentiated, an unexplained decrease in the cell number was observed after few days. One possible explanation for this phenomenon may come from the results obtained in this study: when bone is synthesized the overall scaffold porosity decreased causing an increase on the fluid shear stress that reduces the mechanical viability of the environment for cells to survive.

According to the results obtained in this study, stimuli equivalent to specific tissue phenotypes stabilized within the pores only if a constant pressure was applied to the

scaffold, because the total fluid flow decreased. This suggests that in order to maintain the mechanical stimuli within a physiological range once tissue is formed within the scaffold, the velocity applied should be decreased, instead of being constant as it is currently applied in most of *in vitro* studies. This type of *in silico* studies can contribute to the improvement of the design of scaffolds for tissue engineering (Lacroix et al. 2009). Combining the appropriate material properties (Byrne et al. 2007) with the right scaffold morphology (Olivares et al. 2009) an ideal scaffold can be designed. Additionally, specific mechanical conditions for a bioreactor can be determined in order to maximize the performance of each scaffold.

6.5. CONCLUSION

The method proposed in this study, in which solid and fluid phases were discretized and the effect of both compressive loading and perfusion fluid flow was investigated, allowed capturing the discontinuity of the mechanical stimuli affecting cells seeded within a scaffold over time. Important variations on the fluid shear stress due to formation of new tissue and the corresponding porosity change were detected. If these fluid shear stress variations are not controlled, the formation of tissue within a scaffold may not be possible.

CHAPTER 7
Study of Angiogenesis

7.1. INTRODUCCION

The morphology of constructs has an important influence on the local mechanical stimuli sensed by cells attached to the internal walls of the material. In Chapter 4 it was demonstrated that, according to the pore distribution, the microscopic stimuli within the material can be much higher or lower than the macroscopic stimuli applied to the scaffold. In addition, in Chapter 6 it was found that important oscillations of mechanical stimuli can be transmitted to the cells over time when the scaffolds are subjected to constant perfusion fluid flow. *In vitro*, the perfusion flow plays and important role since it is the mean of transportation of cells, oxygen and nutrients. *In vivo*, the formation of a vascular network (angiogenesis) which supply cells with oxygen and nutrients is essential for their survival.

Checa and Prendergast (2009) proposed a mechanobiological model to simulate capillary network formation and its effect on tissue growth in a bone/implant interface using the lattice modeling approach. This model includes individual cell processes like proliferation, migration, differentiation and apoptosis and simultaneously uses consecutive lattice points to represent capillaries. This model was also applied to a simplified scaffold for bone tissue engineering (Checa and Prendergast 2010), relating the number of cells initially seeded into the scaffold to the rate of vascularization and the penetration of the vascular network. The effect of the mechanical load magnitude applied to the scaffold on bone formation and capillary growth was also studied. The

mechanobiological model of Checa and Prendergast (2009) was applied to a scaffold of regular geometry, i.e. constant pore size and pore distribution. Therefore the effect of the irregular morphology has not been studied.

The objective of this study is to investigate angiogenesis and tissue differentiation within the pores of a CaP scaffold with irregular morphology. To achieve this, the method presented in Checa and Prendergast (2009) was used to simulate the processes. It was hypothesized that the vascular network formed and the distribution of differentiated tissue are critically affected by the morphology of the scaffold.

7.2. METHODS

7.2.1. Material Sample and Computed Reconstruction

The cylindrical section of 1 mm diameter and 0.6 mm height of the glass ceramic scaffold described in Chapter 6 was used (Fig 7.1).

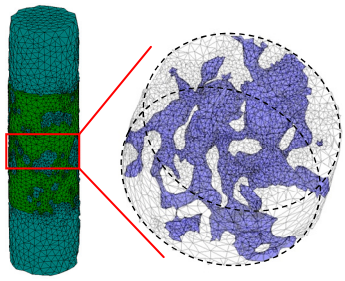

Fig 7.1. Section of the scaffold used for the simulations of angiogenesis and cell differentiation.

7.2.2. FE Model and Computation of Mechanical Stimulus

The mechanical stimulus regulating cell differentiation was defined as $S=\gamma/a+v/b$, where γ was the octahedral shear strain, v was the fluid velocity (in mm/s), and a and b were empirical parameters equal to 0.0375 and 0.003 mm/s respectively (Prendergast et al. 1997). S was computed from the FE model using a poroelastic formulation in Abaqus (Simulia, RI-USA). Unconfined compressive strain in the scaffold was simulated fixing the nodes at the bottom of the sample and applying displacement to the nodes at the top. Null pressure at the outside of the interconnected pores was imposed allowing fluid flow across the boundary.

7.2.3. Angiogenesis and Cell Differentiation Algorithms

Angiogenesis and cell differentiation were simulated within the interconnected pores of the scaffold. This domain was divided in equidistant points (lattice points) forming an orthogonal grid (Fig 7.2). Each point represented the volume space that can be occupied by one cell and its extracellular matrix. The distance between each point was 10 μm.

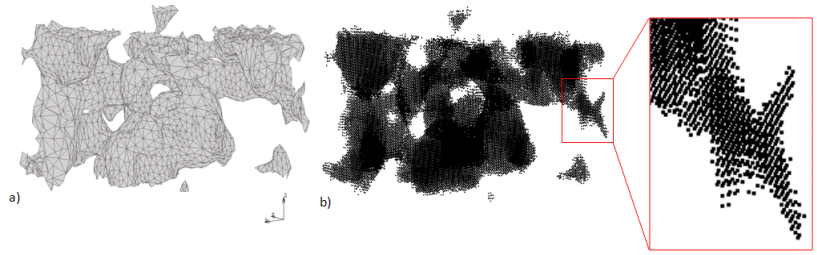

Fig 7.2. a) Pore mesh and b) lattice points were the cell activity is simulated

Cell activity was mimicked in the lattice points following Bernoulli probability distributions; it means that an event occurred with a probability p or not with a probability (1-p) (Checa and Prendergast 2009). A schematic flow chart of the methodology is showed in Fig 7.3 and the parameters and probabilities used in this study are summarized in Table 7.1. Since the degradation rate of phosphate glasses is very slow (less than 2% of weight in 80 days (Navarro et al. 2003)), scaffold degradation was not simulated and the mesh and the lattice did not change. Each iteration represented one day.

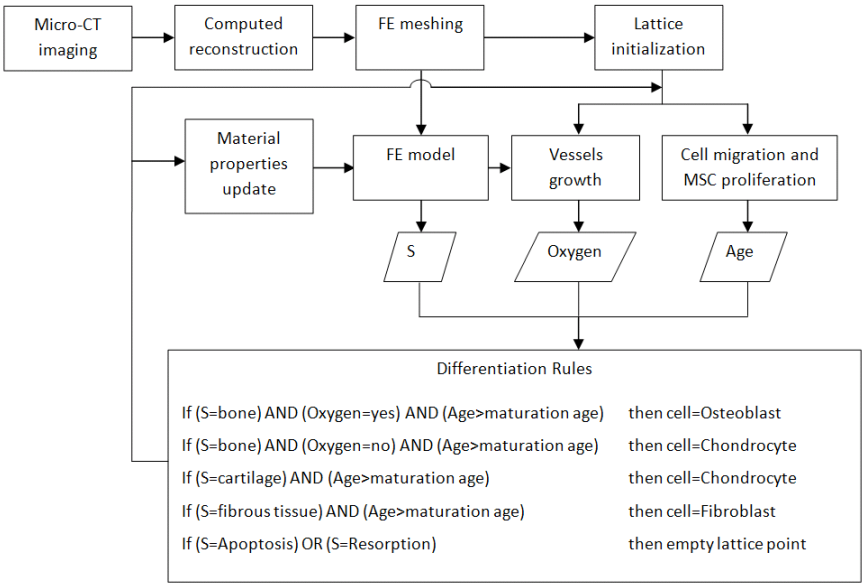

Fig 7.3. Schematic representation of the algorithm used to simulate angiogenesis and tissue differentiation.

Table 7.1. Parameters used in the Algorithm of angiogenesis and cell differentiation.

Cell type	Process	Probability/Rate /Frequency	Reference
MSCs	*In vivo* initialization	0.3	Checa and Prendergast (2010)
MSCs	*In vitro* seeding initialization	N(1.5,0.45)	
MSCs	Differentiation	0.3	Isaksson et al. (2008)
Osteoblasts	Apoptosis	0.15	Isaksson et al. (2008)
Chondrocytes	Apoptosis	0.1	Isaksson et al. (2008)
Fibroblasts	Apoptosis	0.05	Isaksson et al. (2008)
MSCs	Proliferation	0.6	Isaksson et al. (2008)
Osteoblasts	Proliferation	0.3	Isaksson et al. (2008)
Chondrocytes	Proliferation	0.2	Isaksson et al. (2008)
Fibroblasts	Proliferation	0.55	Isaksson et al. (2008)
	Oxygen diffusion distance	100 μm	Carmeliet and Jain (2000)
MSCs Fibroblasts	Migration rate	30 μm/h	Appedu and Shur (1994)
ECs	Initialization	0.1	Checa and Prendergast (2009)
ECs	Vessel branching	$\begin{cases} 0 & \text{if length}<10 \\ (1/20)*\text{length}-1/2 & \text{if } 10<\text{length}<30 \\ 1 & \text{if } 30<\text{length} \end{cases}$	Checa and Prendergast (2009)
ECs	Vessel rate of growth	$\begin{cases} -(33/5)*S+33 & \text{if } S<5 \\ 0 & \text{if } S>5 \end{cases}$	Checa and Prendergast (2009)
ECs	Vessel direction of growth	Random direction with p=0.4 Previous direction with p=0.2 VEGF direction with p=0.4	Checa and Prendergast (2009)

7.2.4. MSCs and ECs Initialization

Two different cases of MSCs initialization were simulated. In the first case, called *in vitro* seeding, an *in vitro* MSCs seeding previous to the scaffold implantation was assumed, consequently MSCs were attached to the walls of the material at the beginning of the simulation. In the second case, called *in vivo* colonization, no previous *in vitro* seeding was performed, then it was assumed that MSCs were initially located at the outside of the interconnected pores.

At the beginning of the simulation, each lattice point at the surface of the scaffold, or at the outside of the interconnected pores according to the case, had a probability for locating a cell. In the first case, this probability was based on the mechano-regulatory stimulus S corresponding to the lattice point and had a Gaussian distribution with mean 1.5 and variance 0.45. These mean and variance were fixed so that the mean value of the initial number of MSCs corresponded to an *in vitro* seeding efficiency of 40% (Lopez-Heredia et al. 2008). In the second case, the probability was 0.3. Initially, every MSC had a maturation age of 1 and it was increased by 1 each iteration. For both cases of MSCs initialization, ECs were located at the outside of the interconnected pores; each unoccupied lattice point had a probability of 0.1 of locating a cell.

7.2.5. MSCs Differentiation

Every MSC with a maturation age higher than 5 differentiated with a certain probability. If a cell differentiated, the phenotype was assigned according to the mechano-regulatory stimuli S corresponding to the specific location of the cell. When S corresponded to osteoblastic differentiation, oxygen supply was taken into account. If there were one or more ECs within the surrounding space corresponding to the oxygen diffusion distance around the MSC, the cell differentiated into an osteoblast. Else, it differentiated into a chondrocyte.

7.2.6. Cell Apoptosis

Any osteoblast, chondrocyte or fibroblast located in a lattice point whose mechanical stimulus did not support that cell phenotype led to apoptosis with a probability p. Additionally, if the stimulus S was higher than 6, the cell became apoptotic.

7.2.7. Cell Proliferation

Every cell proliferated with a probability p. If a cell proliferated, mitosis occurred and the cell was replaced by two daughter cells. The new cells occupied two points selected at random within the original location and its empty neighbouring locations.

7.2.8. Cell Migration

Every MSC and fibroblast migrated; it means that they moved to any empty point beside them. The new position was selected at random. If there were no unoccupied neighboring locations then migration stopped. Since osteoblasts and chondrocytes are less motile, migration was not simulated.

7.2.9. Angiogenesis

Blood vessels were represented as a continuum sequence of lattice points occupied by ECs. For the angiogenesis process, the direction and the rate of growth of each vessel, and its probability of branching were defined. The direction of growth was assigned according to three cases. In the first case the direction was assigned randomly, in the second case the direction was the same than the previous growth direction and in the last case the vessel grew towards the region with the highest concentration of chondrocytes under a mechanical stimulus corresponding to osteoblasts (representing the VEGF influence). The rate of growth was defined as a function of the mechanical stimulus at the front of the vessel. The probability of branching was assigned according to the length of the vessel. Each vessel grew according to its defined variables. Functions and probabilities are shown in Table 7.1.

7.2.10. Material Properties

After each iteration, the element material properties (Young´s modulus, Poisson´s ratio, permeability and bulk modulus) were computed as an average of the properties for the tissue phenotypes predicted in the lattice points within the element in the last 10 iterations (Lacroix et al. 2002). Material properties are shown in Table 7.2.

Table 7.2. Material properties used in the FE models of the simulations of angiogenesis.

	Granulat. Tissue[a]	Mature Bone[a]	Immat. Bone[a]	Cartilage[a]	Fibrous Tissue[a]	Glass Ceramic
Young´s modulus (MPa)	0.2	6000	1000	10	2	455[b]
Poisson´s ratio	0.167	0.3	0.3	0.167	0.167	0.33[b]
Permeability (10^{-14} m^4/Ns)	$4x10^6$	37	10	0.5	1	1
Bulk modulus grain (MPa)	2300	13920	13920	3700	2300	13920
Bulk modulus fluid (MPa)	2300	2300	2300	2300	2300	2300

a Lacroix et al. 2002
b Lacroix et al. 2006

7.2.11. Simulations

In order to study the effects of the total strain magnitude and the MSCs seeding mode on the tissue formation process, four cases were simulated, varying the compressive strain (0.5% and 1%) or varying the initial cell seeding (*in vitro* and *in vivo*), see Table 7.3.

Table 7.3. Simulations using different compressive strain magnitudes and MSCs initialization modes.

Simulation	Total Compressive Strain	MSCs initialization
1	0.5 %	*In vitro* seeding
2	0.5 %	*In vivo*
3	1.0 %	*In vitro* seeding
4	1.0 %	*In vivo*

7.3. RESULTS

The growth of vessels and cell differentiation over time in a cross section through the center of the scaffold for all simulations is shown in Fig 7.4. Most of the capillaries started growing from the periphery of the sample at iteration 1 and were blocked by the walls of the scaffold, with only a few vessels branching. Therefore, pores located at the surface of the sample were well vascularized but pores at the center were not. MSCs proliferated and started filling the scaffold during the first iterations. A rapid differentiation of cells into osteoblasts and chondrocytes was predicted between iterations 10 and 20 when the first stem cells achieved the maturation age. When an *in vitro* cell seeding was simulated (Simulations 1 and 3), at iteration 20 the pores were filled with MSCs, osteoblasts and chondrocytes. At iteration 30 most of the stem cells had differentiated and after 100 iterations the dynamics of proliferation, differentiation, and apoptosis was stable. When an *in vivo* cell migration was simulated (Simulations 2 and 4), homeostasis was achieved at iteration 200 because cells had to migrate from the exterior of the scaffold and took more iterations to fill the pores.

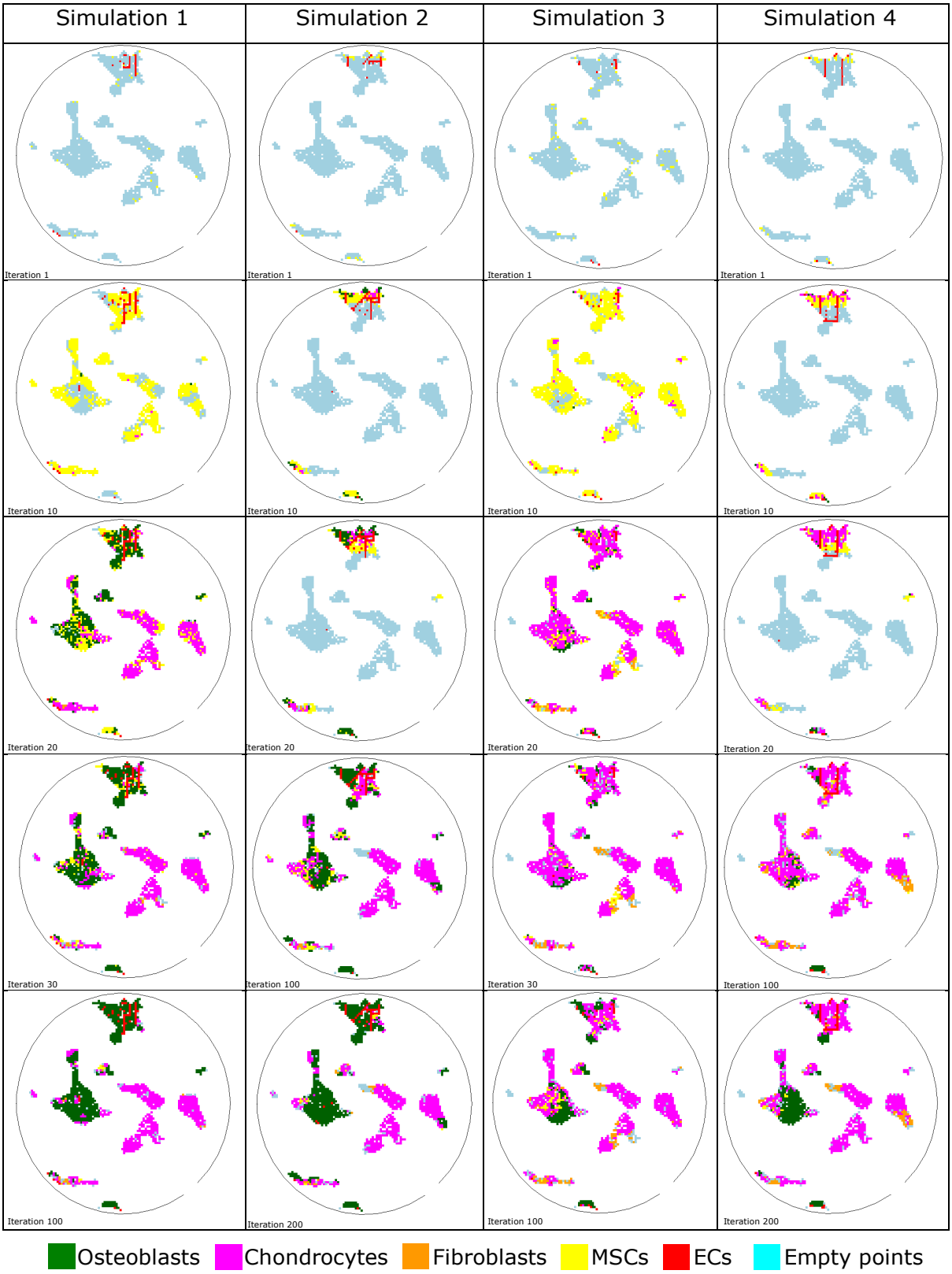

Fig 7.4. Vessels formation and tissue differentiation over the simulations.

The evolution of the effective Young´s modulus during the simulation is shown in Fig 7.5. When cells started differentiating, the stiffness of the sample started increasing. Throughout the simulation the effective scaffold Young´s modulus increased from 26.44 MPa to 41.14 MPa for simulation 1, to 43.15 MPa for simulation 2, to 28.19 MPa for simulations 3, and to 28.46 MPa for simulation 4 (Fig 7.5).

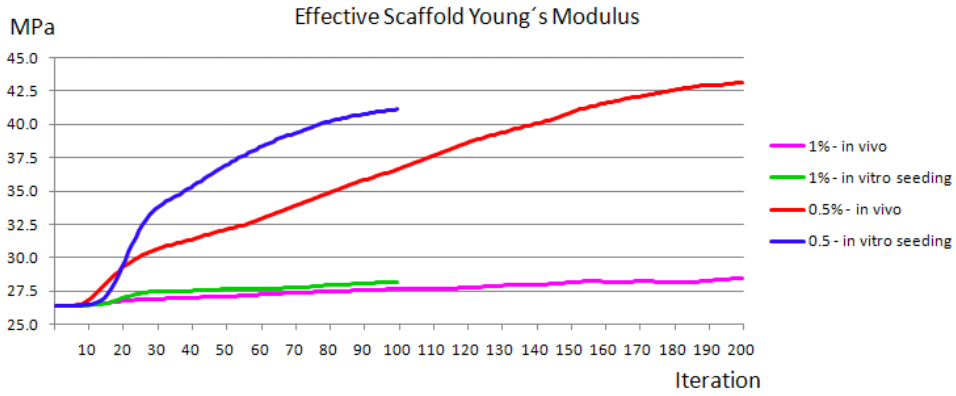

Fig 7.5. Effective scaffold Young´s modulus over the simulations.

The mechano-regulatory stimulus S (as opposed to tissue type in Fig 7.4) influencing each lattice point at the first and last iterations is shown in Fig 7.6.

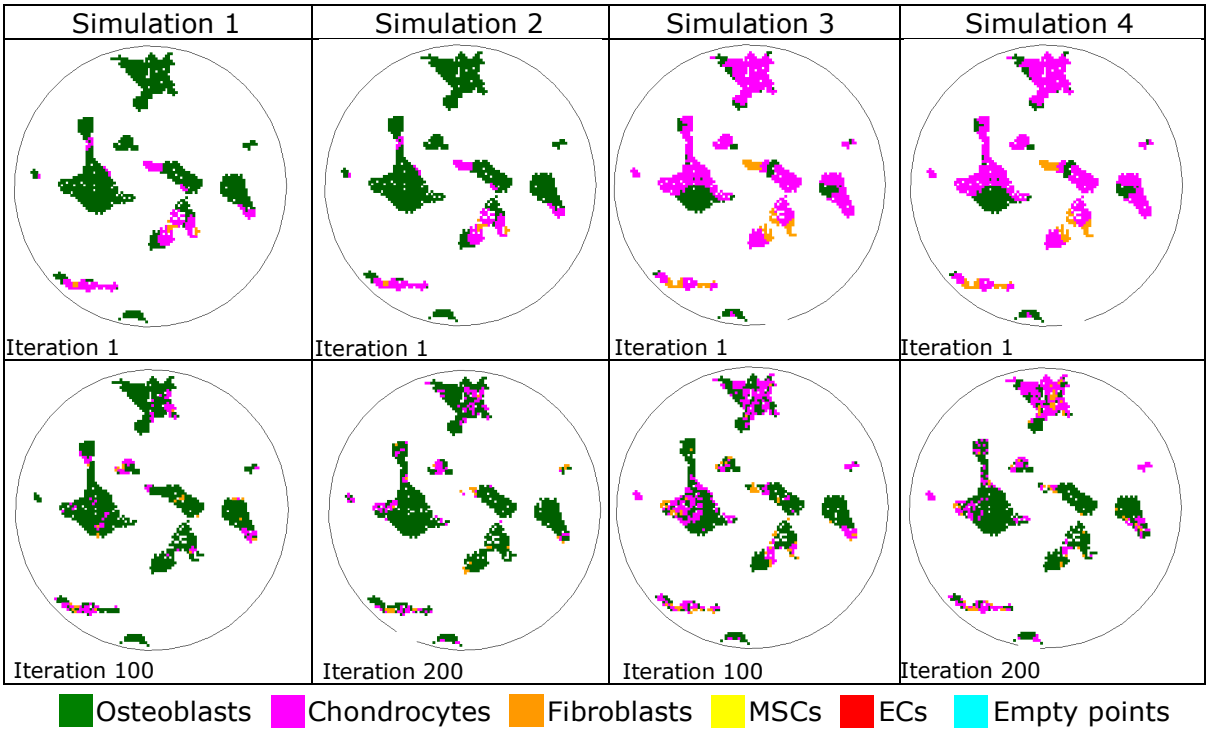

Fig 7.6. Mechano-regulatory stimuli distribution over the simulations.

At iteration 1 it was not possible to find a direct relation between pore size and stimuli, since simultaneous stimuli corresponding to bone, cartilage and fibrous tissue were computed in most of the pores. When 0.5% of deformation was applied (Simulations 1 and 2), stimuli corresponding to bone was predicted in most of the pore volume. When de applied deformation was increased to 1% (Simulations 3 and 4) cartilage stimuli instead of bone stimuli dominated the volume (Fig 7.6). At the end of the simulations, the stimuli distribution is different because of the increase in the scaffold stiffness described below. Most of the mechanical stimuli predicted were those of bone formation when 0.5% of deformation was applied and those of bone and cartilage formation when 1% of deformation was applied (Fig 7.6).

Although most of the stimuli corresponded to bone formation, different types of tissue were predicted within the pores of the sample (Fig 7.7). When the total strain applied was 0.5% of deformation, 70% of pore volume corresponded to bone stimuli but, because of the lack of oxygen, only 40% of the cells in this volume differentiated into osteoblasts. At the end of the simulations 40% of the pore volume was filled with osteoblasts, 40% with chondrocytes and 3% with fibroblasts (Fig 7.7). Osteoblasts were predicted in the pores located at the periphery of the sample (well vascularized regions), whereas chondrocytes were predicted in the internal pores (poor vascularized ones) and fibroblasts were predicted in the narrow regions where there was a high fluid flow (Fig 7.8). When the total strain was increased to 1% of deformation, 45% of pore volume corresponded to bone stimuli but, only 11% of the pore volume was filled with osteoblasts. At the end of the simulations of high stain (1% of deformation) 11% of the pore volume was filled with osteoblasts, 59% with chondrocytes, and 8% with fibroblasts (Fig 7.7). Chondrocytes were predicted in both, internal and external pores (Fig 7.8).

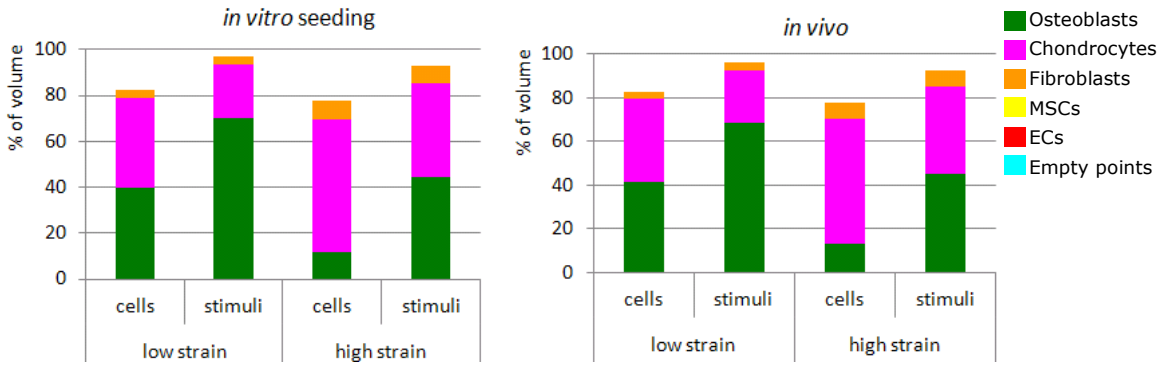

Fig 7.7. Histograms of cell differentiation and mechano-regulatory stimulus distributions at the end of the simulations.

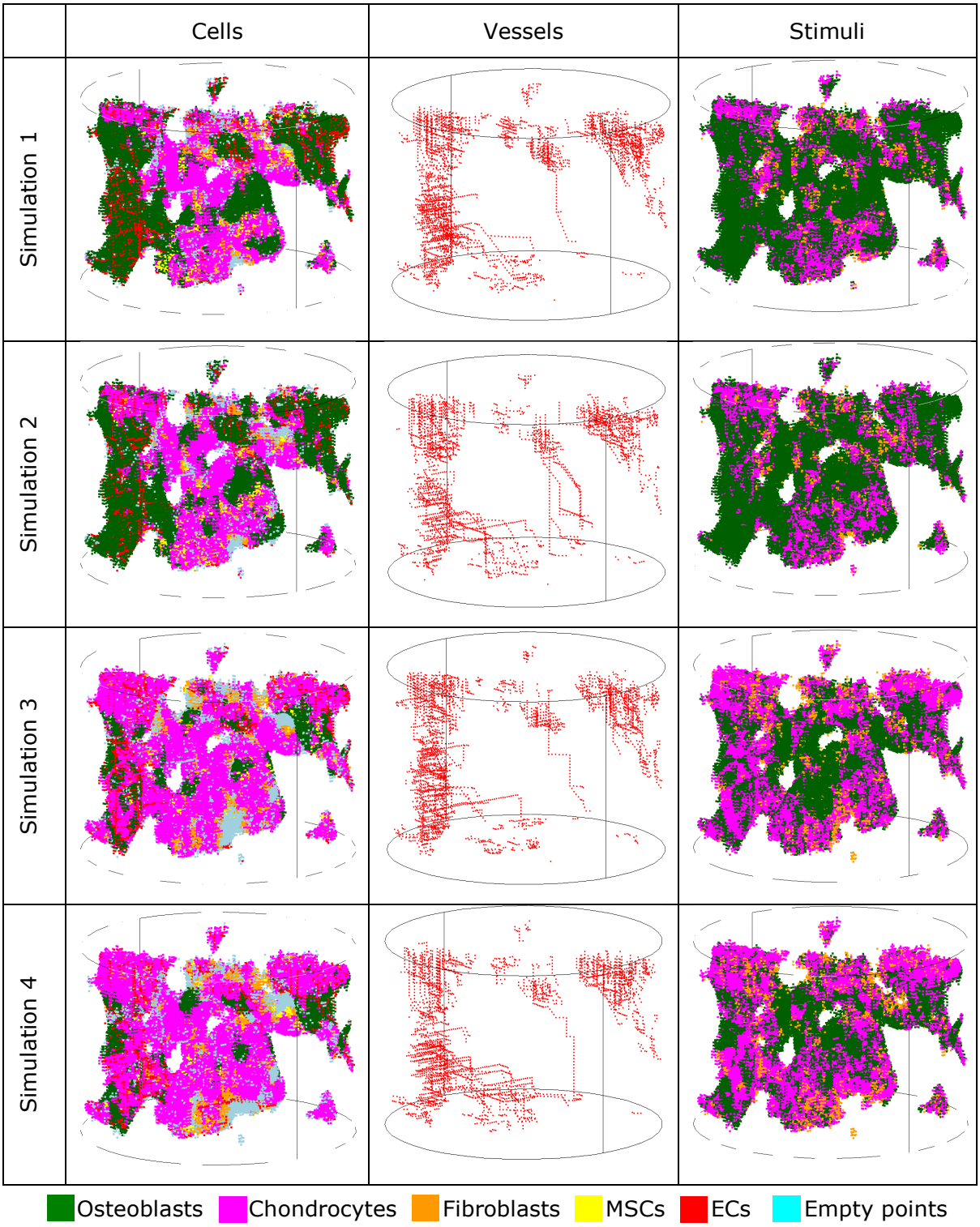

Fig 7.8. Cells distribution compared to mechanical stimuli distribution at the end of the simulations

The vascular network formation was not very sensitive to the MSCs seeding mode. Similar distributions of vessels were predicted whether an *in vitro* seeding or an *in vivo* colonization was simulated (Fig 7.7 and Fig 7.8). The MSCs seeding mode did not have either an evident effect on the distribution of tissue at the end of the simulation. Nevertheless, when previous *in vitro* seeding was simulated, the cells migrated and proliferated faster than when *in vivo* colonization was simulated (Fig 7.4).

For the magnitudes of mechanical strain studied (0.5% and 1% of total deformation), there was not a noticeable effect on angiogenesis. Similar vessel networks were observed in both cases of strain (Fig 7.8). Nevertheless different types of tissues were observed within the pores of the sample according to the mechanical strain applied (Fig 7.7 and Fig 7.8). When 0.5% of deformation was simulated osteoblasts were predicted in well vascularized regions and chondrocytes in poor vascularized ones. When the total strain was increased to 1% of deformation, chondrocytes were predicted in both, internal and external pores.

7.4. DISCUSSION

In this work we set out to investigate vascularization and tissue formation inside a glass ceramic scaffold of 21% of interconnected porosity with irregular morphology. It was predicted that scaffold walls blocked blood vessel growth and consequently, most of the vessels did not reach the center of the sample and a vascular network was mainly formed in the external pores. Therefore, when a compressive strain of 0.5 % was applied, 70% of the pore volume was under a mechanical stimulus favorable for bone formation; however, because of the lack of oxygen in some regions, MSCs differentiated into chondrocytes instead of osteoblasts and only 40% of bone was formed. In the scaffold with regular morphology studied by Checa and Prendergast (2010) full vascularization was achieved and consequently cell differentiation depended mainly on the mechanical stimuli. This difference suggests that in terms of the architecture of the samples, it is necessary to ensure a structure that not only has high porosity and interconnectivity, but also that the space between pores allows vessels to reach the center of the scaffolds and form a vascular network.

The magnitude of the mechanical strain applied to the sample had an important effect on tissue differentiation. When the compressive strain was increased from 0.5% to 1%, osteogenesis decreased from 40% to 15%. This result showed that the sensitivity of cell differentiation to small changes in the magnitude of the strain should be considered in *in vivo* experiments where bone chambers are used to apply controlled

mechanical stimuli. Additionally, when the material is implanted directly into bone, the performance of the scaffold can change depending on the implantation site because of the variation of the loads and therefore the mechanical stimuli along the bone.

MSC seeding conditions did not affect the final pattern of differentiated tissue. Similar results were obtained when *in vivo* or *in vitro* MSC seeding were simulated. The effect of increasing the number of cells seeded in the scaffold was not studied. Checa and Prendergast (2010) predicted that when the number of seeded cells was increased, the space for angiogenesis was decreased and a lower number of vessels was predicted. In this study, most of the vessels were formed at iteration one, then they were blocked and the rest of the space was filled with cells proliferating. When *in vivo* seeding was simulated, similar results than Checa and Prendergast (2010) were obtained; differentiation occurred first in the external pores and then in the internal ones, the tissue formation was slower than in the case of *in vitro* seeding.

The algorithm of mechanoregulation has been validated for bone healing (Isaksson et al. 2006a). A study of the parameters used in the algorithm of angiogenesis was done and its limitations were discussed in detail by Checa and Prendergast (2010). Here, the base line model parameters were used. Some parameters that are regulated by growth factors were simulated as random, for instance the differentiation rate, considered constant. The fact that cells do not migrate to regions where there is no oxygen was not considered by the algorithm, so pores in the center of the sample, where angiogenesis did not occur, could be actually empty instead of being occupied by chondrocytes. The results of this study were consistent with the *in vivo* observations of Del Valle et al. (2007) for the macroporous CaP scaffolds and Jones et al. (2007) for the hydroxyapatite scaffolds. Del Valle et al. (2006) found that blood vessels were present near the surface of the cement and that bone growth occurred mainly in the peripheral pores. They affirm that the lack of bone tissue penetration in the central part of the implant was due to the limited interconnectivity between adjacent pores. Jones et al. (2007) showed that approximately 40 % of pores occupied by bone tissue were near the surface and this fraction dropped within 1 mm of the periphery where most pores were free of bone ingrowth. The use of sample specific models to compare *in vivo* and *in silico* results can be useful to improve the development of this kind of models. Bone ingrowth into biomaterials in *in vitro* or *in vivo* experiments can be assessed using μCT images (Porter et al. 2007, Van Lenthe et al. 2007).

The mechanoregulation model of Prendergast et al. (1997) predicts fibrous tissue formation when the mechano-regulatory stimuli is higher than 3. However, cells can undergo apoptosis under high levels of strain (Kearney et al. 2008). In order to take

this effect into account, a maximum limit was included in the model, if the mechanical stimuli were higher than 6 no tissue was differentiated. In the studied scaffold, the percentage of pore volume affected by stimuli out of the physiological range, being resorption or apoptosis, increased from 17% to 22% when the mechanical strain was increased from 0.5% to 1% of compression. This increment was low (only 5%), because the magnitude of the mechano-regulatory stimuli S in most of regions where apoptosis occurs was much higher than the maximum limit applied. Consequently, the obtained results were not sensitive to the assumed value of 6 for the limit between fibrous tissue formation and apoptosis.

At the beginning of the simulation, there was not a clear correlation between stimuli and pore size or pore location, different stimuli were observed within every pore. It was studied in Chapter 4 that the octahedral strain depends on the thickness of the scaffold walls and the fluid velocity on the pore interconnectivity making the distribution of the mechano-regulatory stimuli not evident. When tissue growth was simulated, the scaffold stiffness increased and consequently stress and strain were better distributed across the material. At the end of the simulation the stimuli were mostly in favor of bone formation. Because the mechanical stimuli changed over time due to the formation of new tissue, investigations on the effect of mechanical loading on the distribution of mechanical stimuli within an empty scaffold help to determine the behavior of the scaffold, but they are not enough to predict the success of the material once tissue starts to differentiate. Consequently, a dynamical analysis is necessary to understand the contribution of the geometry and to predict the mechanoregulation within scaffolds for bone tissue engineering.

7.5. CONCLUSION

This study provided information on the dynamics of mechanical stimuli, angiogenesis and tissue differentiation within the interconnected pores of a CaP scaffold with irregular morphology caused by mechanical compressive strain. Different types of tissues were predicted into the scaffold depending not only in the mechanical stimuli distribution but also in the blood vessel network formation. Osteogenesis was not predicted in most of the pores at the center of the scaffold. This information contributed to the understanding of the effect of angiogenesis and mechanical stimuli on tissue differentiation within the CaP scaffolds. Such kind of studies combined with *in vivo* and *in vitro* experiments are essential to the improvement of scaffold development.

CHAPTER 8
Conclusions

8.1. SUMMARY OF RESULTS

The architecture of a CaP cement and a glass ceramic scaffolds was reconstructed in 3D using μCT images. Pore distribution, shape and interconnectivity were studied. The pores were not well interconnected and distributed throughout the scaffolds. A higher pore concentration was detected at the bottom side than at the top side, additionally pores were not well interconnected between them or with the exterior of the scaffolds.

When the scaffolds were subjected to compressive load, stresses and strains at the solid phase followed Gaussian distributions with mean value consistent to the value of global strain applied. Most of scaffold walls were under compression and no peaks of strain were predicted. When tissue formation was simulated within the scaffold pores, the apparent stiffness of the scaffold increased and the magnitude of mechanical stimuli within the pores decreased.

When perfusion fluid flow was simulated, fluid velocity, pressure and shear stress did not follow a specific distribution. Some pores presented fluid flow almost nil while in some others the velocity increased between 100 and 1000 times the inlet fluid velocity. Peaks of fluid velocity and shear stress that may be associated to cell death were predicted. When tissue formation was simulated, the fluid shear stress predicted depended on the boundary conditions applied to the scaffold and the parameters used for the simulations. When tissue was differentiated and filled the scaffold pores, if a

constant inlet velocity was used, the fluid shear stress increased up to a level of cell death. However, if a constant pressure was used the total fluid flow decreased and the fluid shear stress remained within levels viable for cell survival.

When angiogenesis was simulated, vascularization was not predicted in the pores at the center of the scaffold due to the low porosity and pore interconnectivity of the material. The lack of vessels in most of scaffold pores caused the prediction of cartilage instead of bone in almost 30% of the pore volume. Additionally, the predicted tissue was highly sensitive to the magnitude of the load. An increase from 0.5% to 1% of total deformation of the scaffold caused a decrease of 29% on the predicted bone tissue.

8.2. LIMITATIONS

Only two scaffolds were used for the simulations. Moreover, because of the complexity of the structure and the computational cost necessary to mesh and to model such materials, only one section of each scaffold was studied. However, the sections were representative of the structure and the models illustrated well the correlation between the morphology of the scaffolds and the distribution of the mechanical stimuli.

The resolution of the μCT images were 7.8 x 7.8 x 12.2 μm^3, therefore, pores of size lower than this magnitude were not detected. The porosity of the CaP scaffold is divided in micro-porosity which corresponds to the intrinsic porosity of the material and macro-porosity which is the one that account for tissue differentiation. The macro-porosity was well detected by the μCT.

The methods proposed in this study to investigate the mechanoregulation of tissue differentiation were based on the concept of Prendergast et al. (1997). This concept does not include biological factors that affect cell activity and tissue differentiation different than mechanical stimuli. However, it has been demonstrated to be the most suitable to predict *in vivo* regenerative processes, in particular for the use of fluid flow. In this thesis, the method developed at Chapter 6 (the study of the mechanoregulation of tissue differentiation when the scaffold is subjected to perfusion fluid flow and compressive load) neither includes biological factors; modifications to the original concept were performed in order to take into account the effect of the perfusion fluid flow. The method used at Chapter 7 (the study of angiogenesis and tissue differentiation) proposed by Checa and Prendergast (2009) includes the effect of the VEGF into cell migration and the effect of oxygen availability into cell

differentiation. No other theory has been used to study tissue differentiation in scaffolds for tissue engineering.

The main limitation of this thesis was the lack of validation. The parameters used to model tissue as an elastic solid were taken from literature. The appropriate viscosity necessary to model tissue as a fluid flow is unknown. The parameters for the angiogenesis model were taken also from the literature. The obtained results were very sensitive to the parameters used, especially when using viscosity to model tissue maturation. For this reason it was not possible to conclude about the efficiency of the scaffolds for cell seeding or tissue differentiation or about the exact mechanical loads that should be applied to the scaffolds in order to optimize their performance. However, the results illustrate the differences between the macro mechanical stimuli applied and the micro mechanical stimuli within the scaffold pores generated by the scaffold morphology and the changes of mechanical stimuli over time due to tissue formation. These results can be an explanation of the difficulties faced currently *in vitro* to seed cells or to differentiate tissue.

Tissue formation was modeled changing the material properties, Young´s modulus, Poisson´s ratio, viscosity, and permeability. Since the development of constitutive equations assumes continuity at the material properties, this approximation represents a limitation.

8.3. CONTRIBUTIONS

This study investigated the distribution of mechanical stimuli in scaffolds of irregular morphology and the mechanoregulation of tissue differentiation when the scaffolds are subjected to perfusion fluid flow and compressive loads. Additionally, the mechanoregulation of angiogenesis and tissue differentiation under compressive loading was studied. Most of previous biomechanical studies of scaffolds for tissue engineering had investigated the mechanical stimuli distribution without including the time course of tissue differentiation and the consequent changes in the specific mechanical stimuli transmitted to the cells. The studies of tissue differentiation that had considered the variation on the mechanical stimuli transmitted to the cells over time had been limited to investigate the effect of compressive loading and most of them had been performed in simplified scaffolds. In this thesis, for the first time, a modified version of the mechanoregulation concept of Prendergast et al. (1997) was used to evaluate the dynamic mechanical stimuli acting in a real scaffold under

perfusion fluid flow in addition to compressive loading. And for the first time the methodology of angiogenesis modeling developed by Checa and Prendergast (2009) was applied to a scaffold of irregular morphology.

The methodology proposed in this thesis allowed to predict the discontinuity of the mechanical stimuli distribution, not only at the initial state of a cell culture but also over time. The results of this approach could not have been obtained using continuum models that do not account for the real architecture of the constructs.

The results obtained enlighten that:

1) The relation between applied macro mechanical stimuli, scaffold morphology, micro mechanical stimuli at each point of the construct, and tissue differentiated within a scaffold is not trivial. Because the entire structure is interconnected, the distribution of mechanical stimuli in each specific point depends on the rest of the scaffold. A change of morphology due to tissue differentiation in any place of the scaffold affects the distribution of mechanical stimuli at the overall scaffold.

2) It is necessary to guarantee a minimum level of pore size and interconnectivity that permits tissue formation without closing the pores, allowing the medium with oxygen and nutrients to continue flowing without increasing too much the fluid velocity and the fluid shear stress.

3) There is not a universal magnitude of fluid flow or compressive load that can be applied to scaffolds within bioreactors in order to maximize the seeding efficiency or the tissue differentiated. The magnitude of mechanical stimuli used to stimulate cells depends on the specific scaffold morphology and ideally, it should be computed numerically for each case.

4) The magnitude of mechanical stimuli applied over time to scaffolds within bioreactors may not need to be constant. In particular, when tissue starts to be differentiating, the fluid velocity should be decreased during the culture period in order to maintain the level of mechanical stimuli within a physiological range. The pattern of mechanical stimuli over time specific for each scaffold should be computed according to the state of tissue differentiation and maturation.

8.4. FUTURE PERSPECTIVES

Future work should be directed towards coupling numerical models with *in vitro* and *in vivo* approaches in order to increase the understanding of the process of mechanoregulation of tissue differentiation within scaffolds and therefore improve the success of biomaterials and scaffolds development. In particular future efforts should be addressed to:

1) Modeling the whole scaffold. Higher computational capacity is needed, as well as better computational techniques that allow automatic meshing reducing the necessary hand made process.

2) Integration of the solid and fluid models used to determine the combined mechanical stimuli affecting the cell, as well as their integration to poroelastic models in order to simulate tissue formed within the scaffold pores.

3) Validation of the different parameters used in the simulations. In particular, the levels of mechanical stimuli used for tissue differentiation and for cell death, the magnitude of the material properties used for modeling tissue as linear elastic solid and as fluid flow, and the time used for the transition on the material properties that represents tissue maturation.

4) Modeling specific cell activity in the study of the mechanoregulation under *in vitro* conditions, including the initial number of cells, the number of necrotic (or apoptotic) cells because of high stimuli, the interaction between cells and the interaction between cells and material.

5) Studying different scaffolds and different materials using sample specific *in vitro* and *in silico* experiments in order to compare tissue differentiated and tissue predicted over time.

6) Determining the pattern of mechanical stimuli over time, that optimized the performance of the scaffold in terms of cell differentiation.

References

Adachi T, Osako Y, Tanaka M, Hojo M and Hollister S (2006) Framework for optimal design of porous scaffold microstructure by computational simulation of bone regeneration. Biomaterials 27:3964-3972

Almirall A, Delgado JA, Ginebra MP and Planell JA (2004) Effect of albumen as protein-based foaming agent in calcium phosphate bone cement. Key Eng Mater 254-256:253-256

Ament CH and Hofer EP (2000) A fuzzy logic model of fracture healing. J Biomech 33:961–968

Appedu PA and Shur BD (1994) Molecular analysis of cell surface β-1,4-galactosyltransferase function during cell migration. Proc Natl Acad Sci, USA, 91:2095-2099

Avila G, Martínez S, Del Valle S, Ginebra MP and Planell JA (2005) Alcobe X. Study of porous glass ceramic made by foaming egg white. In: Proceedings of the international conference on porous ceramic materials, Bruges, Belgium, 20–21 October 2005

Bacabac RG, Smit TH, Cowin SC, Van Loon JJWA, Nieuwstadt FTM, Heethaar R and Klein-Nulend J (2005) Dynamic shear stress in parallel-plate flow chambers. J Biomech 38:159-167

Bailon-Plaza A and Van Der Meulen MCH (2001) A Mathematical Framework to Study the Effects of Growth Factor Influences on Fracture Healing. J Theor Biol 212:191-209

Biot MA (1941) General theory of three-dimensional consolidation. J Appl Phys 12:155-164

Byrne DP, Lacroix D, Planell JA, Kelly DJ and Prendergast PJ (2007) Simulation of tissue differentiation in a scaffold as a function of porosity, Young´s modulus and dissolution rate: Application of mechanobiological models in tissue engineering. Biomaterials 28:5544-5554

Caplan AI (2010) Mesenchymal Stem Cells: The Past, the Present, the Future. Cartilage 1:6-10

Carmeliet P (2000) Mechanisms of angiogenesis and arteriogenesis. Nat Med 6:389-395

Carmeliet P (2003) Angiogenesis in health and disease. Nat Med 9:653-660

Carmeliet P and Jain RK (2000) Angiogenesis in cancer and other diseases. Nature 407:249-257

Carter DR and Beaupré GS (2001) Skeletal function and form. Cambridge university press.

Carter DR, Beaurpé GS, Giori N and Helmes J (1998a) Mechanobiology of skeletal regeneration. Clin Orthop Rel Res 355S:S41-S55

Carter DR, Blenman PR and Beaupré GS (1988) Correlations between mechanical stress history and tissue differentiation in initial fracture healing. J Orthopaed Res 6:736-748

Carter DR and Giori N (1991) Effect of mechanical stress on tissue differentiation in the bony implant bed. In: J. Davies editor. The Bone-Biomaterial Interface. University of Toronto Press, pp 367-79

Carter DR, Helms JA, Tay BK and Beaupre GS (1998b) Stress and strain distributions predict tissue differentiation patterns in distraction osteogenesis. In: Trans. 44th Orthop Res Soc, p 234

Carter DR and Wong M (1988) The role of mechanical loading histories in the development of diarthrodial joints. J Orthop Res 6:804-816

Cartmell SH, Porter BD, Garcia AJ and Guldberg RE (2003) Effects of Medium Perfusion Rate on Cell-Seeded Three-Dimensional Bone Constructs in Vitro. Tissue Eng 9:1197-1203

Chao EYS and Inoue N (2003) Biophysical Stimulation of Bone Fracture Repair, Regeneration and Remodeling. European cells and materials 6:72-85

Charles-Harris M, Del Valle S, Hentges E, Bleuet P, Lacroix D and Planell JA (2007) Mechanical and structural characterization of completely degradable polylactic acid/calcium phosphate glass scaffolds. Biomaterials 28:4429-4438

Checa S and Prendergast PJ (2009) A mechanobiological model for tissue differentiation that includes angiogenesis: A lattice-based modeling approach. Ann Biomed Eng 37:129-145

Checa S and Prendergast PJ (2010) Effect of cell seeding and mechanical loading on vascularization and tissue formation inside a scaffold: a mechano-biological model using a lattice approach to simulate cell activity. J Biomech 43:961-968

Cioffi M, Boschetti F, Raimondi MT and Dubini G (2006) Modeling evaluation of the fluid-dynamic microenvironment in tissue-engineered constructs: a μCT based model. Biotechnol Bioeng 93:500-510

Claes LE and Heigele CA (1999) Magnitudes of local stress and strain along bony surfaces predicts the course and type of fracture healing. J Biomech 32:255-266

Claes LE, Heigele CA, Neidlinger-Wilke C, Kaspar D, Seidl W, Margevicius KJ and Augat P (1998) Effects of mechanical factors on the fracture healing process. Clin Orthop Rel Res 355S:S132-S147

Cowin SC (2002) Mechanosensation and fluid transport in living bone. J Musculoskelet Neuronal Interact 2:256-260

Del Valle S, Miño N, Muños F, González A, Planell JA and Ginebra MP (2007) In vivo evaluation of an injectable macroporous calcium phosphate cement. J Mater Sci: Mater Med 18:353-361

Doblare M, Garcıa JM and Gomez MJ (2004) Modelling bone tissue fracture and healing: a review. Eng Fract Mech 71:1809-1840

Fassina L, Visai L, Asti L,Benazzo F, Speziale P, Tanzi MC and Magenes G (2005) Calcified matrix production by SAOS-2 cells inside a polyurethane porous scaffold, using a perfusion bioreactor. Tissue Eng 11:685-700

Filmon R, Retailleau-Gaborit N, Grizon F, Galloyer M, Cincu C, Basle MF et al. (2002) Non-connected versus interconnected macroporosity in poly(2-hydroxyethil methacrylate) polimers. An X-ray microtomographic and histomorphometric study. J Biomater Sci Polym Ed 13:1105-1117

Garcıa JM, Kuiper JH, Doblare M and Richardson JB (2002) A numerical model to study the mechanical influences on bone fracture healing. Acta of Bioengineering and Biomechanics 4. Proceedings of the 13thConference of European Society of Biomechanics

Geris L, Andreykiv A, Van Oosterwyck H, Vander Sloten J, van Keulen F, Duyck J and Naert I (2004) Numerical simulation of tissue differentiation around loaded titanium implants in a bone chamber. J Biomech 37:763-769

Geris L, Gerisch A, Vander Sloten J, Weiner R and Van Oosterwyck H (2008a) Angiogenesis in bone fracture healing: a bioregulatory model. J Theor Biol 251:137-158

Geris L, Vandamme K, Naert I, Vander Sloten J, Duyck J and Van Oosterwyck H (2008b) Application of mechanoregulatory models to simulate peri-implant tissue formation in an in vivo bone chamber. J Biomec 41:145-154

Geris L, Vander Sloten J and Van Oosterwyck H (2010) Connecting biology and mechanics in fracture healing: an integrated mathematical modeling framework for the study of nonunions. Biomech Model Mechanobiol. In press

Ginebra MP (2009) Cements as bone repair materials. In: Planell JA, Best SM, Lacroix D, Merolli A. editors Bone Repair Biomaterials. CRC Press. (S1), pp. 394–395 :

Glowacki J, Trepman E and Folkman J (1983) Cell shape and phenotypic expression in chondrocytes. Proc Soc Exp Biol Med 172:93-98

Hildebrand T, Laib A, Müller R, Dequeker J and Rëgsegger P (1999) Direct Three-Dimensional Morphometric Analysis of Human Cancellous Bone: Microstructural Data from Spine, Femur, Iliac Crest, and Calcaneus. J Bone Miner Res 14:1167-1174

Hiu-Yan Y, Ling Q, Kwong-Man L, Ming Z, Kwok-Sui L and Chun-yiu CJ (2005) Novel approach for quantification of porosity for biomaterial implants using microcomputed tomography (μCT). J Biomed Mater Res B 75:234-242

Holtorf HL, Sheffield TL, Ambrose CG, Jansen AJ and Mikos AG (2005) Flow perfusion culture of marrow stromal cells seeded on porous biphasic calcium phosphate ceramics. Ann Biomed Eng 33:1238-1248

Huiskes R (2000) If bone is the answer, then what is the question? J Anat 197:145-156

Isaksson H, van Donkelaar CC, Huiskes R and Ito K (2006a) Corroboration of mechanoregulatory algorithms for tissue differentiation during fracture healing: comparison with in vivo results. J Orthopaed Res 24:898-907

Isaksson H, van Donkelaar CC, Huiskes R and Ito K (2008) A mechano-regulatory bone-healing model incorporating cell-phenotype specific activity. J Theor Biol 252:230-246

Isaksson H, Wilson W, van Donkelaar CC, Huiskes R and Ito K (2006b) Comparison of biophysical stimuli for mechano-regulation of tissue differentiation during fracture healing. J Biomech 39:1507-1516

Jaecques SVN, Van Oosterwyck H, Muraru L, Van Cleynenbreugel T, De Smet E, Wevers M, Naert I and Ver Sloten J (2004) Individualised, µCT-based finite element modelling as a tool for biomechanical analysis related to tissue engineering of bone. Biomaterials 25:1683-1696

Jones CA, Arns CH, Sheppard AP, Hutmacher DW, Milthorpe BK and Knackstedt MA (2007) Assessment of bone ingrowth into porous biomaterials using µCT. Biomaterials 28:2491-2504

Karageorgiou V and Kaplan D (2005) Porosity of 3D biomaterial scaffolds and osteogenesis. Biomaterials 26:5474-5491

Kearney EM, Prendergast PJ and Campbell VA (2008) Mechanisms of strain mediated mesenchymal stem cell apoptosis. J Biomech Eng 130:061004

Kelly DJ and Prendergast PJ (2005) Mechano-regulation of stem cell differentiation and tissue regeneration in osteochondral defects. J Biomech 38:1413-1422

Kelly DJ and Prendergast PJ (2006) Prediction of the optimal mechanical properties for a scaffold used in osteochondral defect repair. Tissue Eng 12:1509-2519

Khayyeri H, Checa S, Tägil M, O´Brien FJ and Prendergast PJ (2010) Tissue differentiation in an in vivo bioreactor: in silico investigations of scaffold stiffness. J Mater Sci: Mater Med. In press.

Khayyeri H, Checa S, Tägil M and Prendergast PJ (2009) Corroboration of mechanobiological simulations of tissue differentiation in an in vivo bone chamber using a lattice-modeling approach. J Orthopaed Res 27:1659-1666

Kuiper JH, Ashton BA and Richardson JB (2000a) Computer simulation of fracture callus formation and stiffness restoration. In: Prendergast PJ, Lee TC, Carr AJ, editors. Proc 12th Europ Soc Biomech, p. 61

Kuiper JH, Richardson JB and Ashton BA (1996) Mechanical signals in early fracture callus. In: Vander Sloten J, Lowet G, Van Audekercke R, Van der Perre G, editors. Proc 10th Europ Soc Biomech, p. 154

Kuiper JH, Richardson JB and Ashton BA (2000b) Computer simulation to study the effect of fracture site movement on tissue formation and fracture stiffness restoration. In: European Congress on Computational Methods in Applied Sciences and Engineering ECCOMAS.

Lacroix D, Château A, Ginebra MP and Planell JA (2006) Micro-finite element models of bone tissue-engineering scaffolds. Biomaterials 27:5326-5334

Lacroix D, Planell JA and Prendergast PJ (2009) Computer-aided design and finite-element modelling of biomaterial scaffolds for bone tissue engineering. Phil Trans R Soc A 367:1993-2009

Lacroix D and Prendergast PJ (2002) A mechano-regulatory model for tissue differentiation during fracture healing: analysis of gap size and loading. J Biomech 35:1163-71

Lacroix D, Prendergast PJ, Li G and Marsh D (2002) Biomechanical model to simulate tissue differentiation and bone regeneration: application to fracture healing. Med Biol Eng Comput 40:14-21

Lanza R, Langer R and Vacanti J (2000) In Vitro Control of Tissue Development. Tissue Engineering Bioreactors. In: L.E. Freed and G. Vunjak-Novakovic editors. Principles of Tissue Engineering. Academic Press, 2nd edition, pp 143-156

Lin AS, Barrous TH, Cartmell SH and Guldberg RE (2003) Microarchitectural and mechanical characterization of oriented porous polymer scaffolds. Biomaterials 24:481-489

Liu X and Niebur GL (2007) Bony ingrowth into a porous coated implant predicted by a mechano-regulatory tissue differentiation algorithm. Biomech Model Mechanobiol 7:335-344

Lopez-Heredia MA, Sohier J, Gaillard C, Quillard S, Dorget M and Layrolle P (2008) Rapid prototyped porous titanium coated with calcium phosphate as a scaffold for bone tissue engineering. Biomaterials 29:2608-2615

Maes F, Van Ransbeeck P, Van Oosterwyck H and Verdonck P (2009) Modeling Fluid Flow Through Irregular Scaffolds for Perfusion Bioreactors. Biotechnol Bioeng 103:621-630

Martini FH (1998) editor. Fundamentals of Anatomy and Physiology. Prentice Hall International. 4th edition

Meyer U, Büchter A, Nazer N and Wiesmann HP (2006) Design and performance of a bioreactor system for mechanically promoted three-dimensional tissue engineering. British Journal of Oral and Maxillofacial Surgery 44:134-140

Milan JL, Planell JA and Lacroix D (2010) Simulation of bone tissue formation within a porous scaffold under dynamic compression. Biomech Model Mechanobiol In press.

Milan JL, Planell JA and Lacroix D (2009) Computational modelling of the mechanical environment of osteogenesis within a polylactic acid–calcium phosphate glass scaffold. Biomaterials 30:4219-26

Mow VC, Kuei SC, Lai WM and Armstrong CG (1980) Biphasic creep and stress relaxation of articular cartilage in compression: theory and experiments. J Biomech Eng 102:73-84

Navarro M, Ginebra MP, Clément J, Martínez S, Avila G and Planell, JA (2003) Physicochemical Degradation of Titania-Stabilized Soluble Phosphate Glasses for Medical Applications. J Am Ceram Soc 86:1345-1352

Navarro M and Michiardi A (2008) The Challenge of Combining Cells, Synthetic Materials and Growth Factors to Engineer Bone Tissue. In: Barnes SJ and Harris LP editors. Tissue Engineering: Roles, Materials and Applications. Novapublishers, pp 19-66

Newman AP (1998) Aticular Cartilage Repair. Am J Sports Med 26:309-324

Olivares A, Marsal E, Planell JA and Lacroix D (2009) Finite element study of scaffold architecture design and culture conditions for tissue engineering. Biomaterials 30:6142-6149

Pauwels F (1960) Eine neue Theorie fiber den EinfluB mechanischer Reize auf die Differenzierung des Stu¨tzgewebes. [A new theory on the influence of mechanical

stimuli on the differentiation of supporting tissue. The tenth contribution to the functional anatomy and causal morphology of the supporting structure.] Z Anat Entwicklungsgesch 121: 478

Pauwels F (1973) Atlas zur Biomecanik der Gesmusen und Krauken Hüfte. Springer.

Pauwels F (1980) Gesammelte Abhandlungen zur Funktionellen Anatomie des Bewegungsapparates (Translated by P. Maquet and R. Furlong as Biomechanics of the locomotor apparatus). Springer-Verlag.

Pérez MA and Prendergast PJ (2007) Random-walk models of cell dispersal included in mechanobiological simulations of tissue differentiation. J Biomech 40:2244-2253

Perren SM (1979) Physical and biological aspects of fracture healing with special reference to internal fixation. Clin Orthop Rel Res 138:175–96

Perren SM and Cordey J (1980) The concept of interfragmentary strain. In: Current concepts of internal fixation of fractures. Springer-Verlarg, pp 63–77

Porter B, Zauel R, Stockman H, Guldberg R and Fyhrie D (2005) 3-D computational modeling of media flow through scaffolds in a perfusion bioreactor. J Biomech 38:543-549

Porter BD, Lin ASP, Peister A, Hutmacher D and Guldberg RE (2007) Noninvasive image analysis of 3D construct mineralization in a perfusion bioreactor. Biomaterials 28:2525-2533

Potier E, Noailly J and Ito K (2010) Directing bone marrow-derived stromal cell function with mechanics. J Biomech 43:807-817

Prendergast PJ and Huiskes R (1996) Finite element analysis of fibrous tissue morphogenesis-a study of the osteogenic index using a biphasic approach. Mechanics of Composite Materials 32:209-218

Prendergast PJ, Huiskes R and Søballe K (1997) Biophysical stimuli on cells during tissue differentiation at implant interfaces. J Biomech 30:539-548

Raimondi MT, Moretti M, Cioffi M, Giordano C, Boschetti F, Lagana K and Pietrabissa R (2006) The effect of hydrodynamic shear stress on 3D engineered chondrocyte systems subject to direct perfusion. Biorheol 43:215-222

Ratner BD, Hoffman AS, Schoen FJ and Lemons JE (2004) Biomaterials Science: an introduction to materials in medicine. Academic Press, 2nd edition

Sanz-Herrera JA, Garcia-Aznar JM and Doblare M (2009) On scaffold designing for bone regeneration: A computational multiscale approach. Acta Biomater 5:219-229

Sikavitsas VI, Temenoff JS and Mikos AG (2001) Biomaterials and Bone mechanotransduction. Biomaterials 22:2581-2593

Stops AJF, Harrison NM, Haugh MG, O´Brien PJ and McHugh PE (2010a) Local and regional mechanical characterisation of a collagen-glycosaminoglycan scaffold using high-resolution finite element analysis. Journal of the mechanical behaviour of biomedical materials 3:292-302

Stops AJF, Heraty KB, Browne M, O´Brien FJ and McHugh PE (2010b) A prediction of cell differentiation and proliferation within a collagen-glycosaminoglycan scaffold subjected to mechanical strain and perfusive fluid flow. J Biomech 43:618-626

Van Cleynenbreugel T, Schrooten J, Van Oosterwyck H and Ver Sloten J (2006) µCT-based screening of biomechanical and structural properties of bone tissue engineering scaffolds. Med Bio Eng Comput 44:517-525

van Lenthe GH, Hagenmüller H, Bohner M, Hollister SJ, Meinel L and Müller R (2007) Nondestructive micro-computed tomography for biological imaging and quantification of scaffold-bone integration in vivo. Biomaterials 28:2479-2490

Van Rietbergen B, Weinans H and Huiskes R (1996) Computational strategies for iterative solutions of large FEM applications employing voxel data. Int J Numer Methods Eng 39:2743-2767

Viceconti M, Davinell M, Taddei F and Capello A (2004) Automatic generation of accurate subject-specific bone finite element models to be used in clinical studies. J Biomech 37:1597-1605

Weinans H and Prendergast PJ (1996) Tissue adaptation as a dynamical process far from equilibrium. Bone 19:143-149

Wendt D, Marsano A, Jakob M, Heberer H and Martin I (2003) Oscillating perfusion of cell suspensions through three-dimensional scaffolds enhances cell seeding efficiency and uniformity. Biotechnol Bioeng 84:205-214

Wolff J (1892) Das Gesetz der Transformation der Knochen (Translated by P. Manquet and R. Furlong as The law of bone remodelling in 1986) Springer, Berlin

Yang Y and El Haj A (2005) Enhancement of Mechanical Signals for Tissue Engineering Bone. Top Tissue Eng 2:1-21

Appendix A
Constitutive Equations of a Linear Elastic Solid

A homogeneous material possesses the same material properties at all points. An isotropic material has the same material properties in all directions.

Stress

In continuum mechanics, stress σ is a measure of the average amount of force exerted per unit area of the surface on which internal forces act within a deformable body. The stress is produced as a reaction to external forces applied on the body. Because the body is assumed as a continuum, the stress is distributed continuously within the volume of the body.

The stress defined at a specific point of the body under small deformations is completely defined by the nine components of the Cauchy stress tensor $\boldsymbol{\sigma}$.

$$\boldsymbol{\sigma} = \begin{bmatrix} \sigma_x & \tau_{xy} & \tau_{xz} \\ \tau_{yx} & \sigma_y & \tau_{yz} \\ \tau_{zx} & \tau_{zy} & \sigma_z \end{bmatrix}$$

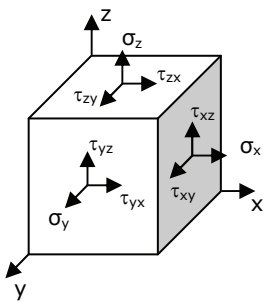

Normal stresses σ_i act on a plane normal to the axis i. Shear stresses τ_{ij} act on a plane normal to the axis i in the direction of the axis j. According to Newton´s laws of linear and angular momentum conservation, if the body is in static equilibrium (acceleration equal to zero) the sum of forces and moments at the specific point is zero and the stress tensor is symmetric ($\tau_{ij} = \tau_{ji}$).

The mean value of the diagonal elements represents the hydrostatic stress which tends to change the volume of the stressed body.

$$-\frac{(\sigma_x + \sigma_y + \sigma_z)}{3} = p$$

Therefore, the stress can be divided into a part that tend to change the volume and a part that tend to distort the body:

$$\begin{bmatrix} \sigma_x & \tau_{xy} & \tau_{xz} \\ \tau_{yx} & \sigma_y & \tau_{yz} \\ \tau_{zx} & \tau_{zy} & \sigma_z \end{bmatrix} = \begin{bmatrix} -p & 0 & 0 \\ 0 & -p & 0 \\ 0 & 0 & -p \end{bmatrix} + \begin{bmatrix} \sigma_x + p & \tau_{xy} & \tau_{xz} \\ \tau_{yx} & \sigma_y + p & \tau_{yz} \\ \tau_{zx} & \tau_{zy} & \sigma_z + p \end{bmatrix}$$

$$\boldsymbol{\sigma} = -p\mathbf{I} + \mathbf{T}$$

I is the identity matrix and **T** is called the deviatoric stress tensor.

The components of the stress tensor depend on the orientation of the coordinate system at the point under consideration. Therefore, for any state of stress it is always possible to define a new coordinate system on which the maximum and minimum normal stresses act and on which no shear stress act.

$$\sigma = \begin{bmatrix} \sigma_I & 0 & 0 \\ 0 & \sigma_{II} & 0 \\ 0 & 0 & \sigma_{III} \end{bmatrix}$$

where σ_I, σ_{II}, σ_{III} are the principal normal stresses

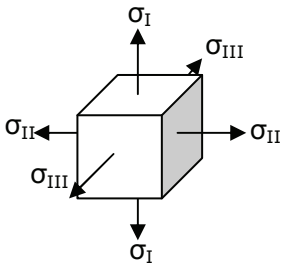

Major principal stress is the principal stress whose absolute value is maximum.

$$\text{major pincipal stress} = \begin{cases} \sigma_I & \text{if } |\sigma_I| > |\sigma_{III}| \\ \sigma_{III} & \text{if } |\sigma_I| < |\sigma_{III}| \end{cases}$$

Considering the principal stress directions as the coordinate axes, a plane in which the normal vector make equal angles with each of the principal axis is called octahedral plane. There are eight such planes. The normal and shear components of the stress tensor on these planes are called hydrostatic stress and octahedral shear stress respectively.

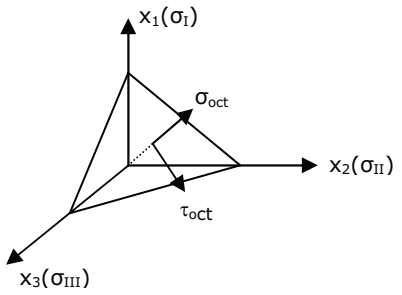

$$\sigma_{oct} = \frac{\sigma_I + \sigma_{II} + \sigma_{III}}{3}$$

$$\tau_{oct} = \frac{1}{3}\sqrt{(\sigma_I - \sigma_{II})^2 + (\sigma_{II} - \sigma_{III})^2 + (\sigma_{III} - \sigma_I)^2}$$

$$= \frac{1}{3}\sqrt{(\sigma_x - \sigma_y)^2 + (\sigma_y - \sigma_z)^2 + (\sigma_x - \sigma_z)^2 + 6(\tau_{xy}{}^2 + \tau_{xz}{}^2 + \tau_{yz}{}^2)}$$

Strain

In continuum mechanics, strain is the geometrical measure of deformation representing the relative displacement between particles in the material body. In a continuous body, a deformation field results from a stress field induced by applied forces or from changes in the temperature field inside the body.

The strain defined at a specific point of the body under small deformations is completely defined by the nine components of the strain tensor **ε**.

$$\boldsymbol{\varepsilon} = \begin{bmatrix} \varepsilon_x & \gamma_{xy} & \gamma_{xz} \\ \gamma_{yx} & \varepsilon_y & \gamma_{yz} \\ \gamma_{zx} & \gamma_{zy} & \varepsilon_z \end{bmatrix}$$

where ε_i is the normal strain in the direction i, and γ_{ij} in the shear strain on the plane ij.

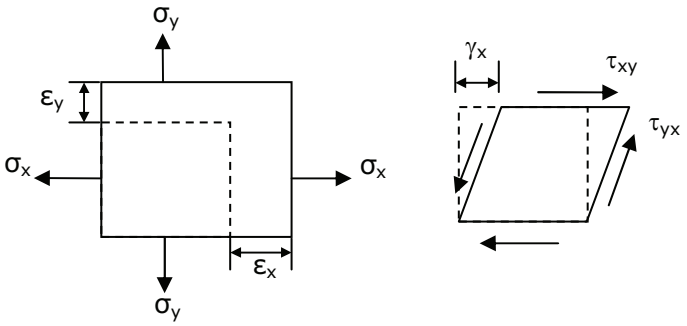

At the coordinate system formed by the principal axis where principal stresses act, principal strain are defined as

$$\boldsymbol{\varepsilon} = \begin{bmatrix} \varepsilon_I & 0 & 0 \\ 0 & \varepsilon_{II} & 0 \\ 0 & 0 & \varepsilon_{III} \end{bmatrix}$$

where ε_I, ε_{II}, ε_{III} are the principal normal strains

The major principal strain is defined as

$$\text{major pincipal strain} = \begin{cases} \varepsilon_I & \text{if } |\varepsilon_I| > |\varepsilon_{III}| \\ \varepsilon_{III} & \text{if } |\varepsilon_I| < |\varepsilon_{III}| \end{cases}$$

For isotropic materials, octahedral strains are referred to the same plane as the octahedral stresses

Octahedral normal strain

$$\varepsilon_{oct} = \frac{\varepsilon_I + \varepsilon_{II} + \varepsilon_{III}}{3}$$

Octahedral shear strain

$$\gamma_{oct} = \frac{2}{3}\sqrt{(\varepsilon_I - \varepsilon_{II})^2 + (\varepsilon_{II} - \varepsilon_{III})^2 + (\varepsilon_{III} - \varepsilon_I)^2}$$

Constitutive Equations

Constitutive equations describe the relationship between stress and strain. For linear elastic materials the derivation of a generalized Hooke's Law in three dimensions for isotropic materials requires the following assumptions:

1. Normal stresses only produce normal strains and do not produce shear strains.

2. Shear stresses only produce shear strains and do not produce normal strains.

3. Material deformations are small, and thus the principle of superposition applies under multiaxial stressing.

The generalized Hooke's Law can be expressed in matrix form as

$$\begin{Bmatrix} \varepsilon_x \\ \varepsilon_y \\ \varepsilon_z \\ \gamma_{xy} \\ \gamma_{yz} \\ \gamma_{zx} \end{Bmatrix} = \frac{1}{E}\begin{bmatrix} 1 & -\nu & -\nu & 0 & 0 & 0 \\ & 1 & -\nu & 0 & 0 & 0 \\ & & 1 & 0 & 0 & 0 \\ & & & 2(1+\nu) & 0 & 0 \\ & \text{Symetric} & & & 2(1+\nu) & 0 \\ & & & & & 2(1+\nu) \end{bmatrix} \begin{Bmatrix} \sigma_x \\ \sigma_y \\ \sigma_z \\ \tau_{xy} \\ \tau_{yz} \\ \tau_{zx} \end{Bmatrix}$$

or more simply $\varepsilon = [S]\sigma$ where [S] is called the compliance matrix. The constant E is the Elastic Modulus or Young's Modulus and the constant G is the Shear Modulus or

the Modulus of Rigidity. The ratio of the lateral strain (due to expansion/contraction of the cross-section) to the axial strain is known as *Poisson's Ratio v*

$$G = \frac{E}{2(1+v)}$$

Stresses may be written as a function of the strains by inverting the compliance matrix. The result is

$$\begin{Bmatrix} \sigma_x \\ \sigma_y \\ \sigma_z \\ \tau_{xy} \\ \tau_{yz} \\ \tau_{zx} \end{Bmatrix} = \frac{E(1-v)}{(1+v)(1-2v)} \begin{bmatrix} 1 & \frac{v}{1-v} & \frac{v}{1-v} & 0 & 0 & 0 \\ & 1 & \frac{v}{1-v} & 0 & 0 & 0 \\ & & 1 & 0 & 0 & 0 \\ & & & \frac{1-2v}{2(1-v)} & 0 & 0 \\ & \text{Symetric} & & & \frac{1-2v}{2(1-v)} & 0 \\ & & & & & \frac{1-2v}{2(1-v)} \end{bmatrix} \begin{Bmatrix} \varepsilon_x \\ \varepsilon_y \\ \varepsilon_z \\ \gamma_{xy} \\ \gamma_{yz} \\ \gamma_{zx} \end{Bmatrix}$$

which can be expressed as $\sigma = [C]\varepsilon$ where [C] is referred to as the stiffness matrix.

Bibliography

Dieter GE (1986) Mechanical Metallurgy. MacGraw-Hill, 3 Ed, New York.

Zienkiewicz OC and Taylor RL (1994) The Finite Element Method. Vol 1: Basic Formulation and Linear Problems. MacGraw-Hill, 4 Edition, London.

Appendix B
Constitutive Equations of a Newtonian Fluid

A fluid flow can be analyzed by two different methods, either by observing the trajectories of specific fluid units, what is commonly termed a Lagrangian representation, or by observing the fluid velocity at fixed positions, which yields an Eulerian representation.

The constitutive equations for a Newtonian fluid are based on the assumption that the fluid, at the scale of interest, is a continuum, in other words it is not made up of discrete particles but rather a continuous substance. The equations are equivalent to the equations for a linear solid elastic. With the application of a small external force, solids respond with a small deformation, however, fluids are easily deformed. In a fluid, the reaction presented to the deformation is not proportional to strain but rather to the speed at which deformation occurs.

Stress

The stress tensor **σ** is defined as:

$$\boldsymbol{\sigma} = \begin{bmatrix} \sigma_x & \tau_{xy} & \tau_{xz} \\ \tau_{yx} & \sigma_y & \tau_{yz} \\ \tau_{zx} & \tau_{zy} & \sigma_z \end{bmatrix}$$

where the σ_i are normal stresses and τ_{ij} shear stresses. The mean value of the diagonal elements represents the hydrostatic pressure p (the static pressure when the fluid is at rest).

$$-\frac{(\sigma_x + \sigma_y + \sigma_z)}{3} = p$$

Therefore, the stress can be divided into a part that would exist if the fluid were at rest and a part related to the fluid motion:

$$\begin{bmatrix} \sigma_x & \tau_{xy} & \tau_{xz} \\ \tau_{yx} & \sigma_y & \tau_{yz} \\ \tau_{zx} & \tau_{zy} & \sigma_z \end{bmatrix} = \begin{bmatrix} -p & 0 & 0 \\ 0 & -p & 0 \\ 0 & 0 & -p \end{bmatrix} + \begin{bmatrix} \sigma_x + p & \tau_{xy} & \tau_{xz} \\ \tau_{yx} & \sigma_y + p & \tau_{yz} \\ \tau_{zx} & \tau_{zy} & \sigma_z + p \end{bmatrix}$$

$$\boldsymbol{\sigma} = -p\mathbf{I} + \mathbf{T}$$

I is the identity matrix and **T** is called the deviatoric stress tensor.

Rate of strain

The fluid velocity **v** is defined as:

$$\mathbf{v} = \begin{bmatrix} u \\ v \\ w \end{bmatrix}$$

were u, v and w are the velocity components in the x, y and z directions respectively.

De gradient of velocity $\nabla\mathbf{v}$ is defined as:

$$\nabla\mathbf{v} = \begin{bmatrix} \frac{\partial u}{\partial x} & \frac{\partial u}{\partial y} & \frac{\partial u}{\partial z} \\ \frac{\partial v}{\partial x} & \frac{\partial v}{\partial y} & \frac{\partial v}{\partial z} \\ \frac{\partial w}{\partial x} & \frac{\partial w}{\partial y} & \frac{\partial w}{\partial z} \end{bmatrix}$$

and can be separated into its symmetric and its anti-symmetric parts, called the rate of strain tensor $\boldsymbol{\varepsilon}$ and the rotation rate tensor $\boldsymbol{\Omega}$:

$$\nabla\mathbf{v} = \begin{bmatrix} \frac{\partial u}{\partial x} & \frac{1}{2}\left(\frac{\partial u}{\partial y} + \frac{\partial v}{\partial x}\right) & \frac{1}{2}\left(\frac{\partial u}{\partial z} + \frac{\partial w}{\partial x}\right) \\ \frac{1}{2}\left(\frac{\partial u}{\partial y} + \frac{\partial v}{\partial x}\right) & \frac{\partial v}{\partial y} & \frac{1}{2}\left(\frac{\partial v}{\partial z} + \frac{\partial w}{\partial y}\right) \\ \frac{1}{2}\left(\frac{\partial u}{\partial z} + \frac{\partial w}{\partial x}\right) & \frac{1}{2}\left(\frac{\partial v}{\partial z} + \frac{\partial w}{\partial y}\right) & \frac{\partial w}{\partial z} \end{bmatrix} + \begin{bmatrix} 0 & \frac{1}{2}\left(\frac{\partial u}{\partial y} - \frac{\partial v}{\partial x}\right) & \frac{1}{2}\left(\frac{\partial u}{\partial z} - \frac{\partial w}{\partial x}\right) \\ -\frac{1}{2}\left(\frac{\partial u}{\partial y} - \frac{\partial v}{\partial x}\right) & 0 & \frac{1}{2}\left(\frac{\partial v}{\partial z} - \frac{\partial w}{\partial y}\right) \\ -\frac{1}{2}\left(\frac{\partial u}{\partial z} - \frac{\partial w}{\partial x}\right) & -\frac{1}{2}\left(\frac{\partial v}{\partial z} - \frac{\partial w}{\partial y}\right) & 0 \end{bmatrix}$$

$$= \boldsymbol{\varepsilon} + \boldsymbol{\Omega}$$

The diagonal elements of the strain tensor are called normal strains and represent the rate of volume expansion.

The sum of normal strains is the divergence of v

$$\text{div}\,\mathbf{v} = \frac{\partial \text{u}}{\partial \text{x}} + \frac{\partial \text{v}}{\partial \text{y}} + \frac{\partial \text{w}}{\partial \text{z}}$$

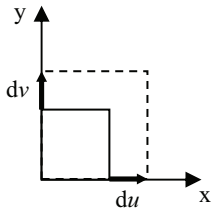

For incompressible flows, div **v** = 0

The off diagonal elements of the strain tensor are called shear strains and represent the rate of shearing deformation.

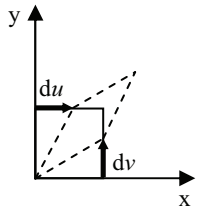

The rotation rate tensor is related to the vorticity that is physically analogous to the angular deformation.

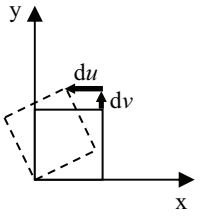

The components of the rate of strain tensor describe motions that are resisted by viscosity; shearing, compression and expansion. The components of the rate of rotation tensor describe motions that are not resisted by viscosity.

As well as the solid, it is always possible to define a new coordinate system on which the maximum and minimum normal stresses act and on which no shear stress act.

$$\boldsymbol{\sigma} = \begin{bmatrix} \sigma_{\text{I}} & 0 & 0 \\ 0 & \sigma_{\text{II}} & 0 \\ 0 & 0 & \sigma_{\text{III}} \end{bmatrix}$$

where σ_{I}, σ_{II}, σ_{III} are the principal normal stresses

$$\boldsymbol{\varepsilon} = \begin{bmatrix} \varepsilon_{\text{I}} & 0 & 0 \\ 0 & \varepsilon_{\text{II}} & 0 \\ 0 & 0 & \varepsilon_{\text{III}} \end{bmatrix}$$

where ε_{I}, ε_{II}, ε_{III} are the principal normal strain-rate

Principal fluid shear stresses can be defined in terms of the principal normal stresses as

$$\tau_{I} = \frac{\sigma_{II}-\sigma_{III}}{2},$$

$$\tau_{II} = \frac{\sigma_{III}-\sigma_{I}}{2},$$

$$\tau_{III} = \frac{\sigma_{I}-\sigma_{II}}{2}$$

Constitutive equations

According to the Stokes law, the stress-strain relations for a isotropic fluid are:

$$\boldsymbol{\sigma} + p\mathbf{I} = 2\mu\left(\boldsymbol{\varepsilon} - \frac{1}{3}\mathrm{div}\mathbf{v}\right)$$

$$p = -k\mathrm{div}\mathbf{v}$$

μ is the viscosity of the fluid and k is the volumetric viscosity.

Therefore,

$$\begin{bmatrix}\sigma_x & \tau_{xy} & \tau_{xz}\\ \tau_{yx} & \sigma_y & \tau_{yz}\\ \tau_{zx} & \tau_{zy} & \sigma_z\end{bmatrix} = -\begin{bmatrix}p & 0 & 0\\ 0 & p & 0\\ 0 & 0 & p\end{bmatrix} + 2\mu\begin{bmatrix}\frac{\partial u}{\partial x} & \frac{1}{2}\left(\frac{\partial u}{\partial y}+\frac{\partial v}{\partial x}\right) & \frac{1}{2}\left(\frac{\partial u}{\partial z}+\frac{\partial w}{\partial x}\right)\\ \frac{1}{2}\left(\frac{\partial u}{\partial y}+\frac{\partial v}{\partial x}\right) & \frac{\partial v}{\partial y} & \frac{1}{2}\left(\frac{\partial v}{\partial z}+\frac{\partial w}{\partial y}\right)\\ \frac{1}{2}\left(\frac{\partial u}{\partial z}+\frac{\partial w}{\partial x}\right) & \frac{1}{2}\left(\frac{\partial v}{\partial z}+\frac{\partial w}{\partial y}\right) & \frac{\partial w}{\partial z}\end{bmatrix}$$

$$-\frac{2\mu}{3}\begin{bmatrix}\mathrm{div}\,v & 0 & 0\\ 0 & \mathrm{div}\,v & 0\\ 0 & 0 & \mathrm{div}\,v\end{bmatrix}$$

The Navier Stokes equations

The Navier Stokes equations are derived from the principles of conservation of mass, momentum, and energy.

Mass conservation:

The principle of mass conservation for a single-phase fluid can be expressed in

differential form as:

$$\frac{D\rho}{Dt} + \nabla(\rho\mathbf{v}) = 0$$

where ρ is the mass density, v is the Eulerian fluid velocity, and t is the time.

Momentum conservation:

The principle of conservation of linear momentum results in:

$$\rho\left(\frac{D\mathbf{v}}{Dt} + \mathbf{v}\nabla\mathbf{v}\right) = \nabla\boldsymbol{\sigma} + \rho\mathbf{f}$$

where σ is the stress tensor and f is the body force per unit mass.

Energy conservation

For incompressible fluids, the principle of conservation of thermal energy is

expressed by:

$$\rho C_p\left(\frac{DT}{Dt} + v\nabla T\right) = -\nabla q + H$$

where T is the temperature, Cp is the specific heat at constant pressure, q is the

thermal flux, and H is the internal heat generated.

Marc solves the Navier-Stokes equations in the fluid under the restrictions that the fluid is considered to be nonreactive, incompressible, single phases, and laminar.

Bibliography

Kundu PK and Cohen IM (2008) Fluid Mechanics. Elsevier Academic Press, 4 Ed, New York.

Pratt LJ (2006) The stress tensor for a fluid and the Navier Stokes Equations. Chapter 3 in Fluid Dynamics of the Atmosphere and Ocean Course. Physical Oceanography Department, Woods Hole Oceanographic Institution, Woods Hole, MA, USA. http://www.whoi.edu/cms/files/adoucette/2006/4/Pedlosky_12.800_Ch3%2706_9199.pdf

Randall DA (2007) The Navier-Stokes Equation. In Selected Notes of David A. Randall. Department of Atmospheric Science, Colorado State University, Fort Collins, Colorado, USA. http://kiwi.atmos.colostate.edu/group/dave/pdf/Navier_Stokes_Equation.pdf

Appendix C
Constitutive Equations of a Poroelastic Material

A porous medium or a porous material is a solid (often called frame or matrix) permeated by an interconnected network of pores (voids) filled with a fluid (liquid or gas). Usually both the solid matrix and the pore network are assumed to be continuous.

The presence of a freely moving fluid in a porous material modifies its mechanical response. Two mechanisms play a key role in this interaction between the interstitial fluid and the porous material: 1) an increase of pore pressure induces a dilation of the porous material, and 2) compression of the porous material causes an increase of pore pressure, if the fluid is prevented from escaping the pore network.

Under drained conditions, excess pore pressure is completely dissipated while under undrained conditions the fluid cannot escape the porous medium.

Linear isotropic poroelastic processes completely described by:

1. The constitutive equations for the porous solid
2. The constitutive equations for the fluid
3. The transport law (Darcy's law)
4. The equilibrium equations
5. The continuity equation

Consistent with the classical continuum approach, any quantity that appears in this description is taken to be averaged over a certain length scale l. This length scale l is assumed to be large (at least by a factor 100) with respect to the length scale of the microstructure (i.e. the typical dimension of the pores), yet small enough to allow the introduction of genuine macroscopic scale material heterogeneity.

Stress

σ is the stress tensor defined in the usual way as the total force per unit area

$$\sigma = \begin{bmatrix} \sigma_x & \tau_{xy} & \tau_{xz} \\ \tau_{yx} & \sigma_y & \tau_{yz} \\ \tau_{zx} & \tau_{zy} & \sigma_z \end{bmatrix}$$

p is the pore pressure, which is a scalar defined as the pressure in an hypothetical reservoir which is in equilibrium with the material (undrained conditions).

Strain

u is the solid displacement vector which follows the movement of the porous solid with respect to a reference configuration.

$$u = \begin{bmatrix} u \\ v \\ w \end{bmatrix}$$

q is the rate of fluid volume crossing a unit area of porous solid. It describes the motion of the fluid relative to the solid.

Two quantities describe the deformation and the change of fluid content of the porous solid with respect to an initial state: the strain tensor **ε** and the variation of fluid content **ζ**. This strain quantities are related to the kinematic variables:

$$\varepsilon = \begin{bmatrix} \frac{\partial u}{\partial x} & \frac{1}{2}\left(\frac{\partial u}{\partial y} + \frac{\partial v}{\partial x}\right) & \frac{1}{2}\left(\frac{\partial u}{\partial z} + \frac{\partial w}{\partial x}\right) \\ \frac{1}{2}\left(\frac{\partial u}{\partial y} + \frac{\partial v}{\partial x}\right) & \frac{\partial v}{\partial y} & \frac{1}{2}\left(\frac{\partial v}{\partial z} + \frac{\partial w}{\partial y}\right) \\ \frac{1}{2}\left(\frac{\partial u}{\partial z} + \frac{\partial w}{\partial x}\right) & \frac{1}{2}\left(\frac{\partial v}{\partial z} + \frac{\partial w}{\partial y}\right) & \frac{\partial w}{\partial z} \end{bmatrix}$$

$$\frac{d\zeta}{dt} = -\frac{dq}{di}$$

where t represents time and i the direction of fluid flow.

Constitutive Equations

The Biot formulation of the constitutive equations for a fluid-filled porous material is based on the assumptions of linearity between the stress (**σ, p**) and the strain (**ε, ζ**), and reversibility of the deformation process (meaning that no energy is dissipated during a closed loading cycle). The strain-stress relation is therefore

$$\begin{Bmatrix} \varepsilon_x \\ \varepsilon_y \\ \varepsilon_z \\ \gamma_{xy} \\ \gamma_{yz} \\ \gamma_{zx} \end{Bmatrix} = \frac{1}{E} \begin{bmatrix} 1 & -v & -v & 0 & 0 & 0 \\ & 1 & -v & 0 & 0 & 0 \\ & & 1 & 0 & 0 & 0 \\ & & & 2(1+v) & 0 & 0 \\ & \text{Symetric} & & & 2(1+v) & 0 \\ & & & & & 2(1+v) \end{bmatrix} \begin{Bmatrix} \sigma_x \\ \sigma_y \\ \sigma_z \\ \tau_{xy} \\ \tau_{yz} \\ \tau_{zx} \end{Bmatrix} + \frac{1}{3H} \begin{bmatrix} 1 & 0 & 0 & 0 & 0 & 0 \\ & 1 & 0 & 0 & 0 & 0 \\ & & 1 & 0 & 0 & 0 \\ & & & 0 & 0 & 0 \\ & \text{Symetric} & & & 0 & 0 \\ & & & & & 0 \end{bmatrix} \begin{Bmatrix} p \\ p \\ p \\ 0 \\ 0 \\ 0 \end{Bmatrix}$$

where E and v are the drained isotropic elastic constants, the Young´s modulus and the Poisson´s ratio respectively, of the material, and H is a constant.

The stress-strain relation is

$$\begin{Bmatrix} \sigma_x \\ \sigma_y \\ \sigma_z \\ \tau_{xy} \\ \tau_{yz} \\ \tau_{zx} \end{Bmatrix} = 2G \begin{bmatrix} \frac{1-v}{1-2v} & \frac{v}{1-2v} & \frac{v}{1-2v} & 0 & 0 & 0 \\ & \frac{1-v}{1-2v} & \frac{v}{1-2v} & 0 & 0 & 0 \\ & & \frac{1-v}{1-2v} & 0 & 0 & 0 \\ & & & \frac{1}{2} & 0 & 0 \\ & \text{Symetric} & & & \frac{1}{2} & 0 \\ & & & & & \frac{1}{2} \end{bmatrix} \begin{Bmatrix} \varepsilon_x \\ \varepsilon_y \\ \varepsilon_z \\ \gamma_{xy} \\ \gamma_{yz} \\ \gamma_{zx} \end{Bmatrix} - \frac{2(1+v)}{3(1-2v)} \frac{G}{H} \begin{bmatrix} 1 & 0 & 0 & 0 & 0 & 0 \\ & 1 & 0 & 0 & 0 & 0 \\ & & 1 & 0 & 0 & 0 \\ & & & 0 & 0 & 0 \\ & \text{Symetric} & & & 0 & 0 \\ & & & & & 0 \end{bmatrix} \begin{Bmatrix} p \\ p \\ p \\ 0 \\ 0 \\ 0 \end{Bmatrix}$$

with $G = \frac{E}{2(1+v)}$

The relation between the dimensionless fluid content ζ and the stress involves the same parameters:

$$\zeta = \frac{\sigma_{x+}\sigma_{y+}\sigma_z}{3H} + \frac{p}{R}$$

where R is an additional constant. Under undrained conditions **ζ**=0, while under drained response **p**=0.

The coefficient 1/H is a measure of the compressibility of the soil for a change in water pressure, while 1/R measures the change in water content for a given change in water pressure.

The constitutive equations can be described in terms of α and K instead of in terms of H and R.

K is the bulk modulus of the material

$$K = \frac{2(1+v)}{3(1-2v)}G$$

α is the ratio of the fluid volume gained (or lost) in a material element to the volume change of that material

$$\alpha = \frac{K}{H}$$

The Darcy´s law

The fluid transport in the interstitial space can be described by the Darcy's law which is an empirical equation for seepage flow in non deformable porous media. Consistent with the current small deformation assumptions and by ignoring the fluid density variation effect, Darcy's law is:

$$q = -\frac{k}{\mu}\left(\frac{dp}{dL} - \rho_f g\right)$$

k the intrinsic permeability having dimension of length squared, μ the fluid viscosity, L is the longitude, g is the body force per unit volume of fluid and ρ_f the fluid density. The intrinsic permeability k is generally a function of the pore geometry. In particular, it is strongly dependent on porosity φ.

The equilibrium equations

Standard considerations of static equilibrium lead to the local stress balance equation

$$\frac{d\sigma}{dx} = -\rho g$$

where g is the body force per unit volume of the bulk material and ρ is the bulk density defined as

$$\rho = (1 - \varphi)\rho_s + \varphi\rho_f$$

where ρ_s and ρ_f are the densities of the solid and the fluid phase, respectively.

The continuity equation

Considerations of mass conservation of a compressible fluid yields the local continuity equation

$$\frac{d\zeta}{dt} + \frac{dq}{dx} = \gamma$$

where γ is the source density (the rate of injected fluid volume per unit volume of the porous solid). It should be noted that the equation is in a linearized form as the fluid density variation effect has been ignored.

Bibliography

Biot MA (1941) General theory of three-dimensional consolidation. J Appl Phys 12:155-164

Detournay E and Cheng AHD (1993) Fundamentals of poroelasticity. Chapter 5 in: Fairhurst C Editor, Comprehensive rock engineering: Principles, Practice and Projects, vol 2, Analysis and Design method. Pergamon Press, Germany. pp 113-171.

Appendix D
Equivalency between a Newtonian Fluid Flow and a Poroelastic Material

The fluid flow in a poroelastic material is described using the Darcy´s law. At a microscopic scale, it is described by the Stokes equations. In a cylindrical pore space or radius *a*, the velocity field is given by the classical Poiseuille solution:

$$v(r) = \frac{1}{4\mu_f}(a^2 - r^2)\left(-\frac{dP}{dx}\right)$$

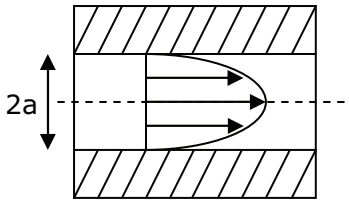

where *r* is the microscopic radial coordinate with respect to the axis of the cylindrical pore space, and *dP/dx* denotes de pressure gradient in the longitudinal coordinate *x*. The fluid is assumed to be incompressible Newtonian fluid of viscosity μ_f. Since the pore pressure is uniform in each section, the pressure gradient is the same at both the microscopic and the macroscopic scale.

If the porosity is defined as:

$$\varphi = \frac{na^2}{R^2}$$

where a is the pore diameter, R is the total diameter and n the number of pores.

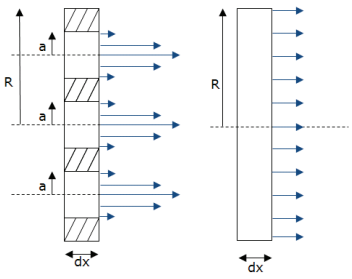

The average flow through the cross section of the elementary volume is thus:

$$Q = \frac{1}{\mu_f}\left(\frac{\varphi a^2}{8}\right)\left(-\frac{dP}{dx}\right)$$

where Q is the total fluid flow, dP/dx is the gradient of pressure and μf is the viscosity of the interstitial fluid flow.

The fist term is the permeability defined as:

$$K = \frac{1}{\mu_f}\left(\frac{\varphi a^2}{8}\right)$$

If a Newtonian formulation is used to determine the average fluid flow, the velocity field can be described also by the Poiseuille solution:

$$v(r) = \frac{1}{4\mu_T}(R^2 - r^2)\left(-\frac{dP}{dx}\right)$$

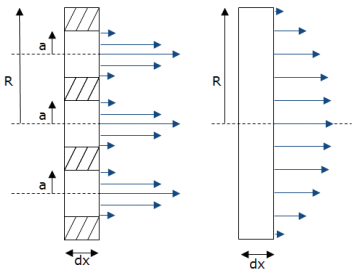

where R is the total diameter, r is the microscopic radial coordinate with respect to the axis of the cylindrical space, and dP/dx denotes de pressure gradient in the longitudinal coordinate x.

The average flow through the cross section of the elementary volume is now:

$$Q = \frac{1}{\mu_T}\left(\frac{R^2}{8}\right)\left(-\frac{dP}{dx}\right)$$

Therefore, making equal the expressions of average fluid flow:

$$K = \frac{1}{\mu_f}\left(\frac{\varphi a^2}{8}\right) = \frac{1}{\mu_T}\left(\frac{R^2}{8}\right)$$

Bibliography

Dormieux L, Kondo D and Ulm FJ (2006) Micro (fluid) mechanics of Darcy´s Law. Chapter 2 in: Microporomechanics. John Wiley & Sons, Chichester. pp 21-61.